THE RADIAL FLOW OF SUPERFLUID HELIUM

OVER A HORIZONTAL SURFACE

and

ION MOBILITY DISCONTINUITIES IN HELIUM II

being a Thesis presented

by

JOHN ALBERT COPE, B.Sc.,

to the

UNIVERSITY OF ST. ANDREWS

in application for

THE DEGREE OF DOCTOR OF PHILOSOPHY

DECLARATION

I declare that this thesis is based on the results of experiments carried out by me, that it is my own composition and has not previously been presented for a Higher Degree.

The work was carried out in the Department of Natural Philosophy, United College, University of St. Andrews, under the direction of Dr. P. W. F. Gribbon, B.Sc., Ph.D.

CERTIFICATE

I hereby certify that Mr. John Albert Cope, B.Sc., has spent a minimum of twelve terms at research work under my supervision, has fulfilled the conditions of Ordinance No. 16 (St. Andrews), and is qualified to submit the accompanying thesis in application for the degree of Ph.D.

Director of Research

UNIVERSITY CAREER

I entered the University of St. Andrews as an undergraduate in October 1956 and graduated B.Sc. with Second Class Honours in Physics in July, 1961.

The research described in this thesis was carried out between October 1961 and April 1965, during which time I held a Research Studentship awarded by the Department of Scientific and Industrial Research, and a University of St. Andrews' Post-Graduate Award.

PUBLISHED PAPERS

1. Gribbon, P. W. F. and Cope, J. A.,
'The Radial Flow of Superfluid Helium Over a Horizontal Surface', Phil. Mag., 8, 2047, (1963)

2. Cope, J. A. and Gribbon, P. W. F.,
'Ion Mobility Discontinuities in Liquid Helium II',
Proc. Conf. Low Temp. Phys., Columbus, Ohio, P. 353, (1965)

3. Cope, J. A. and Gribbon, P. W. F.,
'Vibrating Ions in Liquid He II', Phys. Letters 16, 128, (1965)

4. A paper on the effect of parallel n-fluid flow on ion velocities has been submitted for the Xth Int. Conf. Low Temp. Phys., Moscow, 1966.

5. A criticism of the Huang-Olinto theory for the ion mobility discontinuities including further experimental evidence, has been submitted for publication.

ACKNOWLEDGMENTS

I would like to express my gratitude to Dr. P. W. F. Gribbon for his constant help and advice throughout the period during which the work for this thesis was performed. Dr. Gribbon, who was always available to discuss problems, gave practical help and many valuable ideas.

I am grateful to Prof. J. F. Allen for providing me with the opportunity to do research. His continued interest and attention were a great encouragement.

My thanks are due to Dr. C. G. Kuper and Dr. R. Clark for many profitable discussions with them concerning the theory of the discontinuities.

I would also like to thank the technical staff of the Natural Philosophy Department, University of St. Andrews, and in particular, Mr. J. Gerrard for his many services, including the photographing of my apparatus, Mr. R. Mitchell, for providing liquid helium when required and for advice on technical matters, and Mr. J. McNab for much help in the construction of the apparatus.

I am indebted to the Department of Scientific and Industrial Research for a Research Studentship from 1961-1964, and to the University of St. Andrews for a Post-Graduate Award from 1964-1965.

INDEX

Part I - Radial Flow of Superfluid Helium Over a Horizontal Plate

N.B. Symbols not explained in the text will be found in the notation at the end of the thesis, P.188.

Part II - Ion Mobility Discontinuities in Liquid Helium II

PART I

THE RADIAL FLOW OF SUPERFLUID HELIUM OVER A HORIZONTAL SURFACE

INTRODUCTION

Although film transfer of superfluid helium has been extensively studied, (Jackson and Grimes, Review Article 1958)[1] most observations have been made using vertical surfaces. The behaviour of superfluid helium on a horizontal surface can be quite different, and it was the purpose of this work to study some aspects of this behaviour.

The experiment reported here had three main objectives:

(i) To study the flow of superfluid helium over a horizontal surface

(ii) To look for a contact angle between the bulk liquid and a surface covered by the film

(iii) To observe superfluid helium flowing over a sharp edge.

Section (iii) in particular was stimulated by work on enhanced film transfer into vessels where the rim was close to or even below the bath liquid surface. Allen[2] (1961) reported that enhanced, but apparently measurable, film flow took place into a beaker not only when the rim of the beaker was just at the bath surface but even when the rim of the beaker was as much as 0.6 mm. below the bath surface. It had been expected that such immersion would cause the liquid helium to flow in uncontrollably but this was clearly not the case. It was, therefore, decided to study the phenomena in more detail.

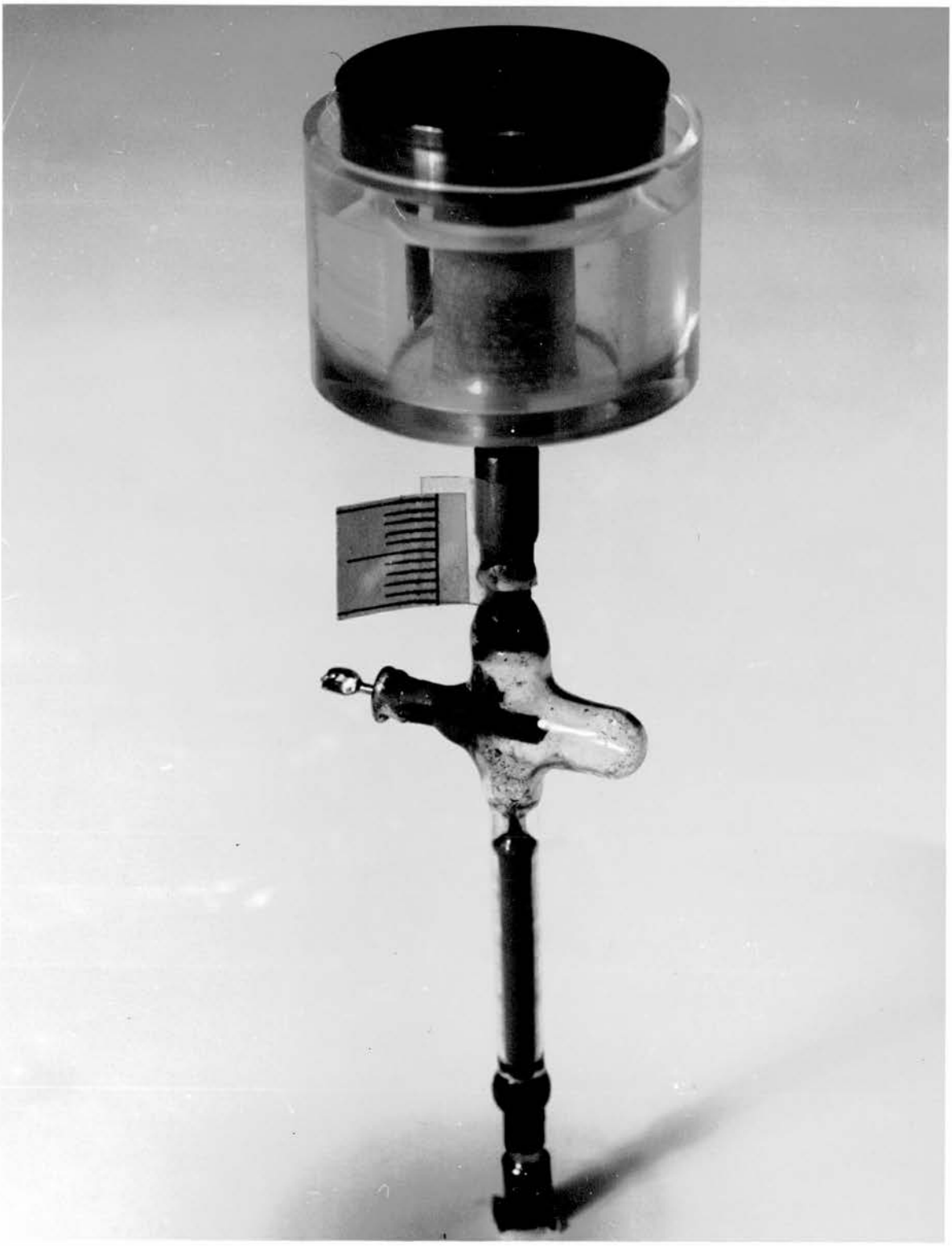

Circular Stainless Steel Plate Used to Observe the

Radial Flow of Superfluid Helium

PLATE 1

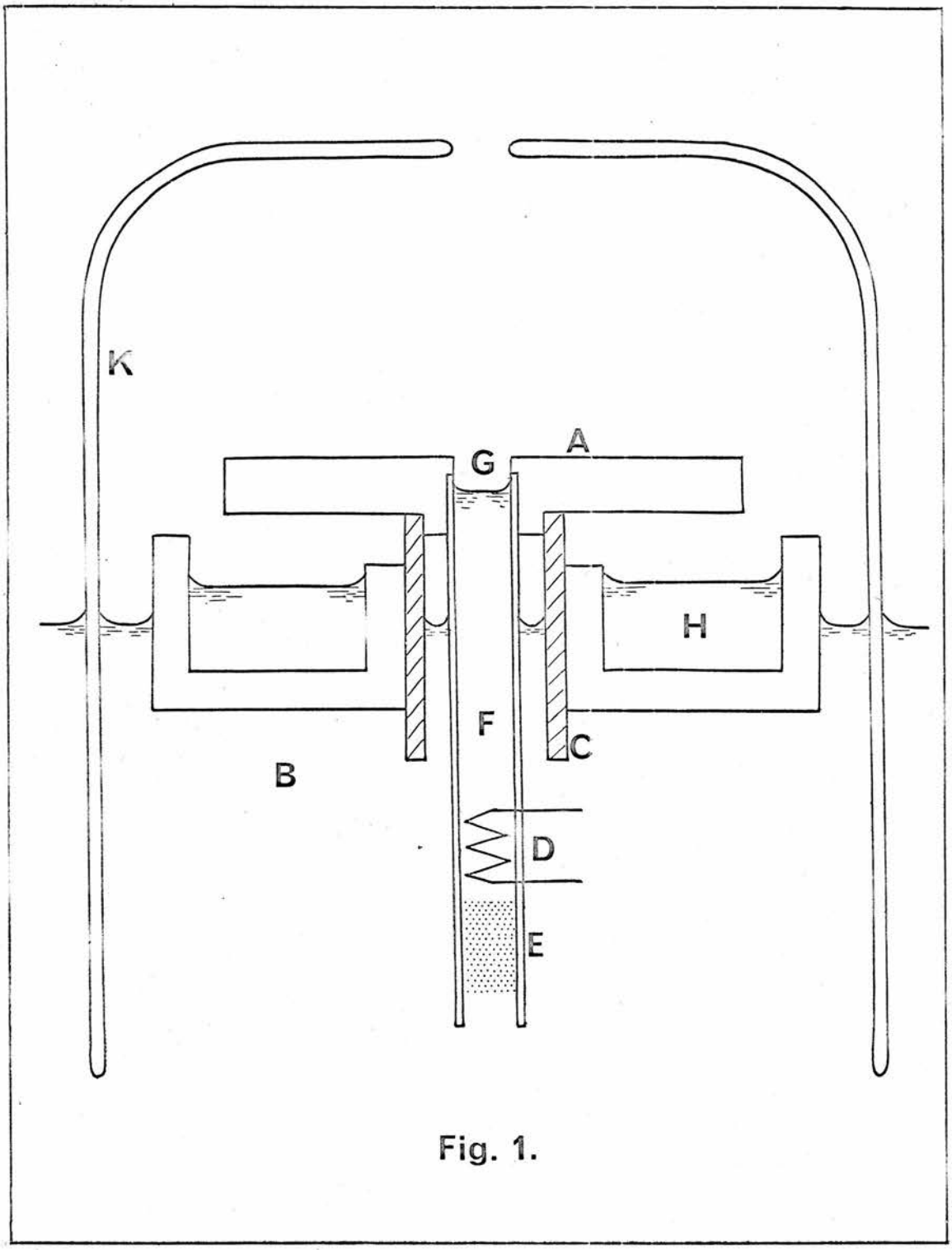

Fig. 1.

APPARATUS

The apparatus used to observe the flow is shown in Fig. 1 and Plate 1. The horizontal polished circular plate A of stainless steel, was 2.8 cm. in diameter and 2 mm. in thickness. The plate surface was lapped to ensure perfect flatness to within 5×10^{-3} cm. Successively finer grades of abrasive were employed, finishing with jewellers rouge which had been allowed to settle in water previously. This gave the finest possible abrasive. The plate was kept in good thermal contact with the helium bath B by a copper tube C soldered to it and dipping into the bath. A 'fountain' pump consisting of a heater D above a 'superleak' E was attached to the plate by the tube F. The heater was made by winding 40 s.w.g. Eureka wire on a plastic former and inserting this into the tube via a Kovar seal. The heater had a resistance of $\approx$ 18 ohms. The 'superleak' was made of two sections of glass tubing, 3 cm. long and 3 mm. inner diameter, packed with jewellers rouge and joined by a glass metal seal. The 'fountain' pump relied on the 'fountain' effect in He II [48] in which n-fluid flows away from the heat source, balanced by a flow of s-fluid towards the heat source. The viscous n-fluid was unable to pass through the 'superleak' E, but the s-fluid passed through with ease. The current in the heater D controlled the rate at which the superfluid component of He II flowed through the 'superleak' and up to the plate through the central hole, G 3 mm. in diameter. Thus the application of heat to heater D caused a rise in liquid level in G.

For high heat inputs He II flowed over the rim of the plate and was collected and measured in a transparent perspex trough H,* which was cemented to C. The apparatus and in particular the surface of the flow plate, were protected from radiation, from excessive evaporation and from dust and

---

* The level in H was measured by a cathetometer.

condensed impurities, by a silvered glass shield K, with small clear strips through which the surface could be viewed. The whole apparatus, including the radiation cover, could be raised and lowered by means of a rod passing through the top of the cryostat. For some experiments a heater was glued under the circumference of the plate. The events on :→

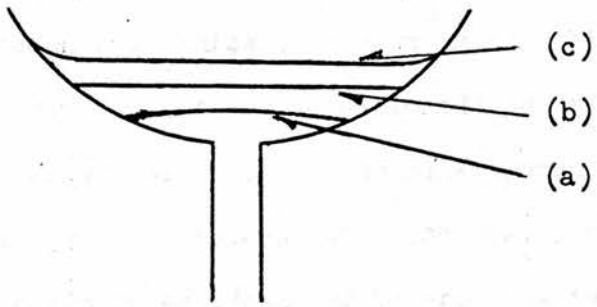

Operation of the cylindrical trough for the measurement of angles of contact, showing three possible liquid levels

(a) Convex upwards.

(b) Perfectly flat

(c) Concave upwards.

The width of the liquid surface when its edges show no curvature (i.e.(b)) together with the radius of curvature of the trough surface gives the angle of contact.

the surface of the plate were observed and measured using a cathetometer.

A subsidiary apparatus was used in an attempt to measure the angle of contact. The flat plate in the above apparatus was replaced by a stainless steel trough. (See Plate 2.) The trough was made from a section of a stainless steel tube whose inner surface, radius 2", was highly polished. The two sides of the trough were closed by perspex windows and made superfluid tight by indium seals. (See opp.)

A modification of this apparatus is shown in Plate 2. In this arrangement the reservoir was filled by dunking, and liquid held in the reservoir by the 'fountain' pump, the heater for which was placed near the reservoir. When the heat supply to the 'fountain' pump was cut off, liquid helium flowed through the 'superleak' to the trough by gravity. A simple trough was made with no 'fountain' pump which could be filled or emptied by film flow or by dunking below the bath surface.

Temperature Measurements

The temperature was measured by measuring the vapour pressure on a standard manometer, since in this region the vapour pressure is strongly dependent on temperature. All measurements were made at a temperature of $1.65^{\circ}K \pm 0.1^{\circ}K$, equivalent to a vapour pressure of 7 mm. of Hg.

A graduated glass beaker was mounted above the apparatus on the support rod and the measured film flow transfer rates out of this gave a good check for contamination. Film flow rates over dirty glass are much greater than over a clean surface.[49]

Cleaning of Plate

Particular attention was paid to surface cleanliness. Washing of the plate in carbon tetrachloride was inadequate as this left a thin film on the surface. The procedure finally adopted was to suspend the plate in the vapour of refluxing carbon tetrachloride for one hour.

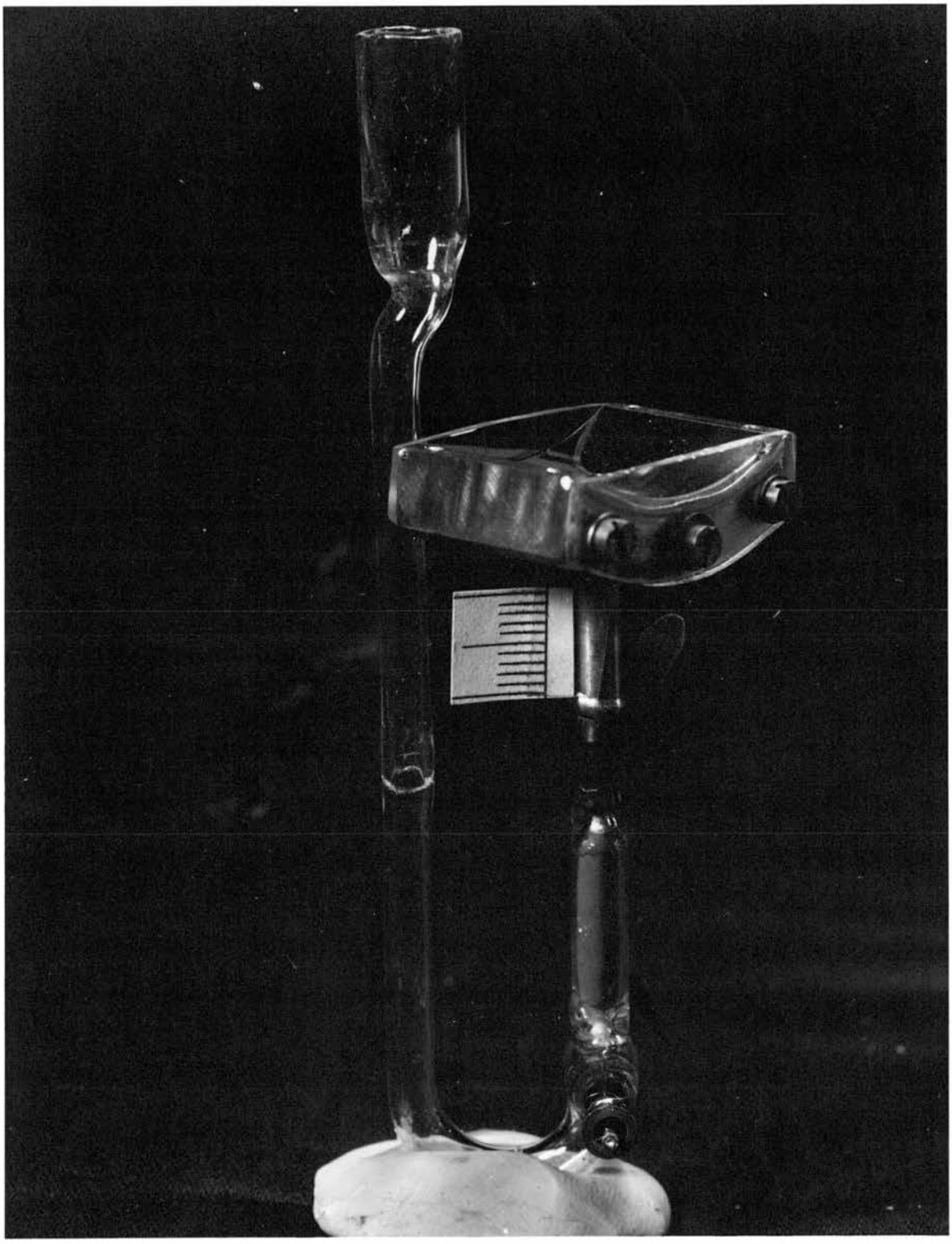

Stainless Steel Trough For Observing Contact Angles

PLATE 2

This method had the double advantage that the liquid washing the surface was newly condensed and therefore pure, also the solvent would be hot and therefore more effective in dissolving unwanted grease.

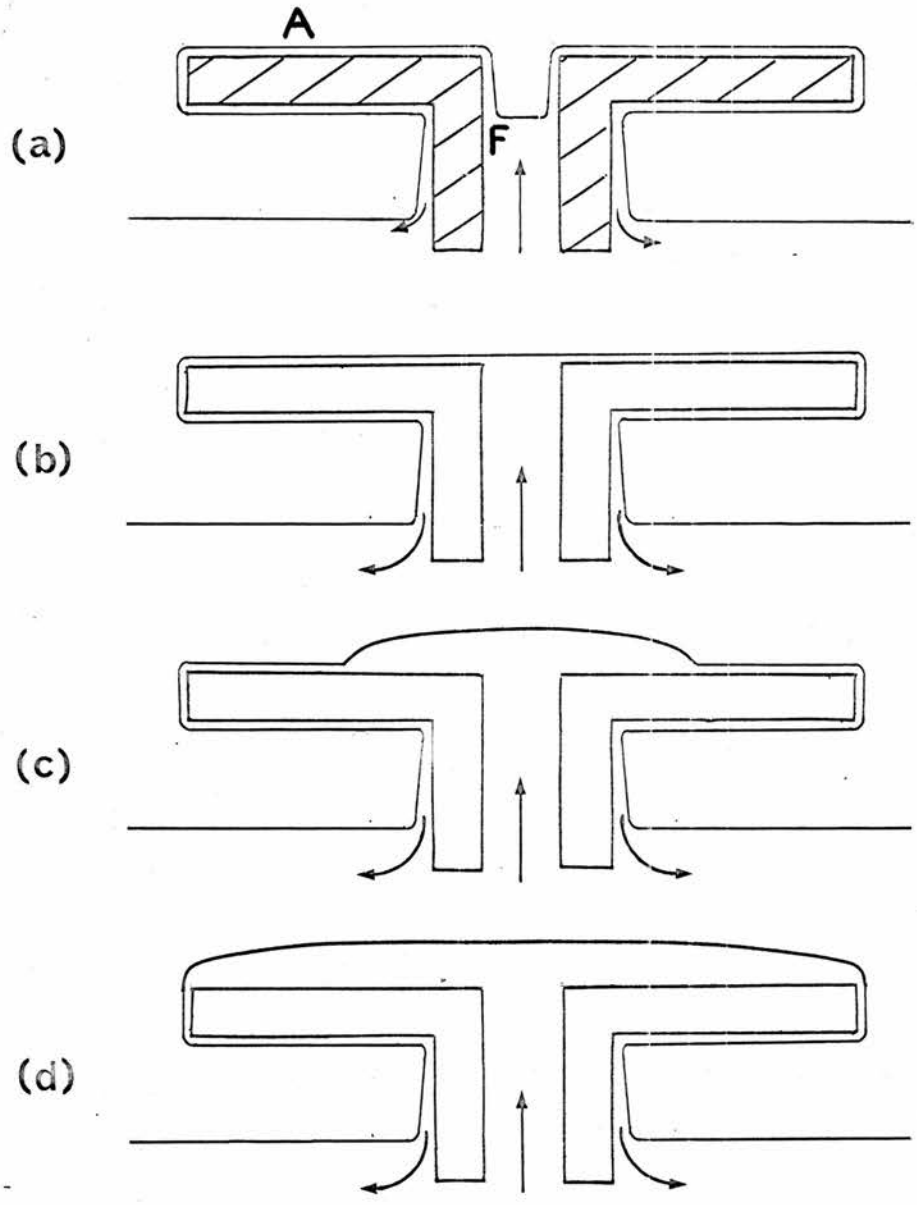

Fig. 2.

RESULTS

In the initial runs using the apparatus with the flat plate, four different situations occurred. These will be described in the order in which they occurred for increasing heat input to the 'fountain' pump and therefore in the order of increasing liquid volume flow to the plate.

(a) With zero input to the heater D, the plate was presumably covered by a static film[1] whose thickness was appropriate to its height above the bath level or above the level in F. With a low heat input to D, the level in F rose and the film on A would thicken accordingly and flow radially outward, as indicated in Fig. 2(a).

(b) As the level in F approached the top of the hole, the film on A thickened considerably, Fig. 2(b), and this was observable as a change in the appearance of the plate surface as viewed by reflected light. The liquid presumably filled the small scratches in the plate surface, thus reducing the amount of diffusely reflected light and giving an apparent darkening of the plate surface.

(c) Further increase of the heat input caused the liquid to form what can be described as a 'dynamic sessile' drop with a sharply defined perimeter between it and the thick film outside it. This is shown schematically in Fig. 2(c).

When the bath liquid was clear of the plate, the surface of the dynamic sessile drop was disturbed by waves radiating from the centre.

(d) When a comparatively large heat input ($\approx$ 15 mW) was supplied to the fountain pump, the dynamic sessile drop extended to the edge of the plate in the manner of Fig. 2(d). Further increase of heat input up to 80 mW caused the height of this 'edge drop' to increase to a maximum $h_m = 0.67 \pm 0.05$ mm.

These topics will now be treated separately.

(a) and (b) - Film Thickness

No attempt was made to measure film thicknesses.

(c) - 'Dynamic Sessile' Drop

This title seems a contradiction in terms.

'Sessile' is meant to imply that bulk liquid is located in one place, over the central hole of the plate.

'Dynamic' refers to the fact that the liquid composing the drop, was constantly changing. Liquid was flowing in from the fountain pump and out by film flow from the drop perimeter.

The perimeter of the drop was clearly defined and the contact angle appeared to be in the neighbourhood of 5 - 10°; accurate measurements of the drop profile were not made.

(i) Transfer Rate from the Drop

In order to determine the fluid flow occurring through the 'sessile' drop, a measuring bath H was fitted beneath the plate.

The copper heat leak C was extended underneath the plate to form a 'skirt.' Liquid flowing from the plate then dripped from this 'skirt' into the measuring bath.

A 'dynamic sessile' drop of the required size, was maintained on the plate and the rise of liquid level in H observed through a cathetometer. Marks on the plate surface proved a means of estimating the drop diameter. This method however, was later superseded by the use of a second cathetometer.

The main difficulty was in keeping the drop constant on the plate. If the heat input to the fountain pump was adjusted to give a sessile

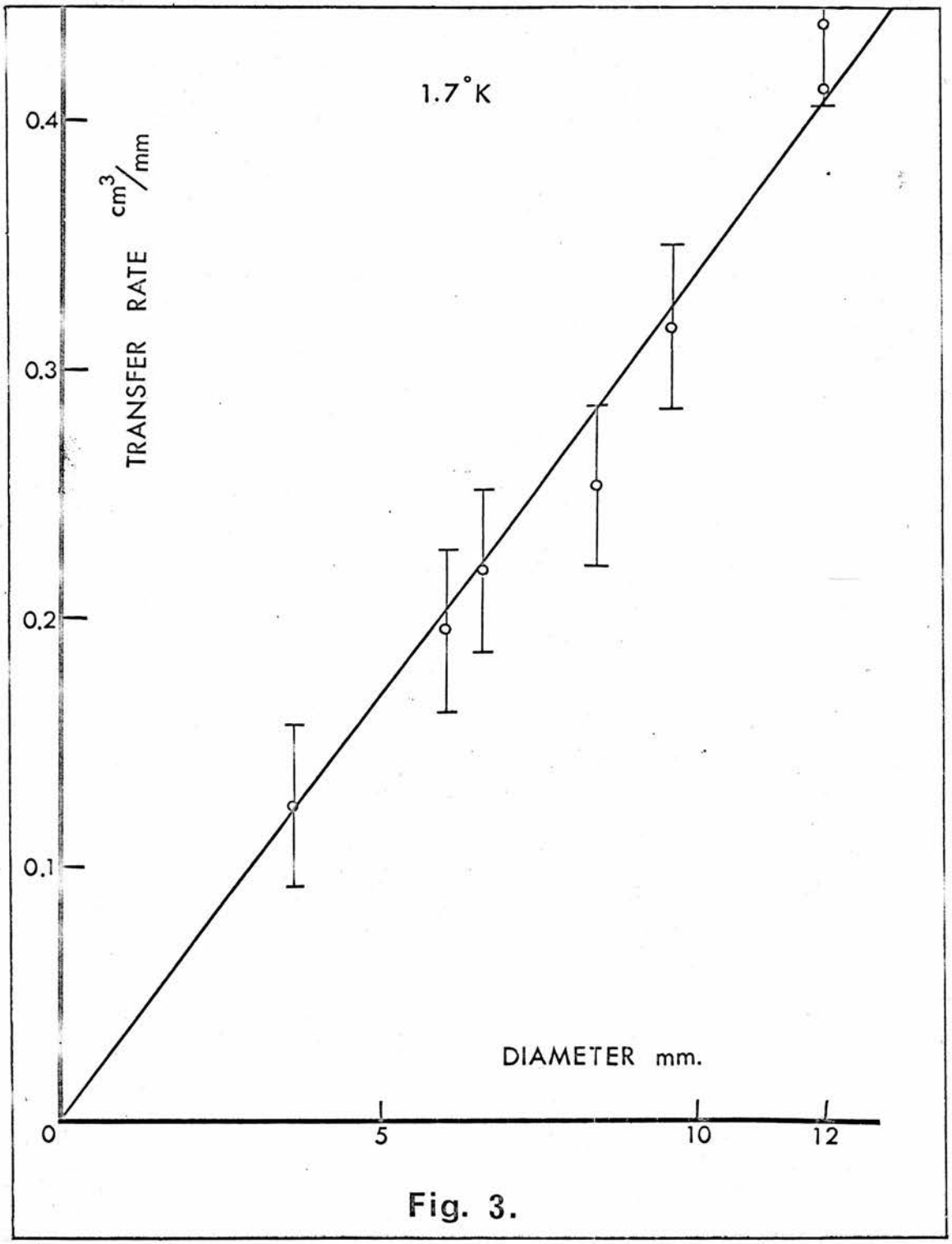

Fig. 3.

drop on the plate and then left unaltered, the sessile drop shrank after a time and the transfer rates were reduced correspondingly. This occurred because, for a fixed heat input, the fountain pump was only able to maintain a constant hydrostatic head[2] above the outer bath level. As the bath level dropped, the top surface of the drop fell correspondingly.

The technique eventually adopted was to set the heater current to a particular value, observe the size of drop formed by this heat input, and measure the initial rate of rise of the level in the bath H. These three operations were accomplished in approximately 10 seconds.

The rate of film flow transfer out of bath H, was measured by observing the bath level after the heat to the fountain pump had been removed. This rate of fall had to be added to the measurements with a drop on the plate, to give the true transfer rates from the 'dynamic sessile' drop. The results are shown in Fig. 3. It can be seen that transfer rates away from the drop were approximately proportional to the drop radius. The transfer rate Q from unit length of the drop perimeter, was $177 \pm 5 \times 10^{-5}$ cm^3 sec^{-1} and independent of drop size. The drop adjusted its size according to the total flow through G.

(ii) Reason for the 'Dynamic Sessile' Drop

The existence and stability of the 'dynamic sessile' drop can be explained in the following way.

Imagine first that a drop exists on the plate under the conditions described. The drop over the central hole consists of bulk liquid flowing radially outwards across the plate under the influence of a

hydrostatic pressure gradient. The film flow outside the drop perimeter, on the other hand, is independent of the pressure head,[1] and consists mainly of the superfluid component. The contribution of the 'normal' component to the film flow is small both because of its small concentration at 1.6°K and because it experiences a large frictional resistance in the comparatively thin film. The velocity and transfer rate by the film will follow the curve given by Atkins.[3]

Since for mass conservation $2\pi vd = \frac{Q}{r}$ = volume/sec/cm. flowing from the 'fountain' pump; for a fixed Q, vd will decrease for increasing r. The film transfer rate $v_f d_f$ outside the drop perimeter will increase with decreasing r in order to conserve mass and also because the film thickens as it approaches the dynamic sessile drop. At the perimeter of the drop the transfer rate due to the film and bulk liquid in the drop are equal.

At the perimeter of the drop there will be a transition between these two regimes of flow; at a certain depth d_o of liquid on the plate, the normal fluid flow will fall off rapidly. Inserting the observed transfer rate $vd \approx 180 \times 10^{-5}$ cm^3/sec. (Page 12) from one cm. of the drop perimeter on Atkins curve[3] of $\log_{10} vd$ versus $\log_{10} d$, would predict a value of $d_o = 2.2 \times 10^{-4}$ cm. and $v_{s_c} = 8$ cm/sec. If the rate of supply of liquid through the 'fountain' pump is Q cm^3/sec., the drop will then adjust its size until

$$Q = 2\pi\, v d_o r \qquad (1)$$

where Q = volume flow/sec.
v = fluid velocity
d = liquid depth
r = radius on the plate
v_f = film velocity
d_f = film thickness

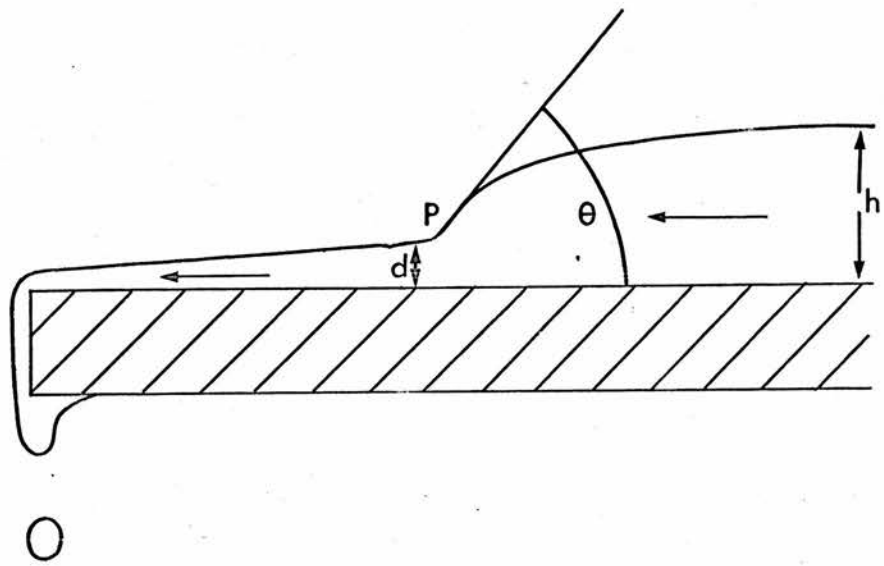

Fig. 5.

Section of "Dynamic Sessile Drop"

Therefore for constant vd_o the radius of the drop is directly proportional to the rate of supply of liquid through the fountain pump as observed. (Fig. 3)

(iii) The Shape of the Sessile Drop

Liquid in the drop has a velocity $v < 10$ cm/sec. and therefore its profile will be approximately that of the stationary sessile drop.* This profile may be calculated in the following way.

For equilibrium at the point P (Fig. 5) the hydrostatic pressure head ρgy must be balanced by the pressure due to surface tension.

$$\therefore \quad \sigma\left[\frac{1}{r_1} + \frac{1}{r_2}\right] = \rho g y \qquad \text{(2)}$$

(Close to the edge of the drop the fluid velocity is higher and the Bernoulli effect introduces a small correction.)

where r_1 = radius of curvature of profile of drop surface

r_2 = " " " in horizontal plane (of drop surface)

σ = surface tension

y = depth below top of drop

ρ = total liquid density

For a large sessile drop $\frac{1}{r_2}$ is negligible.

Now $\frac{1}{r_1} = \frac{d\Psi}{ds} = \frac{d\Psi}{dy}\cdot\frac{dy}{ds} = \mathrm{Sin}\Psi\,\frac{d\Psi}{dy}$

where s = arc length

$\therefore \quad \mathrm{Sin}\Psi\, d\Psi = \frac{\rho g}{\sigma}\, y\, dy$

Integrating and noting that $\Psi = 0$ when $y = 0$

$$\frac{\rho g y^2}{\sigma} = (1 - \mathrm{Cos}\,\Psi)$$

$$\therefore \quad y = \frac{2}{\sqrt{A}}\,\mathrm{Sin}\frac{\Psi}{2} \qquad \text{where } A = \frac{\rho g}{\sigma}$$

---

* Any velocity effects occur in the unobservable drop-film boundary.

PROFILE OF A SESSILE DROP derived from equations (3) and (4) page 17.

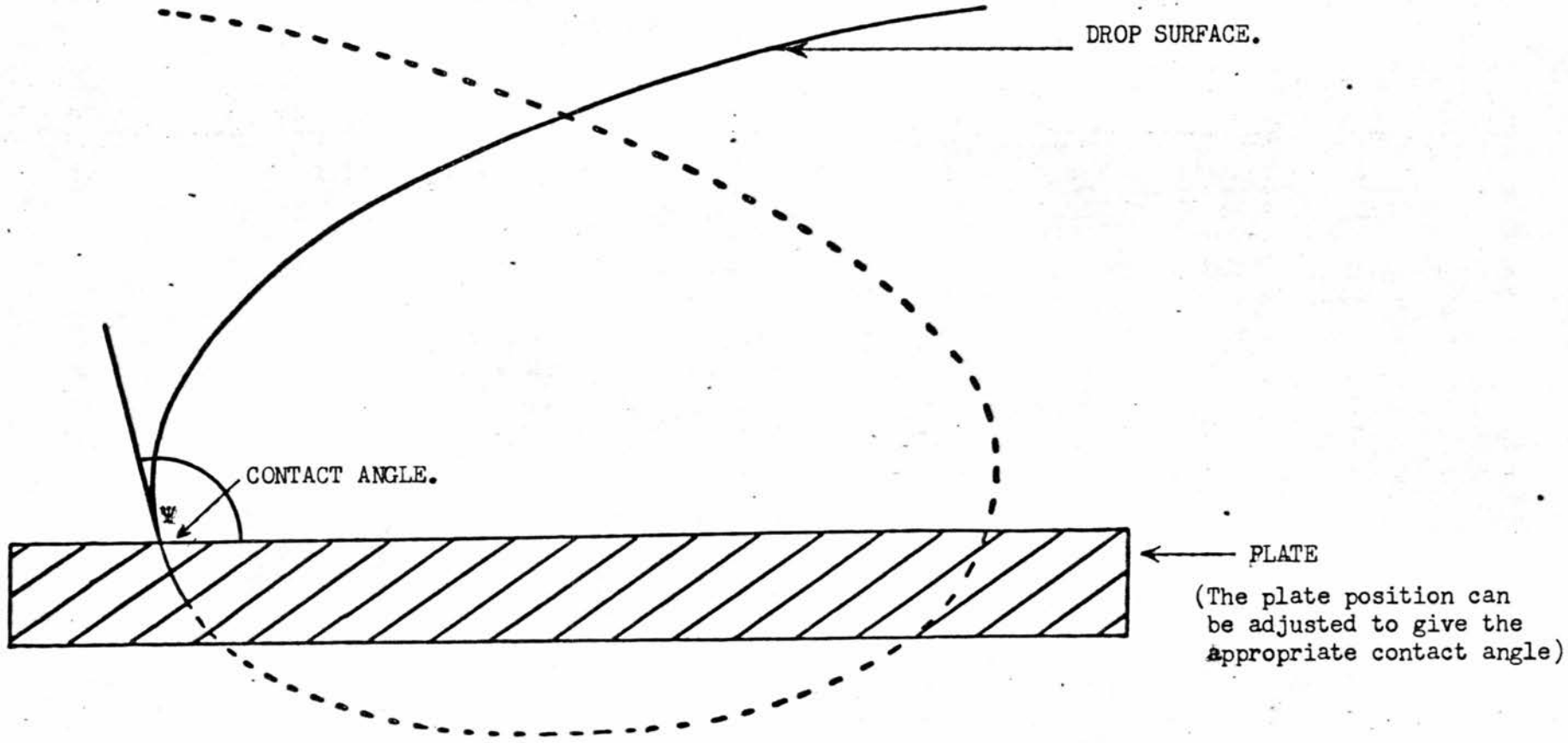

FIG. 6.

Similarly for x

$$\text{Cos.}\Psi \frac{d\Psi}{dx} = Ay = 2\sqrt{A}\ \text{Sin.}\frac{\Psi}{2}$$

$$\therefore\ x = \sqrt{A}\ \log.\frac{\Psi}{4} + 2\sqrt{A}\ \text{Cos.}\frac{\Psi}{2}$$

Substituting e^{-p} for $\tan.\frac{\Psi}{4}$ gives

$$x = 2\sqrt{A}\ (\tanh p - \frac{p}{2}) \qquad \text{----------} \quad (3)$$

and $$y = 2\sqrt{A}\ (\text{sech } p) \qquad \text{----------} \quad (4)$$

The appropriate part of the curve represented by these two equations is shown in Fig. 6. When normalised to the drop height, this curve gives the variation of liquid depth d with r.

(iv) - Comparison with Atkins 'Transfer Rate ' Diagram (See Fig. 6a)

For conservation of mass in the 'dynamic sessile' drop

$$v_s dr = \text{Constant} = 180 \times 10^{-5}\ \text{cm}^3/\text{sec.}$$

Eliminating r from this equation and a graphical solution of d versus r obtained from the above computed profile, gives a relationship between $v_s\dot{d}$ and d. The form of this relationship, plotted on Atkins[3] graph of $\log_{10} vd$ vs $\log_{10} d$, describes completely the phenomena observed on the plate surface. There are three significant sections.

Diameter	Height
mm.	mm.
3.0	0.2 ± 0.02
5.7	0.37
7.0	0.41
9.0	0.26
9.0	0.34
13.2	0.37
16.0	0.34
25.0	0.51

Temperature ≡ 1.6°K

Dynamic Sessile Drop Height

as a Function of Diameter

TABLE I

N.B. The error ± 0.02 mm. is the possible error in the measurement of height. The actual height of the drop is more uncertain than this because of the experimental difficulty of obtaining a height measurement before the drop began to shrink. (Page 12)

Profile of a Typical "Dynamic Sessile Drop"

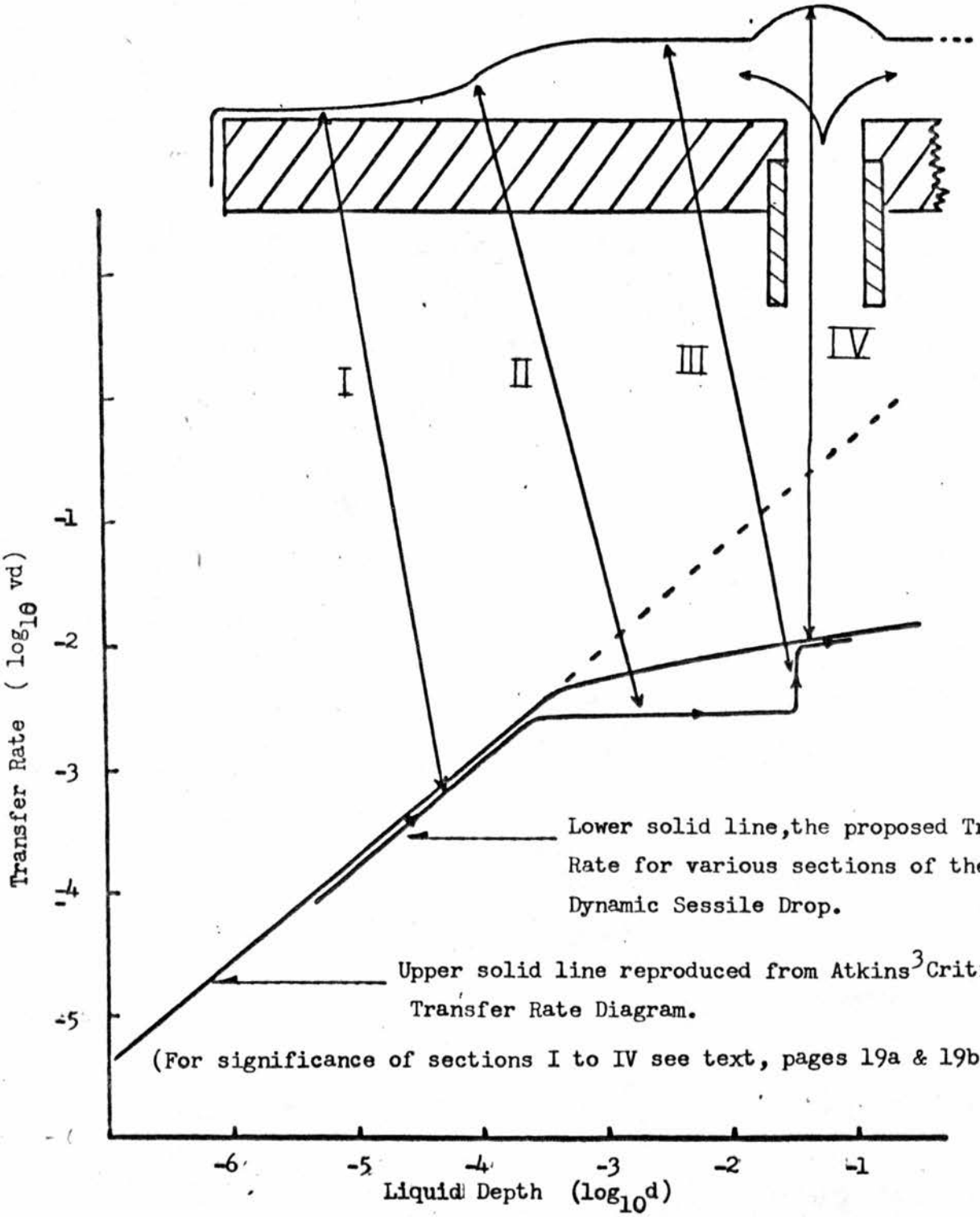

FIG. 6(a)

I. At the edge of the plate where $d \approx 10^{-4}$ cm. flow is by the film only and the transfer rates follow exactly the relationship

$$v_{s_c} d = Cd^{+3/4} \qquad \text{(12)}$$

(van Alphen[53]) where C = Constant $\approx 1 cm^{\frac{5}{4}} sec.^{-1}$ obtained from Atkins transfer rate diagram[53]. The dependence of film thickness on r the distance from the centre of the plate, can be calculated by eliminating v_{s_c} from equation (12) and the mass conservation equation

$$v_s d r = \text{Total volume flow rate} \qquad \text{(13)}$$

The profile of the film outside the dynamic sessile drop of radius 1 cm. is shown in Fig.6(a).

II. Near the perimeter of the dynamic sessile drop at some depth d_o of the liquid, a significant amount of n-fluid enters the flow and a hydrostatic pressure gradient is necessary to maintain this flow. This means that the depth of liquid must increase further with decreasing radius on the plate. In this region, however, the profile of the liquid surface is determined predominantly by surface tension (See equations (3) and (4) P37) and the drop thickens more rapdily than is necessary to accommodate the critical transfer rate. The actual transfer rate across a section in region II of the drop is therefore lower than the critical transfer rate, and pure superflow occurs.

III. Equations (3) and (4) predict that the top surface of the sessile drop is flat to better than 0.01 mm. to within 2 mm. of its perimeter. In this 'flat' region it is obvious that the depth d remains constant while the transfer rate across unit length of the section continues to increase with decreasing radius of the section.

IV. Towards the centre of the drop for sufficiently high heat inputs the transfer rate $v_s d$ reaches the critical values $v_{s_c} d$. On the diagram (Fig.6a) this is where the vertical line, corresponding to region III of constant drop height, cuts the horizontal portion of Atkins transfer rate curve.[3] This horizontal section of the transfer rate curve which was previously associated with the superfluid critical velocity, has now been shown by van Alphen et al[53] to correspond to the onset of classical turbulence. If the drop liquid reaches this critical transfer rate at a radius $r = r_c$ then for $r < r_c$ the transfer rate/unit length perimeter must increase and therefore the turbulence remains and the liquid must increase in depth to accommodate the volume flow. This could account for the comparatively high reading obtained for the height of a drop of diameter (Table I) 25 mm. At high heat inputs small 'bumps' were observed over the centre of the drop, as shown in the figure 6(a).

The edge of the sessile drop is a pseudo hydraulic jump. The increase in drop height near the centre of the plate for large sessile drops is a true hydraulic jump similar in nature to hydraulic jumps occurring in classical liquids.*

(v) - Sessile Drop Height

The height of the drop was measured as a function of radius. The results are shown in Table I. Again the main difficulty in making these measurements was in maintaining the drop steady. An advancing drop tended to be higher than a receding drop of the same radius. All

---

*e.g. tidal bore

the measurements recorded are for approximately stationary drops.

The resulting drop height is 0.35 ± 0.05 mm. independent of drop diameter, provided the drop is clear of the edge of the plate and the central hole.

The first reading for a drop just spanning the hole and the last for a drop almost extending to the edge were discarded as spurious. A reason for the high reading at a drop diameter of 25 cm. is given above. (P.19)

In order to estimate its height, the sessile drop is considered as a container emptying at its perimeter by means of film flow. The maximum velocity of bulk liquid occurs at the drop perimeter where $d_o = 2.2 \times 10^{-4}$ cm. and $v \sim 8$ cm/sec. These values were obtained from plotting the observed $vd = 180 \times 10^{-4}$ on the curve given by Atkins.[3] This maximum velocity occurs when the hydrostatic pressure due to the drop height exactly balances the negative pressure due to the Bernoulli effect.

$$\text{i.e. when } v = \sqrt{2gh} \qquad \text{---------- (5)}$$

Substituting v = 8 cm/sec. gives

$$h = \frac{v^2}{2g} = 0.33 \text{ mm.}$$

a value in remarkably good agreement with the observed drop height of 0.35 mm.

(vi) - Waves

When the outer bath liquid level was below the copper heat leak C, the plate was thermally isolated from the bath liquid. Under these

conditons, the surface of a drop maintained on the plate was disturbed by waves radiating from the central hole. Their frequency f = 5 to 10 cycles/sec. and the velocity u $\sim$ 10 cm/sec. were measured using a stroboscope.

Oscillations of this kind were predicted by Robinson[4] and observed by Manchester and Brown[5] under adiabatic conditions. They used an adiabatic container connected to the bath liquid by a superleak, and initiated the oscillations by discharging a condenser through a heater in the container. They observed oscillations with a frequency of approximately $\frac{1}{2}$ cycle/sec. at 1.6°K.

They predict the theoretical frequency for ideal adiabatic oscillations to be given by

$$\omega_a = \omega_i (1 + \alpha)^{\frac{1}{2}} \qquad \text{----------} \qquad (6)$$

where $$\omega_i = \left(\frac{\rho_s}{\rho} \frac{gA}{\ell a}\right)^{\frac{1}{2}} = \text{Frequency of isothermal oscillations} \qquad \text{-------} \qquad (7)$$

where A = cross-sectional area of the superleak

ℓ = length of superleak

a = cross-sectional area of observation capillary

and

$$\alpha = \frac{aTS^2}{gVC} \left\{1 - \frac{1}{\rho_s} \left(\frac{dP}{dT}\right)_{vap.}\right\} \qquad \text{----------} \qquad (8)$$

where S and C are the entropy and specific heat respectively, of He II, $\left(\frac{dP}{dT}\right)_{vap.}$ is the gradient of the vapour pressure curve, and T is the

* Superfluid velocity through the fine pores of the superleak[3]

$v_{s_c} \approx 50 \text{ cm.sec}^{-1}$.

The volume 0.4 cm^3 above the superleak emptied in approximately 20 secs.

$$\therefore v_{s_c} A = \frac{0.4}{20} \text{ cm}^3\text{sec.}^{-1}$$

$$\therefore \quad A = 4 \times 10^{-4} \text{cm}^2$$

absolute temperature.

When the flat plate used in the author's experiments was clear of the bath liquid, the arrangement was very similar to that of Manchester and Brown.[5]

If the above equations are applied to the case of the sessile drop, 'a' made equal to the area of the drop, say 3 cm.^{2}, and $A = 4 \times 10^{-4}$ cm.^{2} (*see opposite) calculated from measured emptying rates through the superleak, the frequency of oscillations obtained is $\sim$ 6 cycles/sec. in good agreement with the observed frequencies.

The waves once generated at the centre of the plate travel radially outwards and will have a velocity consistent with the depth of liquid on the plate. They are assumed to obey shallow liquid theory[54] in which case the velocity of the waves will be given by

$$v = \sqrt{gh}$$

substituting h = 0.035 cm. gives $v \sim 6$ cm/sec.

The waves on the sessile drop persisted for as long as the drop was maintained on the plate, several minutes in many cases, and showed no signs of being damped. Moreover waves appeared spontaneously on an initially stable sessile drop when the bath level fell below the plate. Both observations suggested that there was a degree of 'positive feed back' in the system, tending to perpetuate wave production. The following mechanism is suggested for this feedback.

When the heater is first switched on n-fluid flows onto the plate and, being unable to escape from the sessile drop, it gives up its

'heat' to the plate, raising its temperature until no temperature gradient exists between the fountain pump and plate. n-fluid flow persists in this direction for a finite time after temperature equilibrium is reached, making the temperature of the plate exceed that of the liquid in the fountain pump. The reverse thermomechanical effect eventually takes over and continues until the original situation is reached. This theory is supported by the observation that waves could not be produced when the bath liquid was in thermal contact with the plate. In this case the plate would always be colder than the liquid in the fountain pump and n-fluid would always flow away from the fountain pump

(vii) - Contact Angle

The existence of the sessile drop has been shown to be a consequence of liquid transfer across the plate by two different regimes of flow; bulk liquid flow and film flow. The angle at which the surface of the drop approaches the plate is therefore not a true contact angle as observed for classical non-wetting liquids. Consideration of the dynamics of liquid flow across the plate showed that a certain height of bulk liquid would accumulate above the centre of the plate. The 'contact' angle observed was then the slope of the predicted sessile drop profile at this depth below the apex.

An attempt was made to measure the contact angle by determining the width of the perfectly flat surface in cylindrical stainless steel troughs. The idea was that, as the liquid level rose in the trough, the angle between the horizontal liquid surface and the trough at the

liquid edge increased and, therefore, at some point the liquid surface would change from convex upwards to concave upwards. (Fig. 6b) The method works well for classical liquids. However for liquid helium there were several reason why the method was completely inadequate.

For example, the perimeter of the expanding pool of liquid in the trough remains nearly constant, a situation quite different from the dynamic sessile drop previously described. The film flowing away from the pool must rise over the edge of the trough. The liquid meniscus on the trough window tended to obscure the surface being observed.

Liquid helium under nearly all circumstances appeared wetting.

Dzyaloshinskii et al[6] have calculated the contact angle for a droplet of liquid resting on a substrate covered by a wetting film of the same liquid. They obtained the chemical potential of the liquid film from a knowledge of the dielectric constant of the liquid and substrate.

$$\text{The contact angle } \theta = \left(\frac{2}{\sigma}\int_{\ell}^{\infty} \mu d\ell\right)^{\frac{1}{2}} \frac{1}{10\ell_{max.}}\sqrt{\frac{h\bar{\omega}}{\sigma}} \qquad \text{---------- (9)}$$

$$\text{where the chemical potential } \mu(\ell) = -\frac{h\bar{\omega}(\varepsilon - 1)}{16\pi^2\ell^3}$$

ℓ = film thickness

ε = dielectric constant

σ = surface tension

Measurements of the helium film thickness give the coefficient of ℓ^3 and hence $h\bar{\omega} \sim 6$ eV.

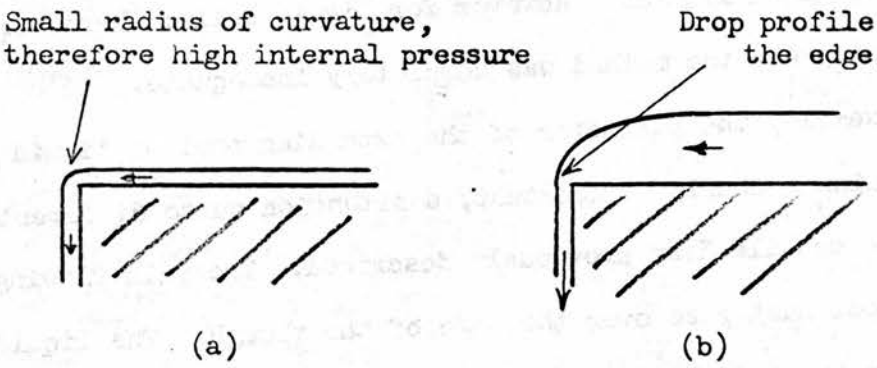

Two ways in which liquid might flow over a sharp edge

(Fig. 6c)

Substituting this value in equation 9, and $\ell_{max.} = 2.2 \times 10^{-4}$ cm. observed here, gives $\theta \sim 0.1^{\circ}$. This is below the limit of observation in the author's experiment.

(d) - Flow over the Edge of a Horizontal Plate

When a comparatively large heat input $\geq$15 mW was supplied to the fountain pump, the dynamic sessile drop extended to the edge of the plate in the manner of Fig. 2(d). / P.8 Further increase in heat input up to 80 mW caused the height of this edge drop to increase to a maximum of 0.67 $\pm$ 0.05 mm.

The problem of the edge drop can be treated classically as a consequence of surface tension and does not involve any superfluid properties directly. The surface of bulk liquid helium, like any classical liquid, cannot follow closely the contour of the substrate when flowing over a sharp edge. The pressure in a classical liquid due to surface tension σ and curvature $\frac{1}{r}$ is $p_o = \frac{\sigma}{r}$.

Flow by a thin layer of liquid over a sharp edge would infer a small value of r, and therefore a high internal pressure head of liquid is required for this kind of flow over the edge. (Fig. 6c) The profile of the bulk liquid on the plate is governed by surface tension and a large hydrostatic head is therefore inconsistent with a small radius of curvature at the edge. Therefore bulk liquid cannot flow over the edge until the edge drop increases in height to the point where the bulk liquid surface at the edge is vertical. One can infer then that the maximum height h_m of an edge drop of a wetting liquid is given by the height above the equator of a classical non-wetting sessile drop; that

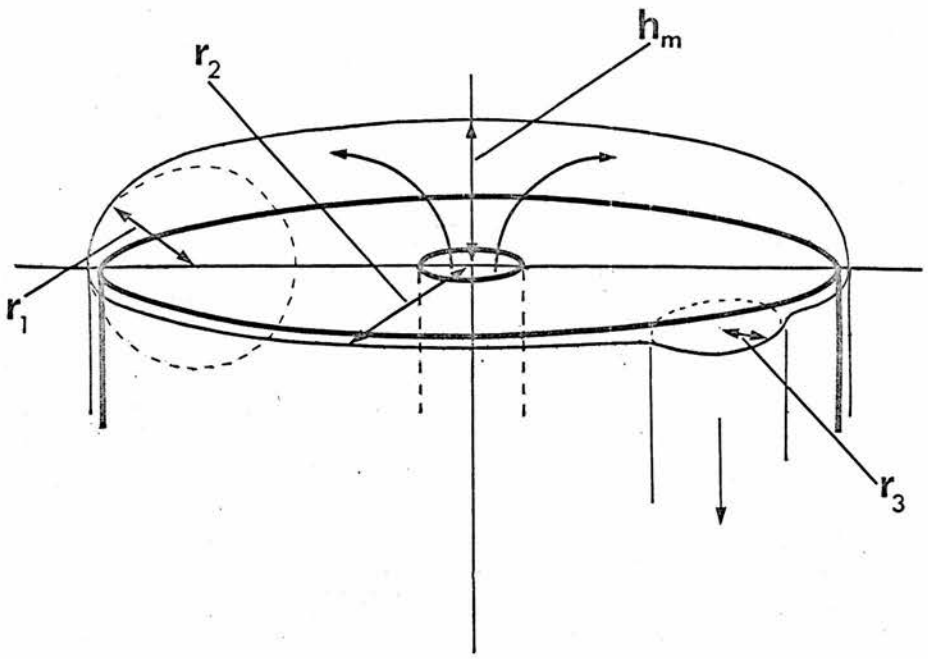

Fig. 7.

is, h_m is reached when the tangent to the edge drop profile at the edge is vertical. When this is so[51]

$$h_m = \left(\frac{2\sigma}{\rho g}\right)^{\frac{1}{2}} \qquad \text{---------- (10)}$$

Substituting the values for liquid helium $\sigma = 0.33$ ergs.cm^{-2} [52] and $\rho = 0.145$ grm.cm.$^{-3}$ gives $h_m = 0.68$ mm. in excellent agreement with the observed $h_m = 0.67$ mm. $\pm$ 0.05 mm.

Looking at the equilibrium conditions which hold for a flowing edge drop, the internal pressure at the edge of the drop must be almost equal to that just below the edge; and Laplace's formula holds

(Pressure at edge of drop) = (Pressure below edge of plate)

$$\sigma\left[\frac{1}{r_1} + \frac{1}{r_2}\right] = \frac{\sigma}{r_3} \qquad \text{---------- (11)}$$

where the radii of curvature are as shown in Fig. 7.

Since in this case r_1, r_2 and r_3 are all positive, it follows that r_2, the radius of curvature in the horizontal plane just above the edge of the drop, must be greater than r_3, the radius of curvature in the horizontal plane just below the edge of the drop. This condition cannot therefore, be satisfied by the liquid pouring uniformly over the whole perimeter surface, since this would give a liquid surface radius $\approx r_2$, but only by it pouring preferentially down one or more narrow columns or rivulets whose effective radii of curvature are given by r_3. This is illustrated in Fig. 7. Since this is the condition for the maximum height of drop h_m, any further supply of liquid to the drop will cause the columns or rivulets to adjust their size and number in order to cope with the increased flow. The same argument could be applied to the

filling of a beaker dipped into a liquid so that its rim was held at a depth $d \leq h_m$ below the surface of the liquid. Filling of the beaker by bulk liquid will be by rivulets which are convex towards the centre of the beaker and the horizontal radius of curvature of the rivulet surface will be greater than the inner radius of the beaker. This could account for the fast filling observed by Allen[2] under conditions when uncontrollable flooding of the beaker might have been expected.

Flow of Benzene over Talc

In order to confirm that the problem of the edge drop was a classical one and not limited to liquid helium, a replica of the circular flat plate was made from Talc (Soapstone.) Benzene was supplied to this plate by a central hole from a 'constant head' device. Benzene completely wets talc and, therefore, it was impossible to maintain a sessile drop on the plate away from the edge.

As soon as liquid flowed onto the plate an 'edge' drop formed which increased in height with the addition of more benzene, until the profile of the drop at the edge became vertical. At this point the drop height was a maximum h_m. A further small addition of benzene caused flow off the plate by a narrow rivulet, exactly as predicted by Laplaces equation, and the drop height fell. If benzene was then supplied to the plate at a rate in excess of the 'leakage' rate, the edge drop again increased in height until the original maximum height was reached, at which point a second rivulet formed on the vertical face of the rim of the plate. This sequence was repeated for increasing flow rates until benzene was pouring over the edge of

the plate in six or seven rivulets and flow instabilities occurred.

In order to measure the maximum height of the edge drop of benzene a special plate was constructed having a corrugated surface as shown.

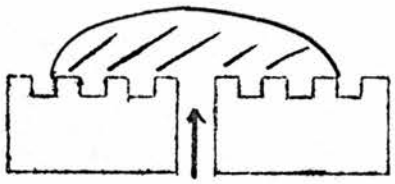

Fig. 8.

Benzene was supplied in a slow stream to this plate. As liquid reached each corrugation, the height of the drop increased until flow over that edge was initiated and the liquid surface would then drop suddenly. The drop height reached a maximum immediately before flow over one of these corrugations and, in this way, several readings for the maximum height of the edge drop were obtained.

The drop was viewed by a cathetometer. The value obtained for the maximum height of an edge drop of benzene was 2.6 ± 0.2 mm. in exact agreement with the value predicted by substituting the surface tension $\sigma = 26.9$ dynes/cm. and density $\rho = 0.88$ gm/cm^3 into equation 10. (P.27

CONCLUSION

In studying the radial flow of liquid helium II over a horizontal surface, it was found that for intermediate liquid supply rates and under isothermal conditions, a dynamic sessile drop could be maintained on the plate surface. This sessile drop, unlike those formed by classical non-wetting liquids, owed its existence to the special flow conditions/present on the plate and not to a finite contact angle. For large liquid supply rates a classical 'edge' drop was formed whose outermost tangent to the profile was vertical. Under non-isothermal conditions the liquid surface on the plate was disturbed by waves due to adiabatic oscillations of the central column of liquid.

by film and bulk liquid

Measurements of the thickness of the film and dynamic sessile drop on the plate should be very instructive. The results should give, in one experiment, a direct confirmation of the curve of transfer rate against liquid depth obtained by Atkins[3] from the results of many different experiments.

PART II

ION MOBILITY DISCONTINUITIES IN HELIUM II

INTRODUCTION

In 1962 Careri[1,5] reported observing periodic discontinuities in the drift velocity of ions in liquid helium for increasing field. He attributed these discontinuities to the creation of quantised vortex rings. At the first critical velocity a vortex ring of unit circulation is created and at subsequent discontinuities, rings with multiple units of circulation occur.

The work reported here had the following aims:-

(a) To prove the reproducibility of the discontinuities

(b) To elucidate the nature of the discontinuities by investigating their dependence on the available parameters

(c) To produce a theory which would predict the observed periodic discontinuities and explain the existence of the giant discontinuity at 28 m/sec., also observed by Careri[2].

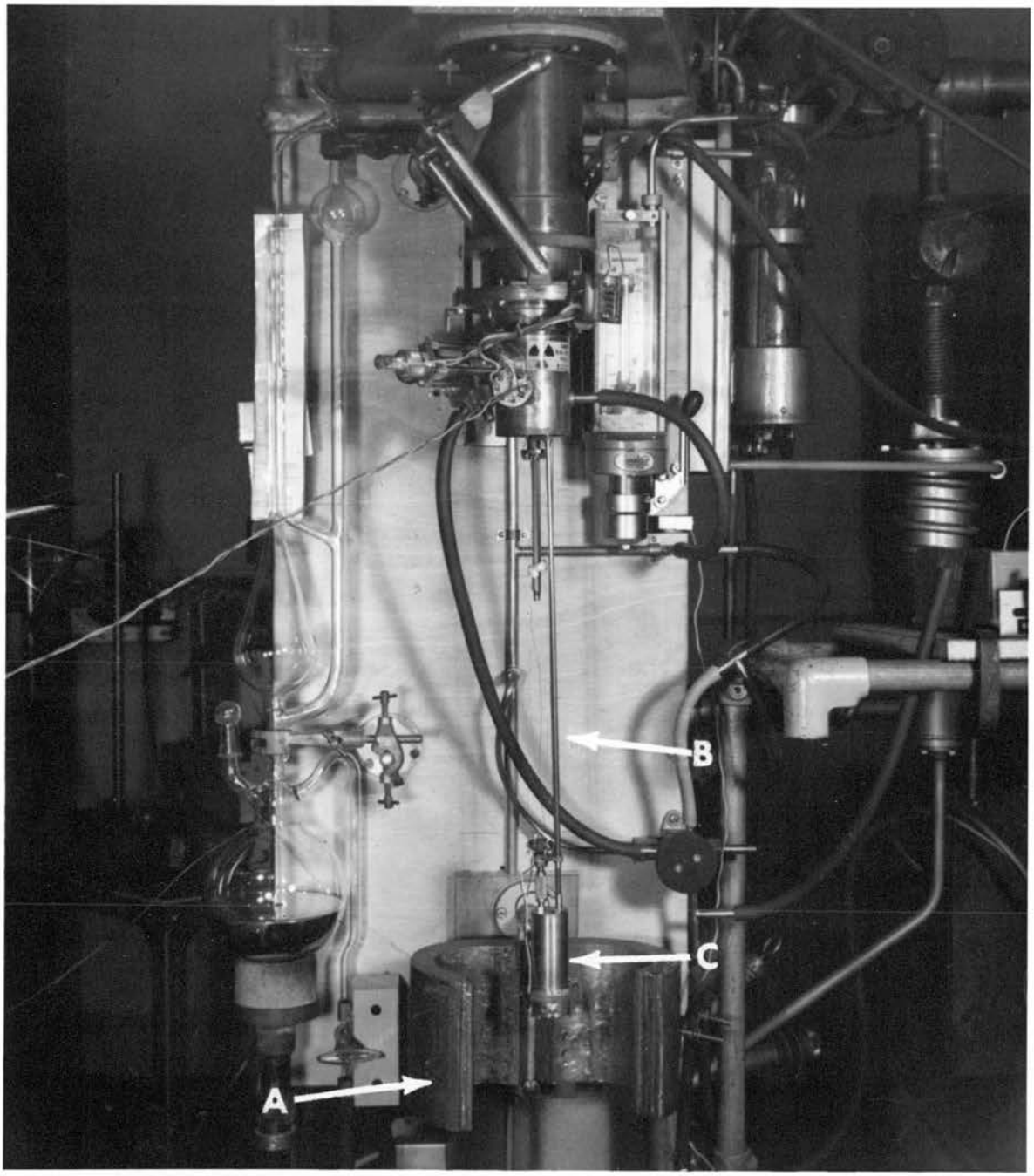

Cryostat for Ion Mobilities

(A) Lead Shield (B) Pumped Current Lead (C) Triode Cell

PLATE 1(a)

PLATE 1(b)

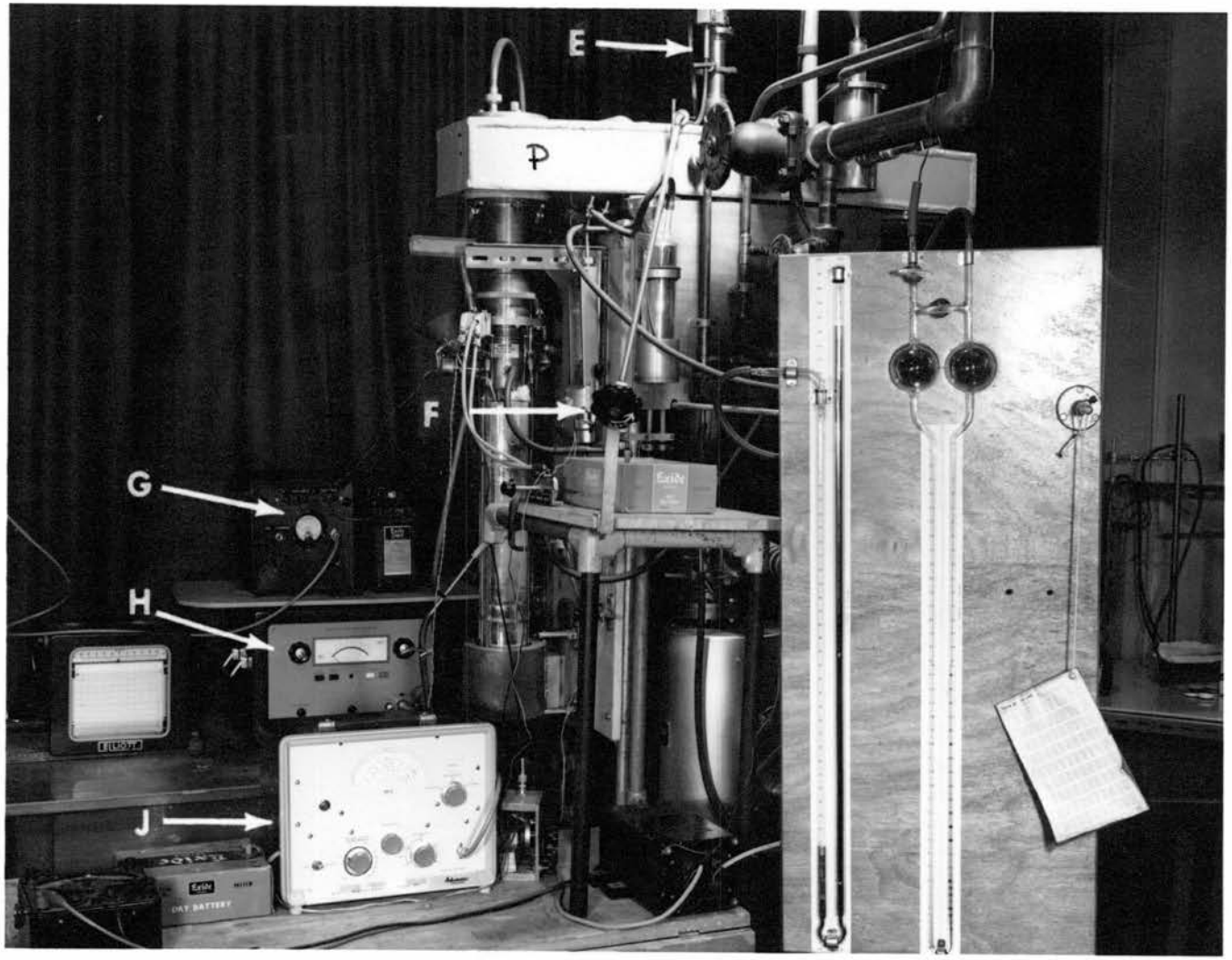

General Arrangement

(E) Fine Pressure Control Valve (F) Remote Control Knob for (E)

(G) Temperature Bridge (H) Electrometer (J) Square Wave Generator

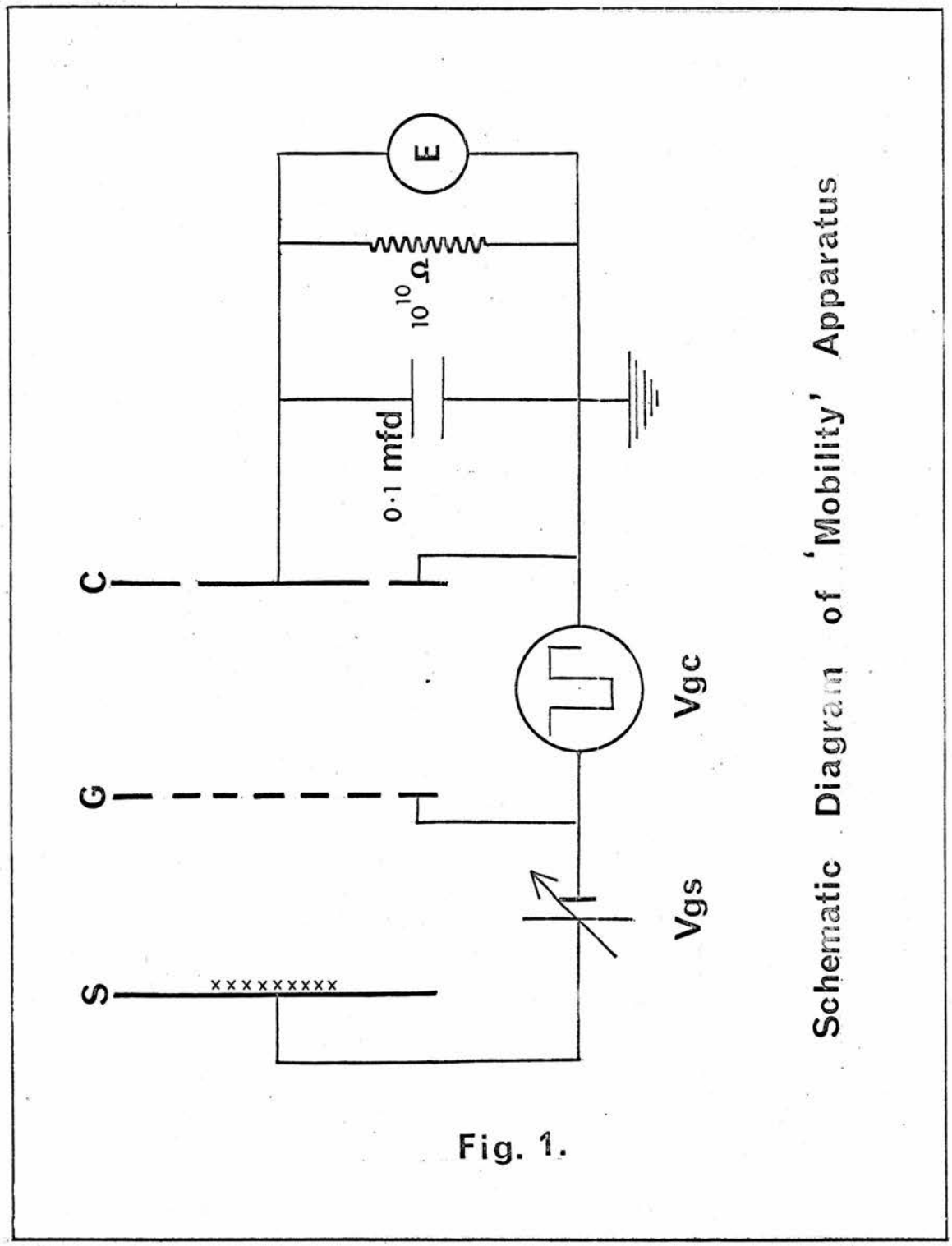

Schematic Diagram of 'Mobility' Apparatus

Fig. 1.

APPARATUS

Fig. 1 shows the arrangement of the eletrical components.

Ions are produced by the radioactive source S and those of the appropriate polarity move towards the grid G in the steady electrical field produced by battery V_{gs}. SG is called hereafter, the 'grid-source' space. The square wave generator V_{gc}, provides an alternating field between the grid and collector C. Ions will move towards the collector during one half cycle of the square wave and return to the grid in the other. For certain values of field and square wave frequency, the ions will be able to reach C where they will be collected and recorded by the electrometer E. As the frequency of the square wave is increased, the number of ions able to reach C is diminished and so the current recorded will decrease. The current arriving at the collector and recorded by the electrometer is given by

$$i = \left(\frac{1}{2} - \frac{d_o \gamma}{\mu E}\right) i_o \qquad \text{----------} \qquad (1)$$

For derivation of equation (1) see Appendix 1.

where i_o = ion current for constant field across the measuring space

= ion current passing through the grid

d_o = grid-collector spacing

γ = applied square wave frequency

μ = ion mobility

E = applied field

Fig. 2.

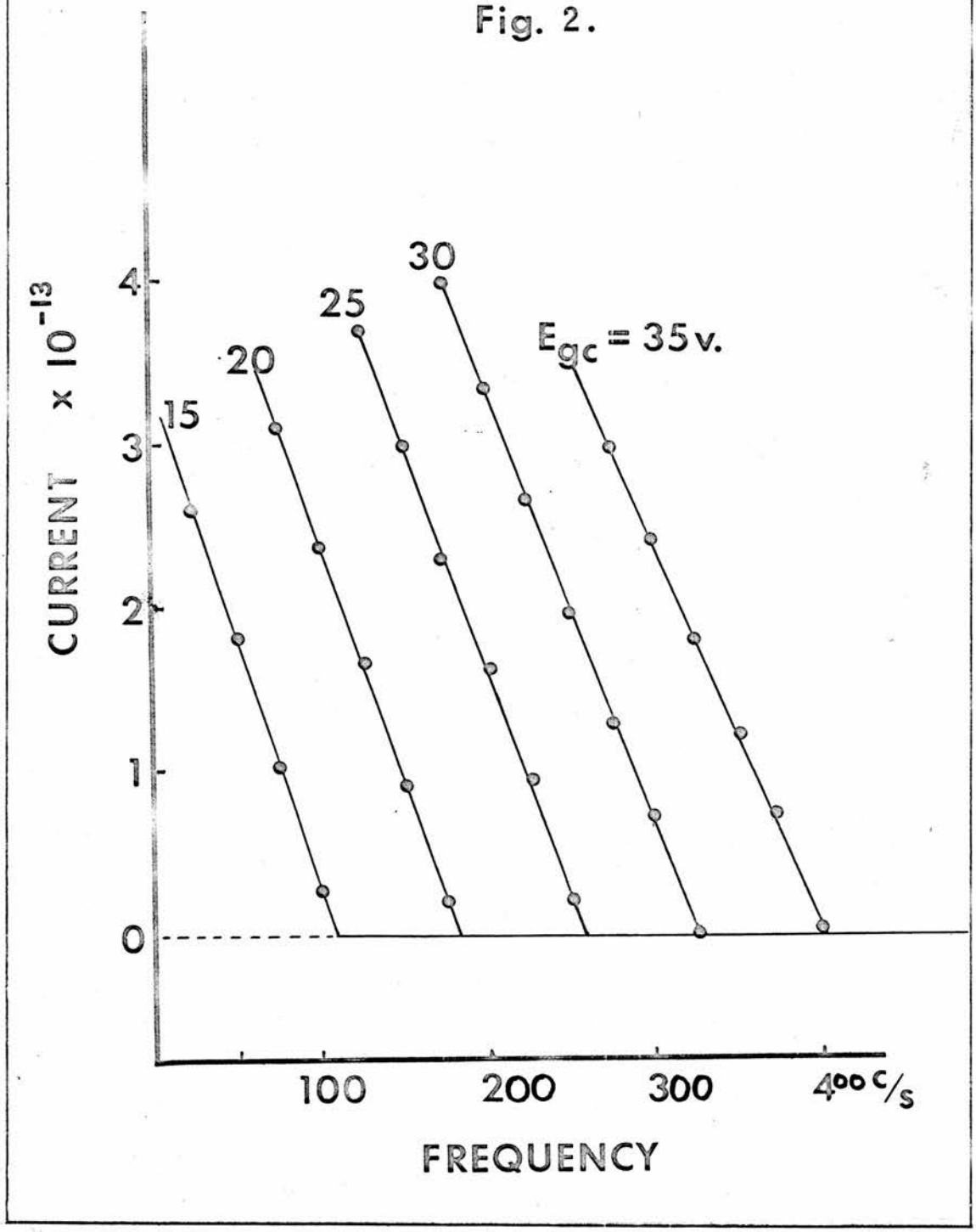
CURRENT x 10^{-13}
4
3
2
1
0
15
20
25
30
E_{gc} = 35 v.
100
200
300
400 c/s
FREQUENCY

When $\frac{d_o \gamma_c}{\mu E} = \frac{1}{2}$, i = 0 and γ_c is the cut-off frequency.

For higher applied frequencies, the current remains zero and does not become negative, since a negative current is meaningless in this context. Fig. 2 shows a typical set of observations of current for increasing frequency at different grid-collector fields E_{gc}.

The current collected will become zero for a given field when the frequency of the applied square wave is sufficiently high that ions cannot traverse the grid collector space in one 'forward' half cycle. With known distance between grid and collector, the frequency at which current reaches zero, henceforth called the 'cut-off frequency', gives the velocity of the ion,

$$\mu E = v = 2\gamma_c d_o$$

The grid collector space is sometimes referred to as the 'measuring space' since it is in this region only that the velocity of the ions is investigated.

The actual apparatus was set up as shown in Plate 1, and connected to an Edwards B9A Booster Pump by means of the large pumping box P. A temperature of 1.3°K could be obtained using the backing pump only. For temperatures between 1.3°K and 0.85°K, the Booster was employed and controlled by the fine control valve E.

Consider now the individual units separately.

1. The 'Triode' Cell (Fig. 3, Plate 2)

The electrodes were silver or silver plated and separated by 'perspex' spacers.

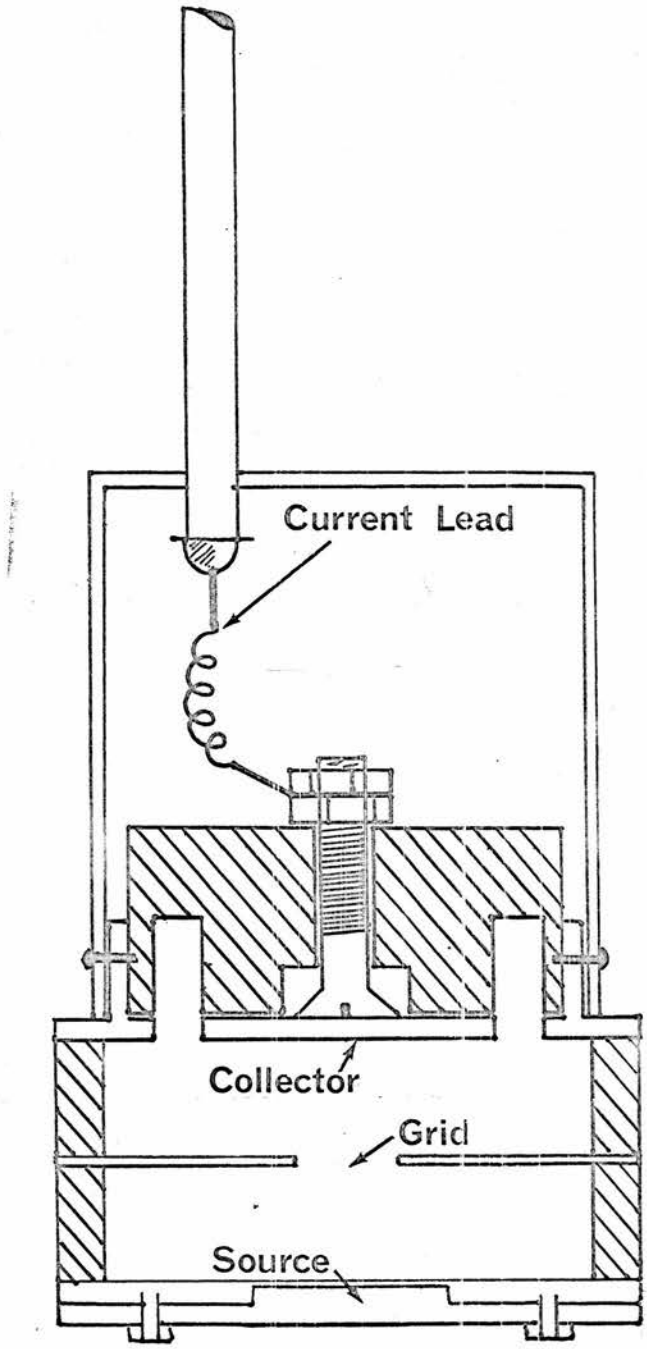

FIG. 3.

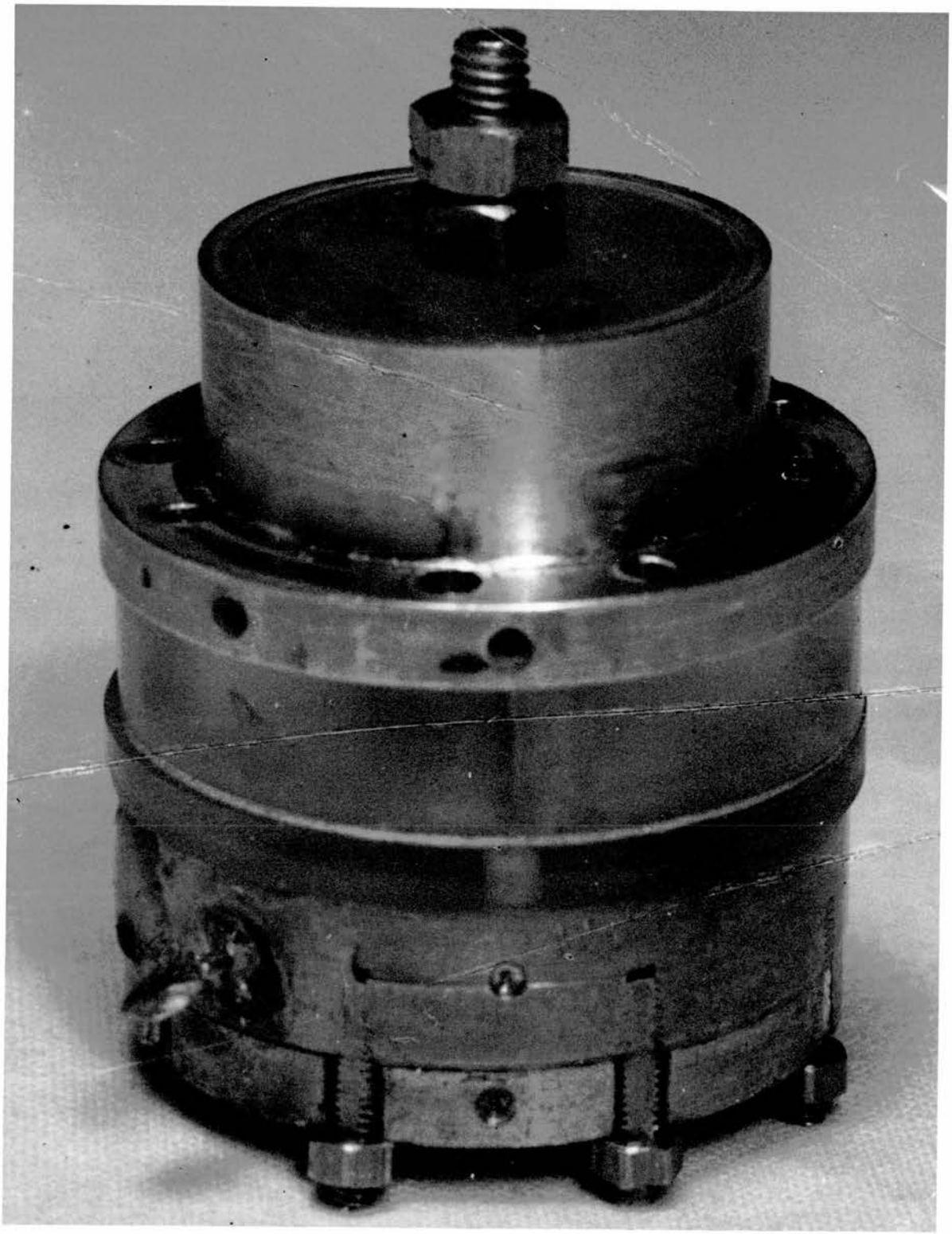

The 'Triode' Cell

PLATE 2

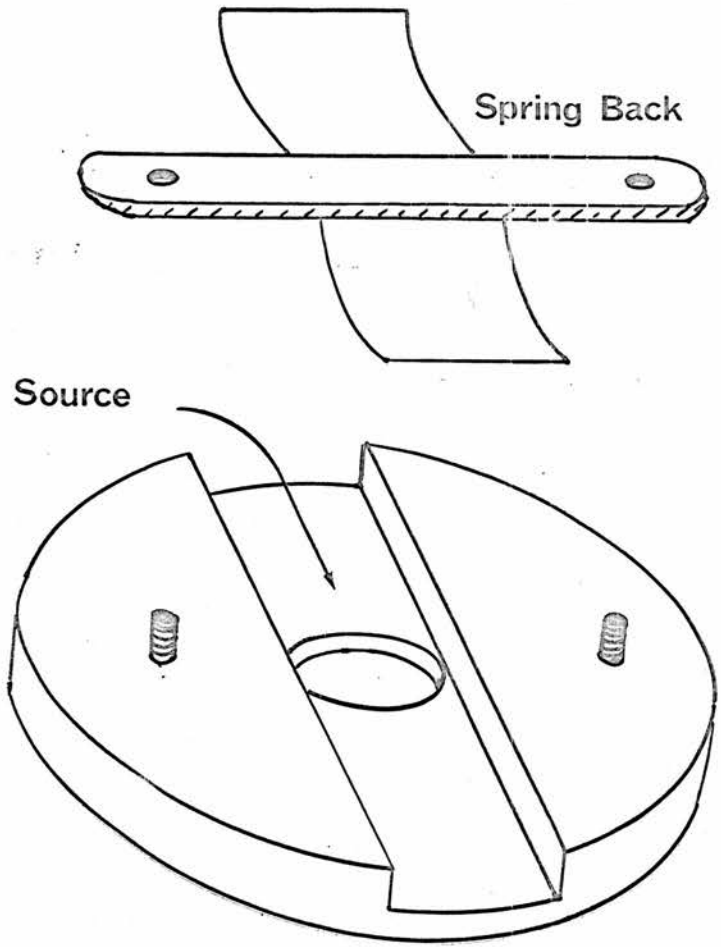

FIG. 4.

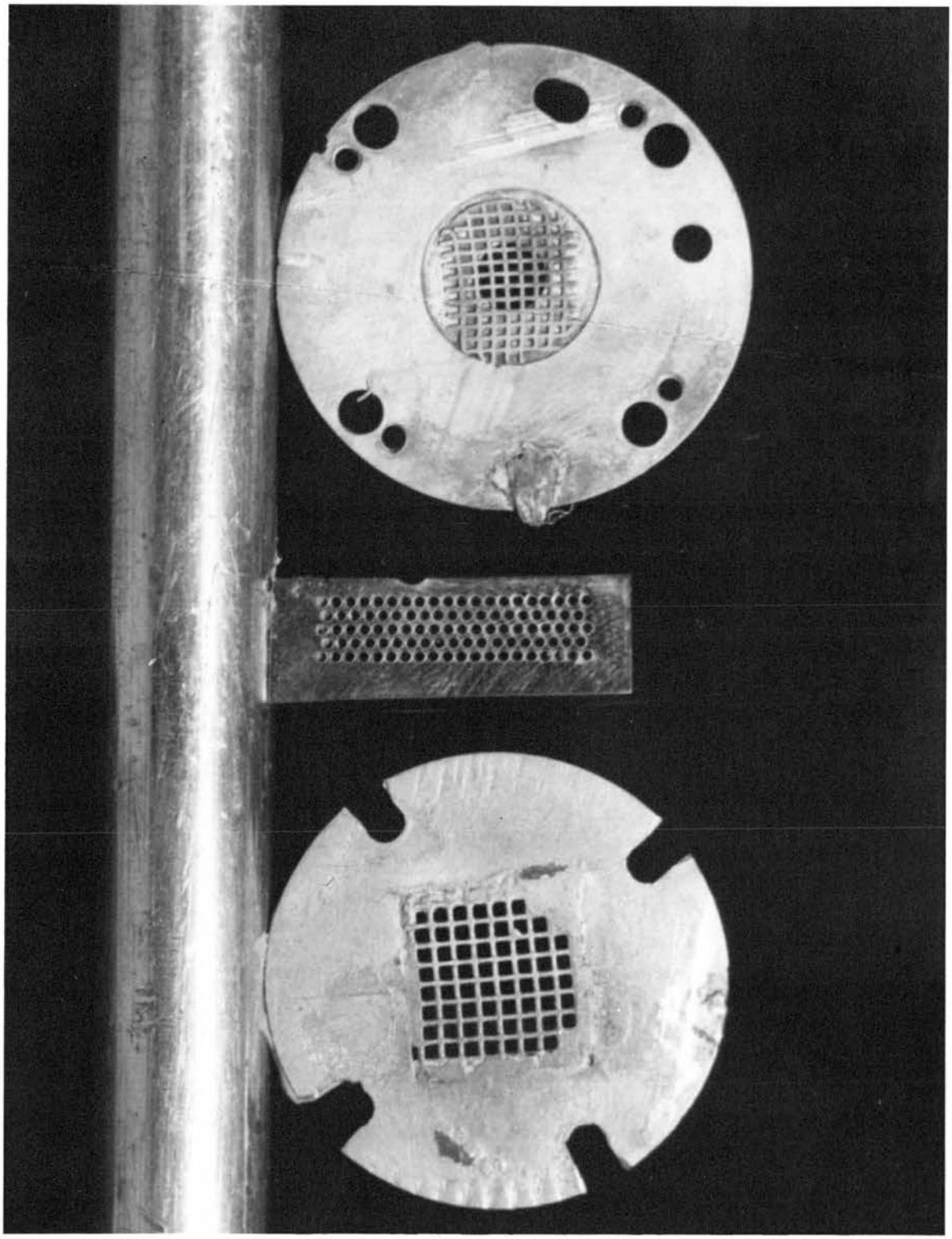

Types of Grid Used

PLATE 3

(a) The Source

The source material eventually chosen was Americium 241. This was supplied by the 'Radio Chemical Centre' Amersham, in the form of a thinly coated silver foil. The strength of this source was 100 microcuries. The advantage of these ready made sources is that they have a protective layer of silver electrodeposited on top of the radioactive layer, which greatly reduces the risk of contamination during use. A 10 microcurie Po 210 source, from the same supplier, was tried first but found to be of insufficient strength. Consultation with the Radiochemical Centre revealed that the stated strength related to the actual quantity of radioactive material deposited on the foil and, even though this was deposited as a thin layer, considerable absorption takes place. Consequently the emission of α-particles was considerably less than anticipated.

Americium 241 emits α-particles of energy ~ 5.4 MeV and a small amount of low energy gamma rays. The radiation hazard from the gamma emission is almost negligible but, as an extra precaution, a 1" thick lead sleeve was made to fit the appropriate part of the dewar A. Outside this shield the radiation was undetectable. (i.e. $\leq$ background count.)

The source holder (Fig. 4) was constructed so as to facilitate rapid mounting and demounting of the radioactive foil.

(b) The Grid (Plate 3)

A very thin flat grid was desired. Thin (.010") copper sheeting was drilled with a regular array of holes, each 0.8 mm. diameter, (Example B.) separated by ≈ 1.5 mm. between hole centres. A circle of this drilled sheet was then soldered over the

hole at the centre of a circular brass plate 0.7 mm. thick. The total diameter of the perforated grid was 8 mm. This grid behaved perfectly well for the majority of the experiments, even though its open area = 0.10 cm^2 was only 20% of the total grid area. An improvement was obtained by making the grid from fine brass wire mesh which was cold rolled until only (.010") thick. (Examples A & C.) In this way a grid with rectangular holes was obtained whose open area/was = 0.14 cm^2 ~30% of the total area. This second grid allowed more ions through, therefore higher currents were recorded and greater accuracy achieved. (See Appendix 2)

The source holder and the grids were silver plated in order to reduce the effects of surface resistance.

(c) The Collector (Fig. 3)

The collecting electrode was made of solid silver soldered onto a brass bolt which held the electrode in place on a perspex base and acted as conductor for the current. The surface of the silver plate was lapped flat and polished with jewellers rouge. The collector diameter 12 mm. was greater than the diameter of the grid 8 mm, in order to ensure collection of all the ion beam.

A guard ring was mounted round the collector in order to maintain a uniform field in the measuring space.

The input resistance to the electrometer was $10^{10}\Omega$, consequently the leakage resistance between the current lead and earth had to be maintained above $5 \times 10^{12}\Omega$, otherwise a significant amount of the current would not pass through the electrometer at all.

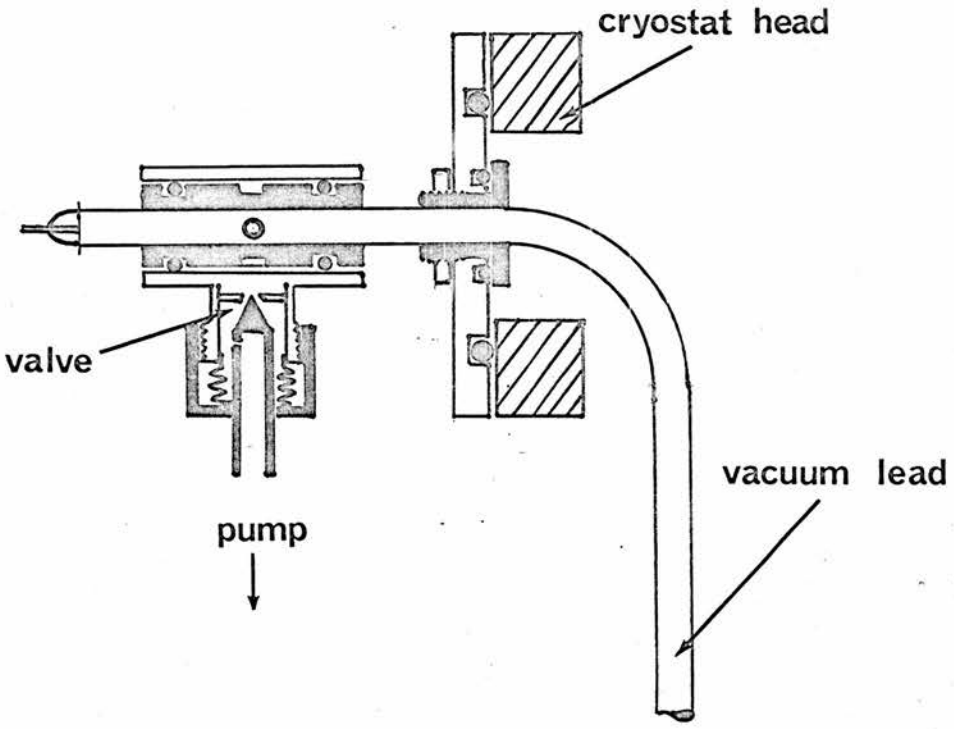

Fig. 5.

The guard ring was separated from the collector by a 'moat' cut out of the perspex base. This groove ensured a long surface leakage path between the collector and guard ring and thus helped to prevent the loss of the ionic current to earth. The inaccessibility of the groove also prevented accidental contamination of the surface with greasy fingers.

2. The Current Lead

Ions arriving at the collector passed through it, up the brass bolt into the shield can, through a short lead to the centre shaft on a Kovar seal, and thence up the pumped coaxial line to the outside of the cryostat head. The coaxial line was constructed of 4 mm. O.D. stainless steel tubing containing a 40 gauge copper wire. The wire was insulated from the walls by passing it through the centre of a length of cellular polyethylene tubing. It was essential for reasons mentioned above, that this insulation remained absolutely dry and greaseless and, therefore, great care was necessary in constructing the leads. Six attempts were made before a lead of sufficiently high insulation was obtained. The ends of the coaxial lead were closed by Kovar seals. The lead, pumped nearly continuously to maintain good conditions, was connected via the valve illustrated in Fig. 5, to a small backing pump. The lead passed through a perspex window in the cryostat head to keep it isolated electrically from the rest of the system.

All insulation measurements were performed using a 'Norma Teraohmmeter' which was capable of detecting leak resistances of the

order of 10^{14} ohms.

Potential to the grid was supplied through an identical coaxial lead.

All other leads were unshielded 40 gauge copper wires.

Once a good earth was found, the system showed very little external pick-up.

A flexible coaxial line fed the signal from the cryostat head to the electrometer input.

3. High Frequency Filter

A large condenser (0.1 μF) was connected between the current lead and earth. This effectively filtered out any undesirable high frequency pick-up and increased the time constant of the electrometer circuit so that the meter reading was automatically an averaged value of the current received over approximately 1 second.

This filter had to have the same high insulation standards required by the rest of the electrometer input circuit. The condenser which had to be of a high quality, was mounted in a metal can fitted with a coaxial socket. The interior of the can was kept dry by the insertion of silica gel dessicant.

4. The Electrometer

This was a vibrating reed, Wayne Kerr precision electrometer. An adaptor on the input containing a high resistance converted the current to an appropriate voltage which the electrometer itself then indicated. Four ranges on the meter, and three alternative input resistors, gave a range of measurable currents from 10^{-8} - 10^{-15} amps for full scale

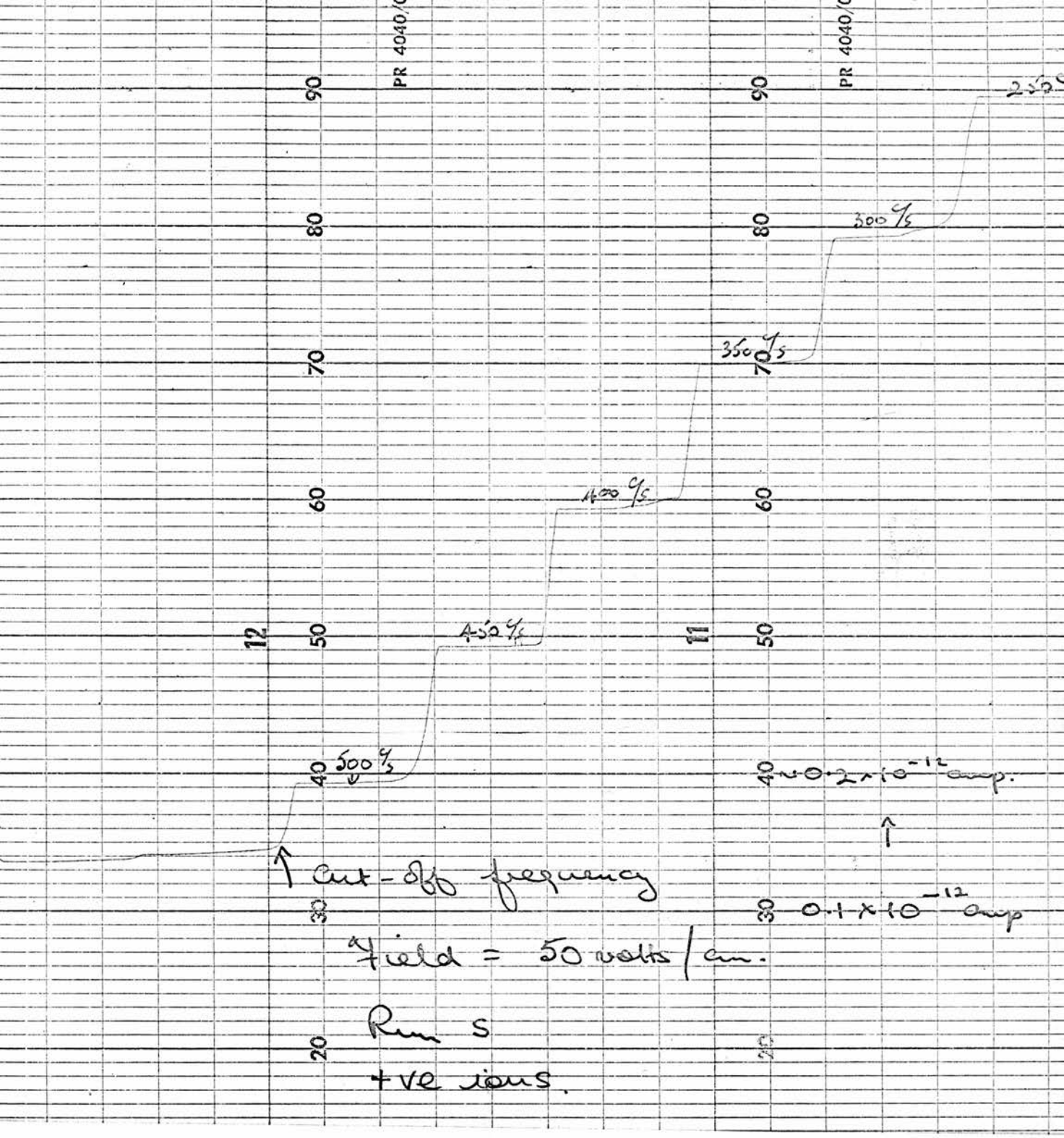
PR 4040/0
90
80
70
60
50
40
30
20
12
11
500 V/s
450 V/s
400 V/s
350 V/s
300 V/s
~0·2×10⁻¹² amp.
0·1×10⁻¹² amp
↑ cut-off frequency
Field = 50 volts/cm.
Rm s
+ve ions.

Fig. 6.

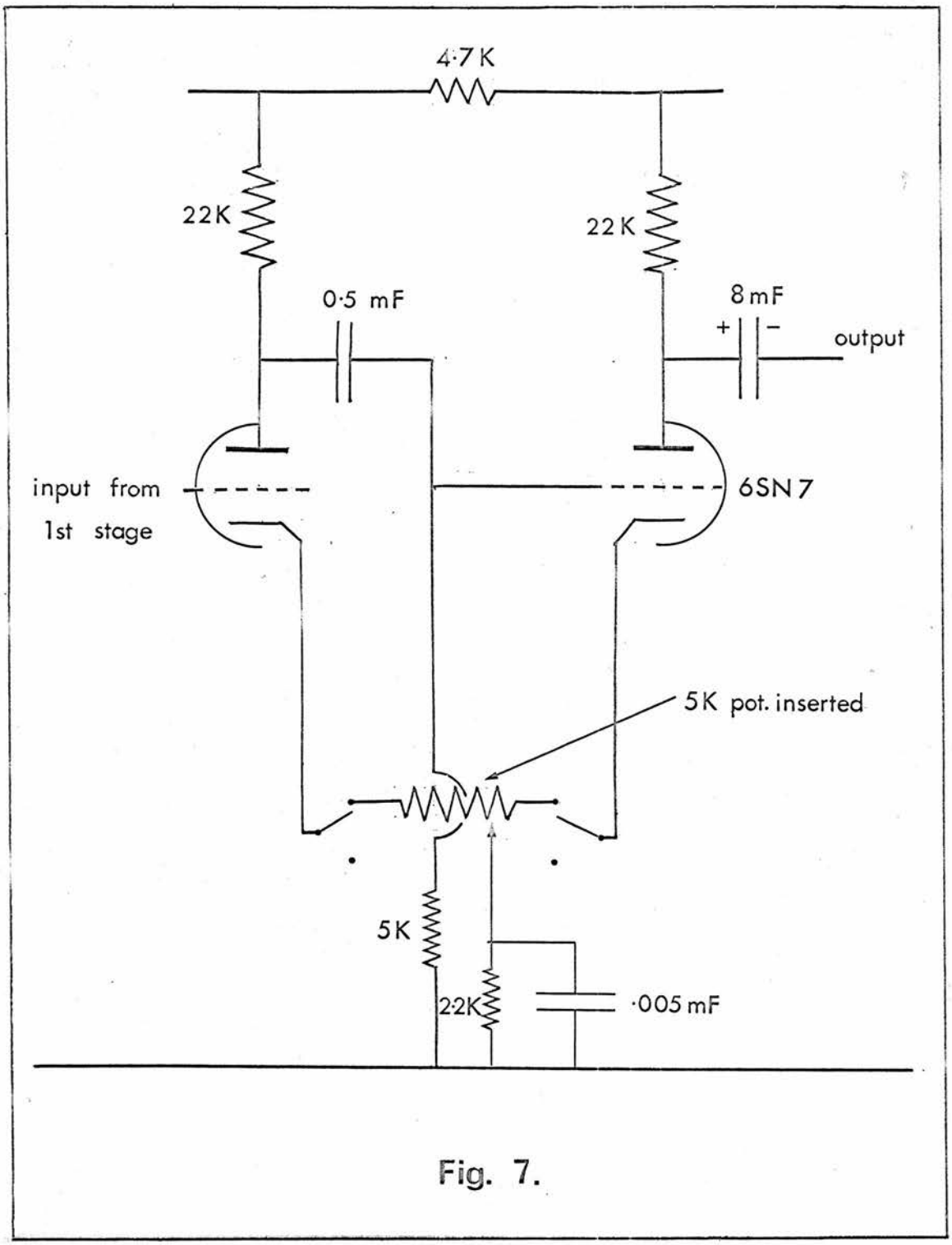
4·7 K
22K
22 K
0·5 mF
8 mF
+
−
output
input from
1st stage
6SN7
5K pot. inserted
5K
22K
·005 mF

Fig. 7.

deflection. The input resistors were $10^8\Omega$, $10^{10}\Omega$, and $10^{12}\Omega$. With the $10^8\Omega$ resistor in the input, there was insufficient sensitivity, but with $10^{12}\Omega$ in place, there was insufficient stability since it was difficult to maintain the insulation much better than $10^{12}\Omega$. For these reasons most of the measurements were performed using a $10^{10}\Omega$ resistance in the input circuit. The electrometer had a pen-recorder output, which was utilised occasionally in conjunction with a Honeywell-Brown Pen Recorder; this was of limited use however, since direct readings, for which there was adequate time, were far more accurate. A typical recorder plot of current against time is shown in Fig. 6.

5. Square Wave Generator

This was a Model H1 Low Frequency Signal Generator. The experiment required a square wave having one pulse longer than the other. The reverse pulse was made 10% longer in order to 'clean' out the grid-collector space between forward pulses. Ions left in the measuring space after a forward pulse would blurr the cut-off frequency. In order to obtain unequal pulse lengths, the above generator was modified as shown in Fig. 7. The insertion of a 5K potentiometer in the cathode circuits of valve V2 unbalanced the time constants of the two resonant circuits. In this way it was possible to make either pulse up to 10% longer than the other.

6. Temperature Measurements

(a) Conventional oil differential and mercury manometers indicated the approximate pressure and hence temperature in the cryostat.

(b) A McLeod Gauge was designed and made to cover the range of pressures most frequently encountered in the ion experiments, that is from 10^{-1} to 10^{-2} mm.Hg. With this, the pressure could be read with an accuracy of $\pm$ 10^{-3} mm.Hg. which corresponds to an uncertainty in temperature of $\pm$ 3 millidegrees at 0.85°K. The McLeod Gauge was connected to a long

stainless steel tube which was inserted via two 'O' ring seals through the cryostat head. This could be adjusted so that its tip was just above the liquid surface. After suitable corrections for the length of the tube, an absolute measure of the helium temperature was obtained. The method, however, was cumbersome and lengthy and so it was used only to calibrate a carbon resistance thermometer which was used as the primary method of temperature measurement.

Carbon Resistance Thermometer

A 50Ω standard Allen-Bradley carbon resistor was mounted below the triode cell in the cryostat. The resistance was measured by a standard bridge network. The ratio arm of the bridge was carefully made using constantan wire for both sections in order to eliminate drift due to temperature fluctuations. The variable resistor was surrounded by a large mass of copper and the whole bridge mounted in a thermally insulated box. A fixed resistor was included in the circuit which could be substituted for the carbon thermometer at any time to check the operation of the bridge. The bridge output was to a sensitive galvanometer. Movement of the galvanometer needle was amplified by an optical lever system. Light from the galvanometer mirror was reflected from a fixed mirror ~1 ft. away and the final image appeared on a screen ~18 ft. away. The sensitivity obtained in this way was as high as 20 cm/millidegree.

Calibration

The carbon resistance thermometer was calibrated by measuring its resistance and the helium vapour pressure at frequent intervals during

the process of cooling below 4.2°K. Pressure measurement became unreliable as a temperature indicator below 1°K, therefore the extrapolation of the resistance temperature curves for the carbon thermometer was used instead.

7. Temperature Control

It was necessary to maintain the temperature constant to within at least a millidegree. At 0.95°K, $\frac{\Delta\mu}{\Delta T} \approx 100$ cm^2/volt.sec./°K. ∴ a change of one millidegree would give a 1% change in mobility. We are looking for changes in mobility of ≈ 6 - 7%. (See also P.58)

The normal heat leak to the helium was ≈ 10 mW, which meant that the Booster Pump was theoretically capable of maintaining a temperature of ≈ 0.85°K. The pumping speed of the Booster Pump was controlled by a fine control baffle valve; if this valve was open a constant amount during one run, the temperature would gradually fall as the run progressed, because as the helium level in the dewar fell, so the heat leak to the liquid would be reduced. The change in temperature was indicated by the galvanometer spot as described in the previous section. To maintain a constant temperature the fine control valve was carefully adjusted so as to maintain a galvanometer spot in one place throughout the run. Temperature drift was usually about 2-3 millidegrees per hour, consequently fine control valve adjustments were quite adequate in controlling the temperature within the desired limits. Occasionally, when for instance the liquid level was falling past the top of the can, a rapid temperature change occurred; results taken during this change were usually discarded.

An attempt was made at producing an automatic temperature control. The galvanometer spot was made to fall on one of two photocells which,

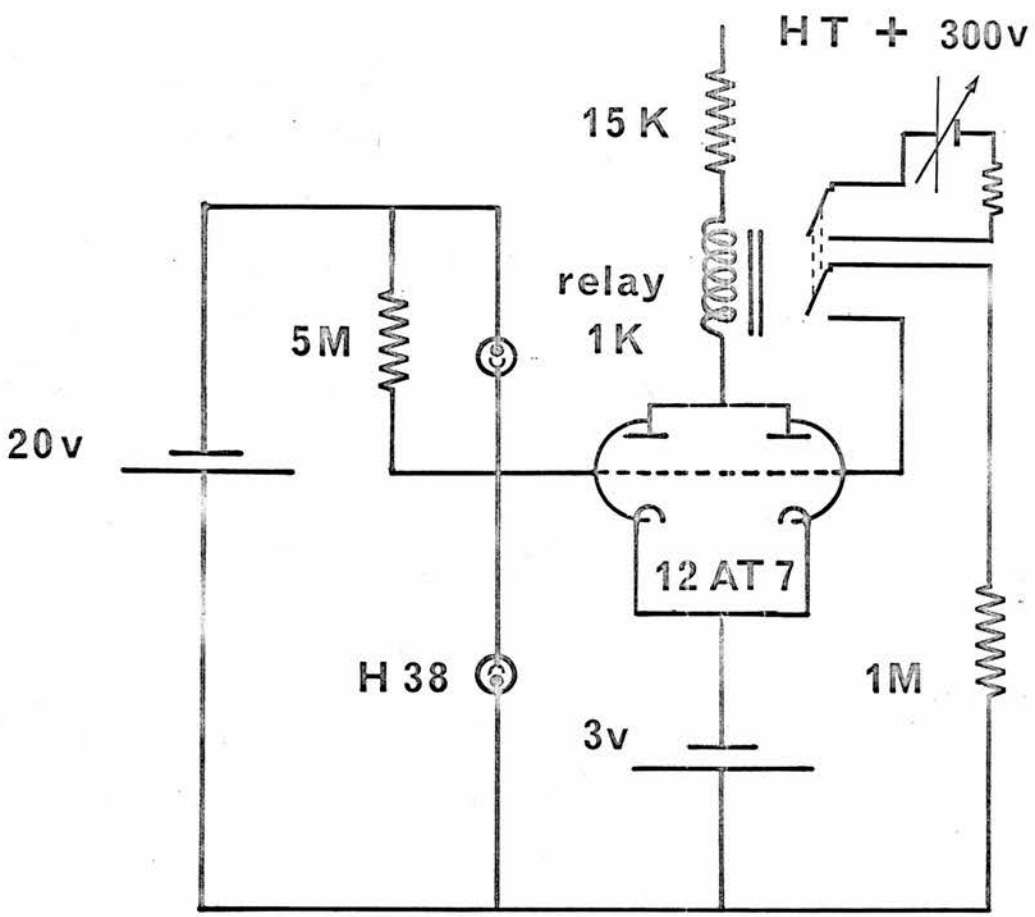

Temperature Control Circuit

FIG. 8.

by means of a simple relay circuit (Fig. 8), switched on or off a small heater in the helium. The method was found unsuitable because small heat inputs were easily accommodated by the pump; large heat inputs produced large temperature fluctuations because the time constant of the heating system was longer than that for the control circuit. In other words, even though the heater was switched off automatically, the temperature still continued to rise until the heater system had dissipated all its heat and until the pump could reduce the pressure in the cryostat to its original value.

Control by the needle valve was quite satisfactory so the technique of automatic control was not pursued further.

8 Telescope

The electrometer and its input circuit, despite good earthing, remained sensitive to people moving near it. The effect was small but to improve results, the electrometer dial was read through a telescope at a distance of ~6 ft. This ensured remoteness and also constant angle of view of the electrometer needle.

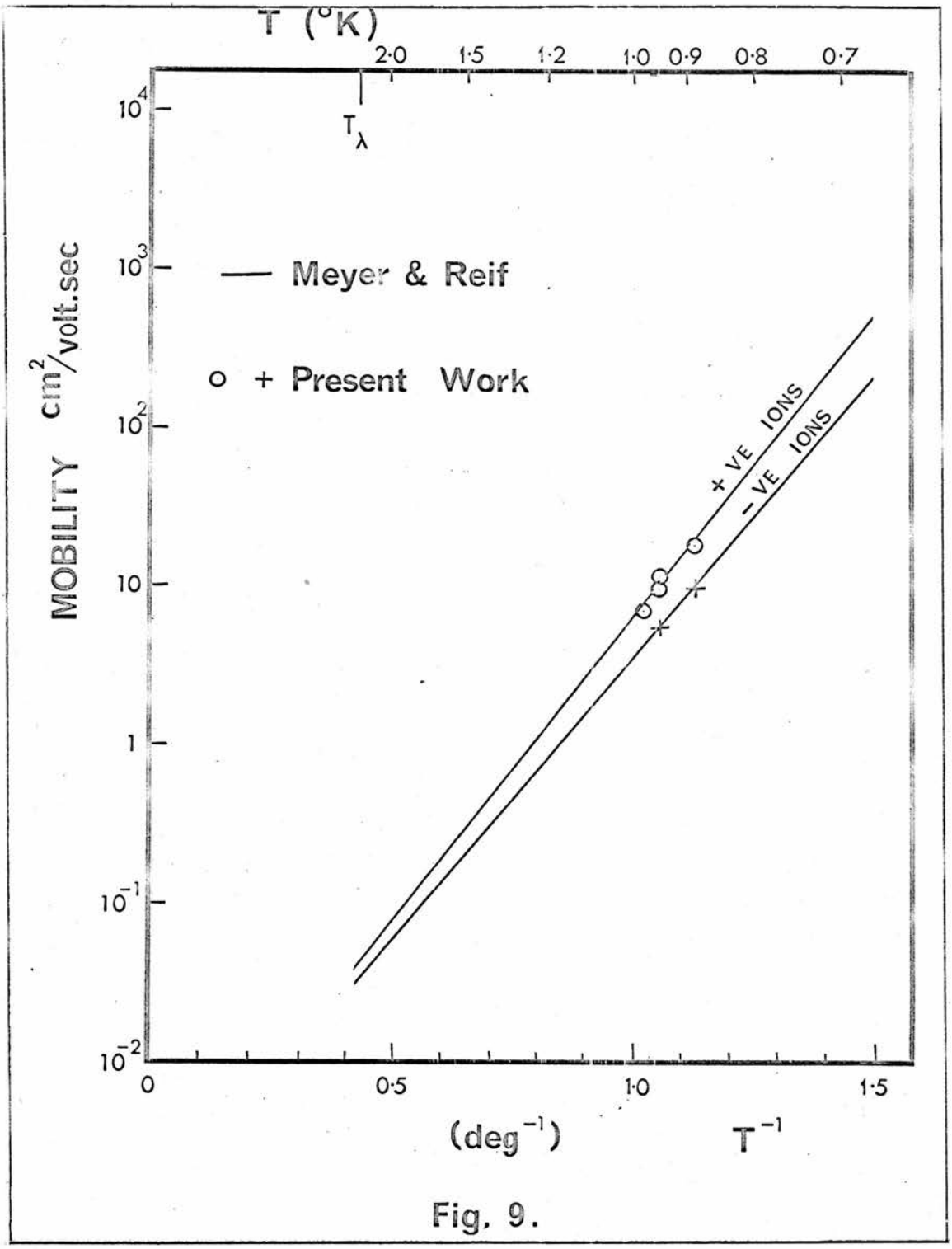
T (°K)
2·0
1·5
1·2
1·0
0·9
0·8
0·7
T_λ
10^4
10^3
10^2
10
1
10^{-1}
10^{-2}
MOBILITY $cm^2/volt.sec$
— Meyer & Reif
o + Present Work
+ VE IONS
– VE IONS
0
0·5
1·0
1·5
(deg^{-1})
T^{-1}

Fig. 9.

$T^{\circ}K$	$\frac{1}{T}$	μ $(cm^2 volt^{-1} sec.^{-1})$
	Positive Ions	
0.968 ± 0.005	1.032	8.31 ± 0.02
0.955	1.048	9.33 ± 0.03
0.953	1.050	9.35
0.931	1.074	11.21
0.928	1.078	11.7
0.921	1.087	12.73
0.918	1.089	14.65
0.915	1.092	16.00
0.94	1.063	12.2 ± 0.5
0.885	1.13	20.3
	Negative Ions	
0.94	1.063	5.9 ± 0.4
0.885	1.13	8.7

Values of Mobility at Different Temperatures Close to $1^{\circ}K$

TABLE I

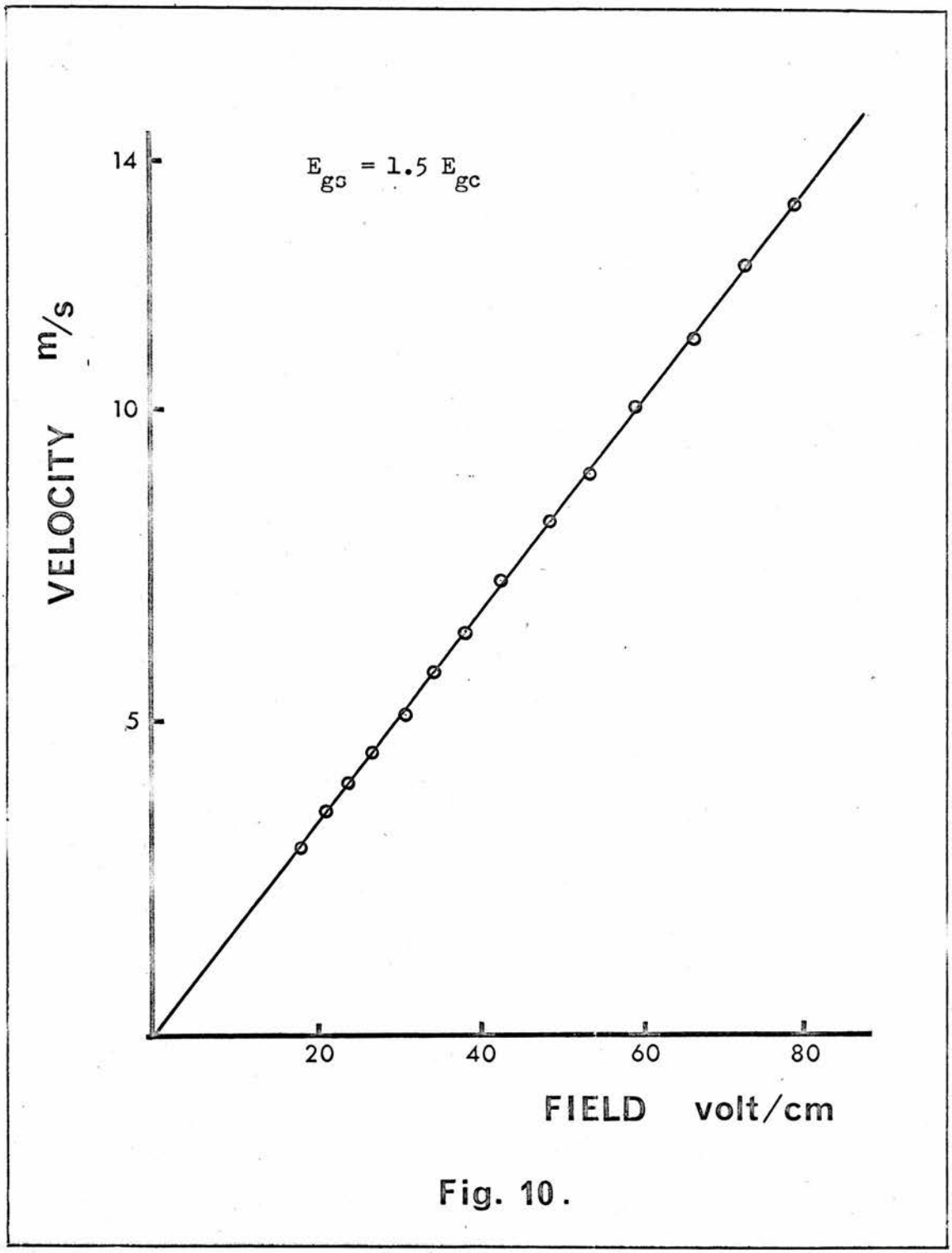

Fig. 10.

N.B. A discontinuity ≤ 2% would not be seen in these velocity field curves

RESULTS

Absolute Value of Mobility

Although not important to the present series of experiments, a few mobility determinations were made at measured temperatures and found to be consistent with the values obtained by previous authors; Meyer and Reif[3], Careri, Cunsolo and Dupre.[4] Table I shows the results from one run in which the temperature was deliberately varied while the applied field $E < E_c^*$ was kept constant. Some of these values are plotted on a graph of μ against $\frac{1}{T}$ and compared with Meyer and Reif's curves, (Fig. 9). The discontinuities were best seen in the very narrow temperature range 0.9 - 1.0°K, consequently, mobility measurements were restricted to this region.

Early Attempts at Observing the Critical Velocity

Variation of Grid-Source Field.

The author performed very many runs before ever observing a discontinuity in the drift velocity of positive ions at ~5 m/sec.

A typical run, showing complete linearity of the velocity-field curves, is shown in Fig. 10. The absence of the discontinuity is shown below to be entirely due to the mode of operation of the cell, in particular the setting of the grid-source field E_{gs}. It seemed reasonable to operate the cell such that E_{gs} should be varied simultaneously with E_{gc}, such that for all measurements $E_{gs} \geq E_{gc}$. This arrangement assured a large ion current emerging from the grid.

---

* E_c = Field at the first discontinuity.

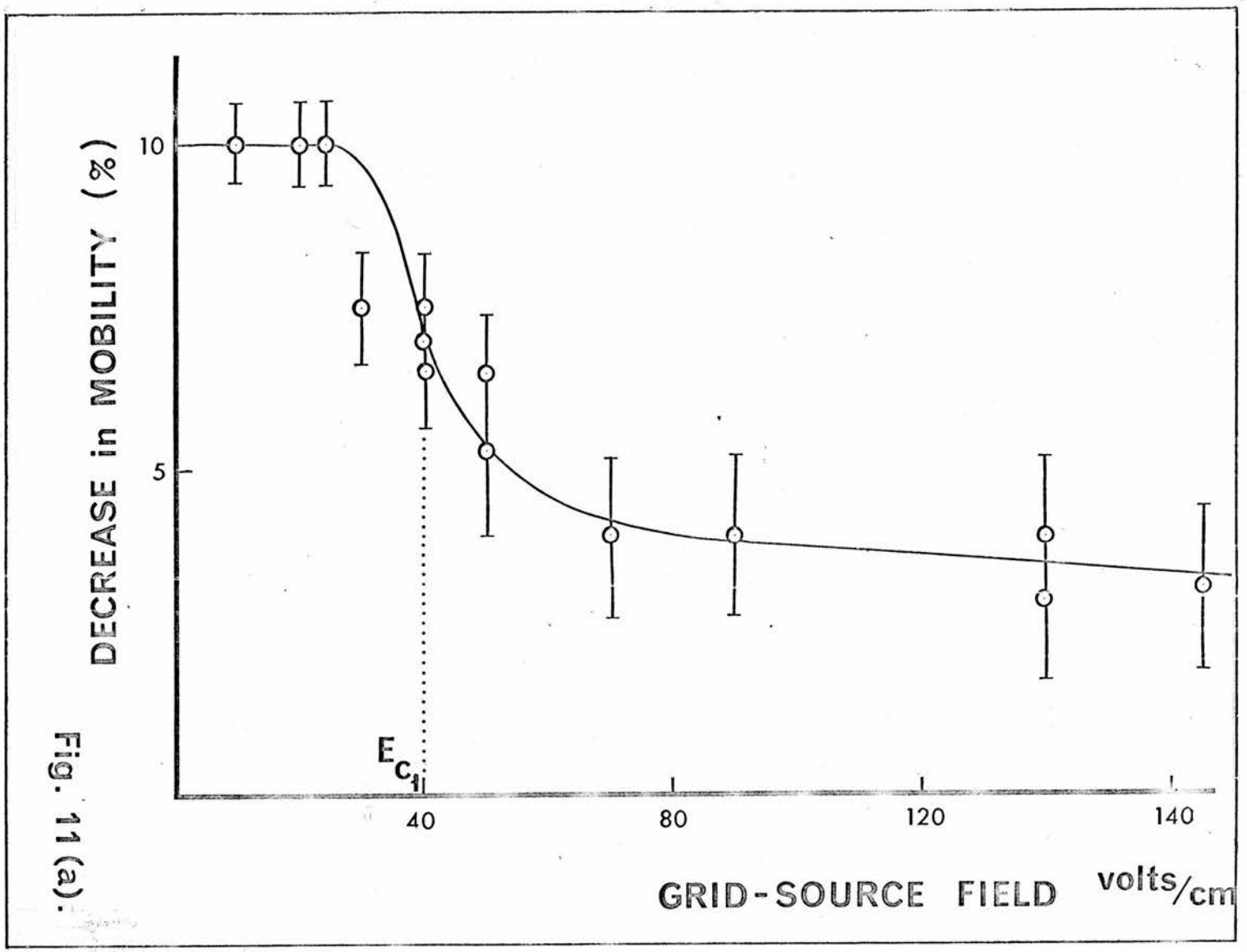
DECREASE in MOBILITY (%)
10
5
E_{c_1}
40
80
120
140
GRID-SOURCE FIELD volts/cm

Fig. 11 (a).

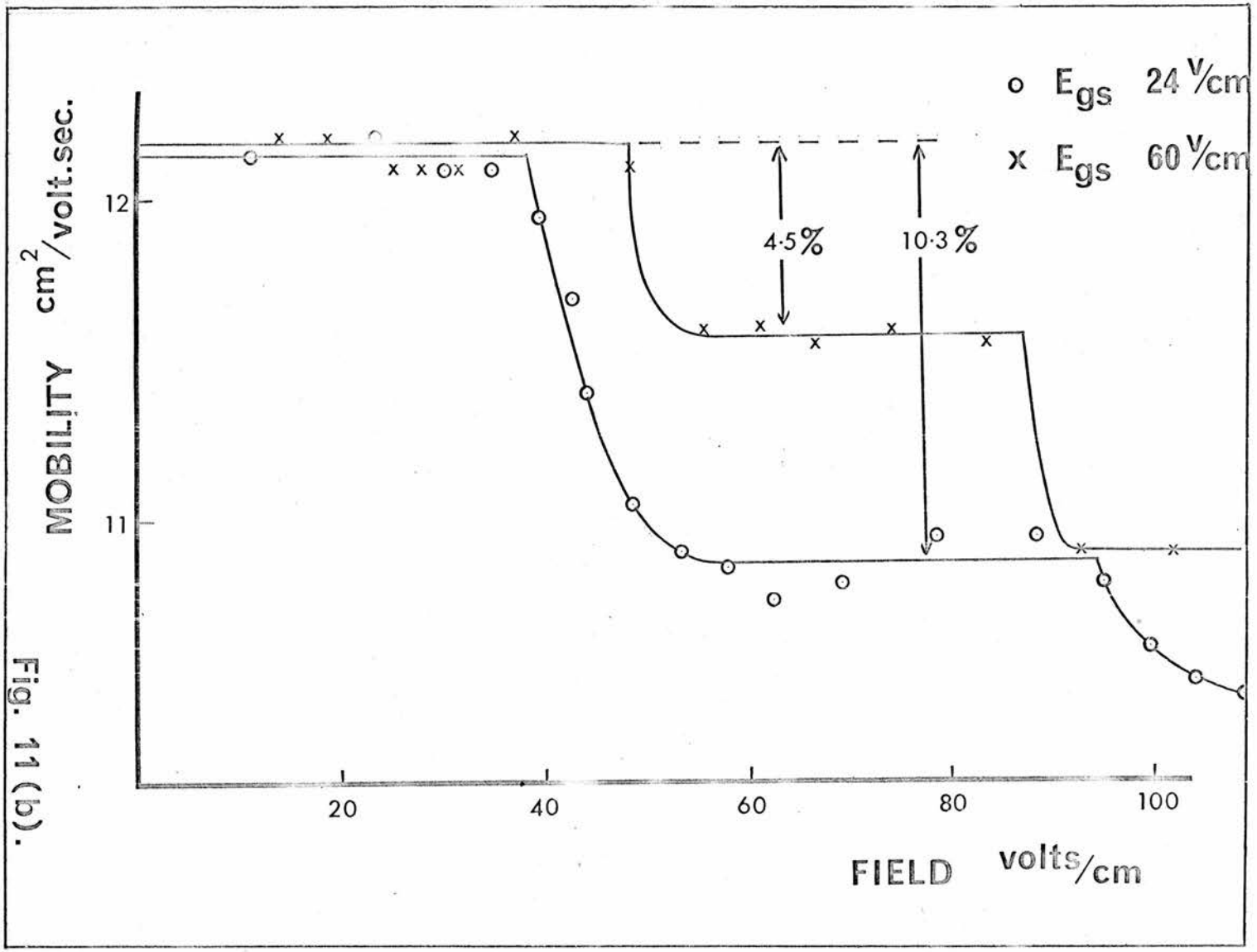
o E_{gs} 24 V/cm
x E_{gs} 60 V/cm
4·5%
10·3%
MOBILITY cm²/volt.sec.
12
11
20
40
60
80
100
FIELD volts/cm

Fig. 11 (b).

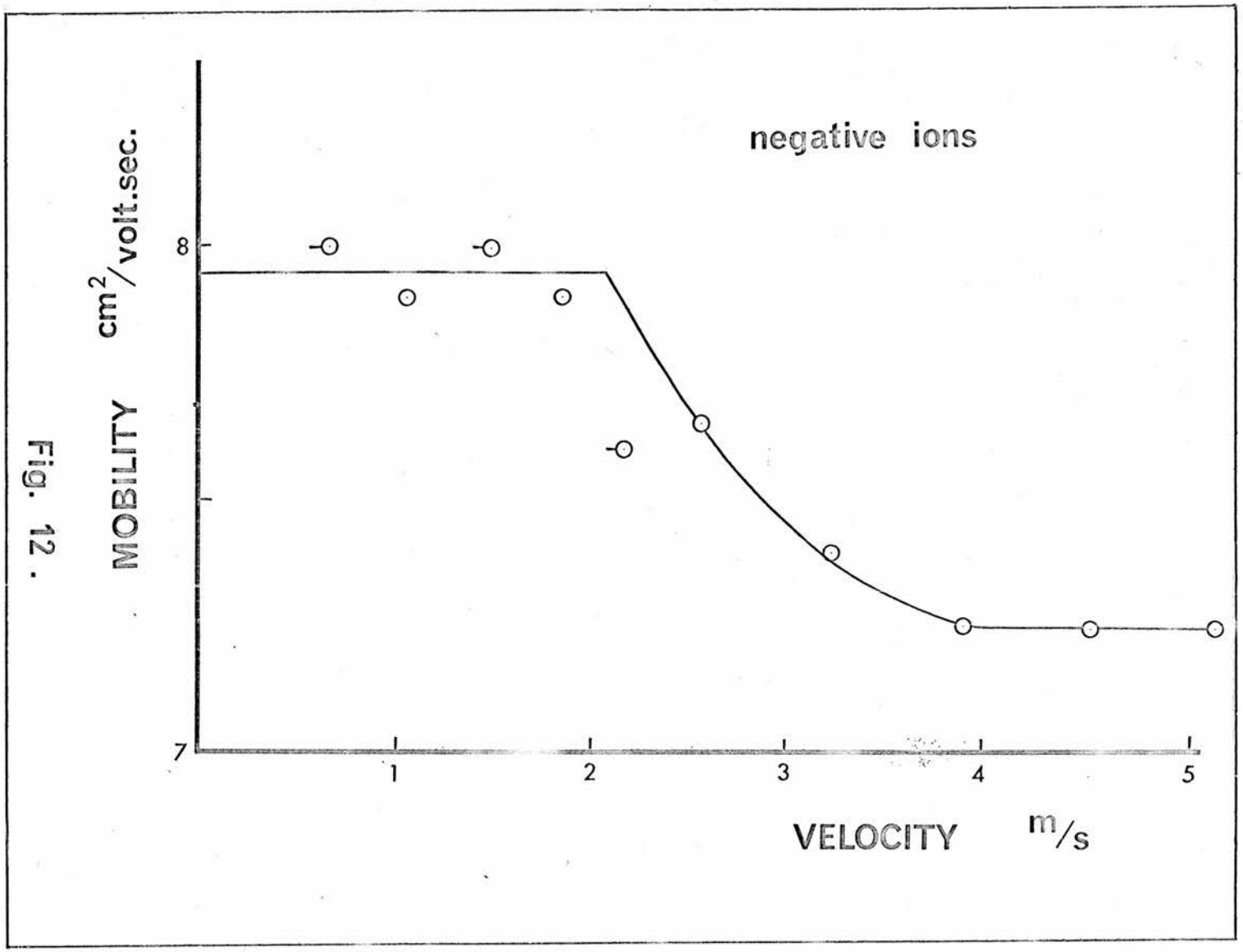

Fig. 12.

During the first fifteen runs in which E_{gs} was maintained equal to E_{gc} and where no discontinuities were observed at 5 m/sec., twelve examples of a discontinuity were observed at a velocity equivalent to ~10 m/sec. These were assumed to be the second discontinuity. The velocity at which the second discontinuity occurs taken from these readings, is 10.35 m/sec. $\pm$ 0.9 m/sec. This is double the value, given below, for the velocity of the first discontinuity.

The discontinuity at 5 m/sec was first observed in a run performed at constant $E_{gs} < E_c$. Thereafter the size of the discontinuity was shown to depend on the grid-source field such that if $\frac{E_{gs}}{E_{gc}} < 0.8$, the drop in mobility at the first step was $6 \rightarrow 10\%$ and if $\frac{E_{gs}}{E_{gc}} > 1.5$, the discontinuity was $\leqslant 3\%$. Figs. 11(a) and 11(b) show this dependence for positive ions; the results were taken from a series of runs where all other parameters were kept constant.

Negative ions were more difficult to measure on account of their lower mobility. Here also it was found that no clear discontinuity could be observed unless the grid-source field was very low. This is presumably why Careri[2] et al have been unable to see the first two discontinuities for negative ions. The author therefore claims the first reported observation of the first discontinuity for negative ions, (Fig. 12).

A similar effect was observed for the second discontinuity for positive ions. For very high fields $E_{gs} > E_{c_2}$* the second step was very difficult to observe.

Within the accuracy of the experiment, the effect of varying E_{gs} from low field $< E_c$ to high field $> E_c$ and vice-versa, was instantaneous.

---

* E_{c_2} = grid-collector field at the second discontinuity.

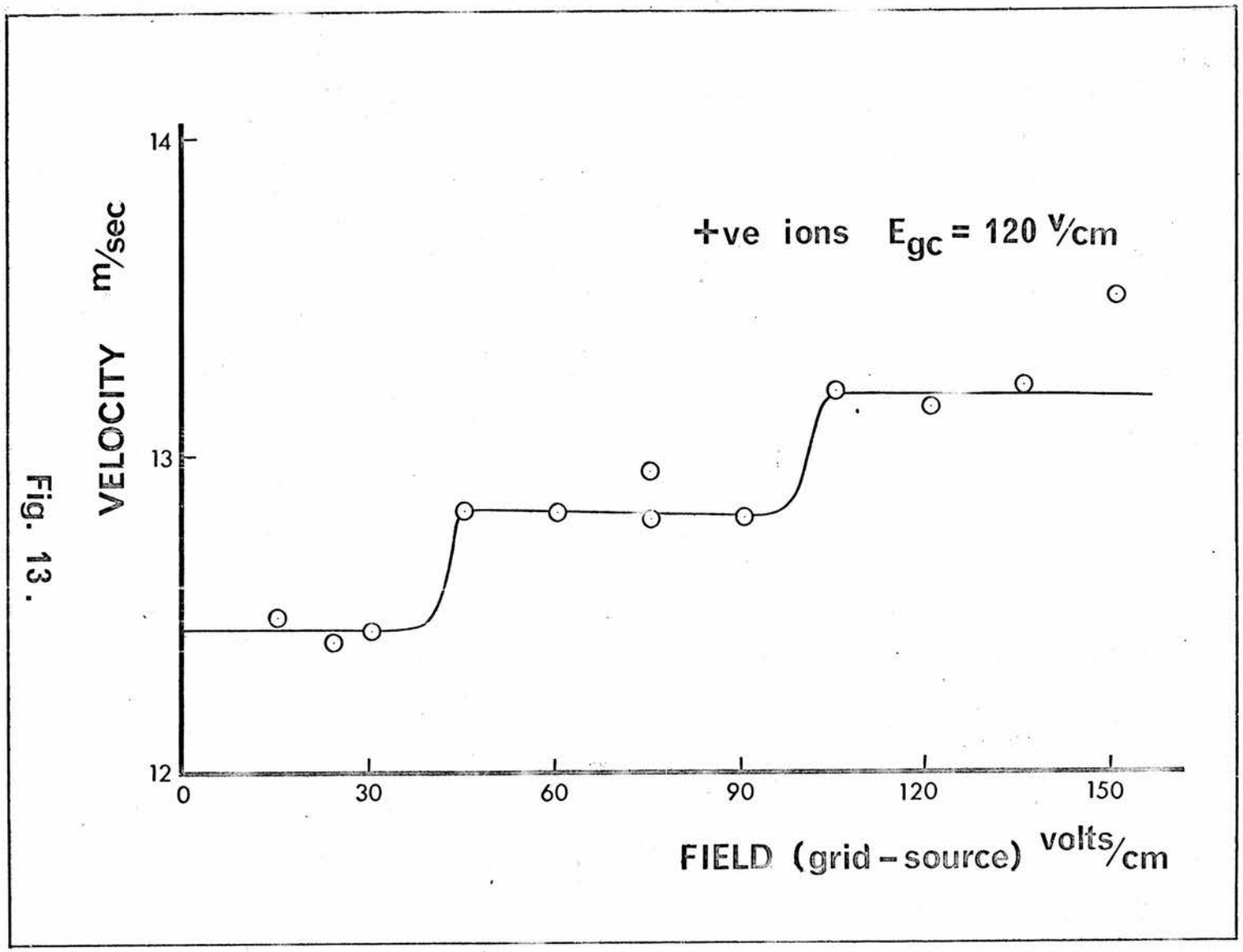
+ve ions E_{gc} = 120 V/cm
VELOCITY m/sec
14
13
12
0
30
60
90
120
150
FIELD (grid – source) volts/cm

Fig. 13.

The time dependence was investigated by setting the grid-collector field to a value $E_{gc} < E_c$, and to a frequency just above cut-off. While keeping E_{gc} constant, E_{gs} was varied from a sub-critical to a super-critical value and the current observed. Previous results (P.58) suggest that the apparent ion velocity for $E_{gc} > E_c$ was enhanced when the grid-source field is increased beyond the critical field, so that now the constant applied frequency would be too low to prevent ions from reaching the collector and a current should be collected. As soon as the grid-source field was altered, the current began to adjust itself reaching its new value in about one minute. The time constant of the electrometer circuit was of this order, consequently the change in current can be considered instantaneous.

The variation in discontinuity size with grid-source field was observed in another way. The velocity of the ions under a constant grid-collector field $E_{gc} > E_c$ was measured for varying grid-source field. The result of such a measurement is shown in Fig. 13. As expected, the velocity of the ions increased when the grid-source field E_{gs} became supercritical, $(>E_{c_1})$ and increased again as E_{gs} passed through the value of field for the second discontinuity (E_{c_2}).

The Critical Velocity

The existence of discontinuities in the field dependent drift velocity of ions as observed by Careri, has therefore been confirmed.

Positive Ions

The value of the critical velocity for positive ions is obtained from the average of 30 runs in which the discontinuity was particularly

Run	Multiple of v_c	v_{c_n}	$\frac{v_{c_n}}{n}$ cm.sec.$^{-1}$
L	v_{c_3}	741 ± 8	247
	v_{c_3}	622	207
J	v_{c_2}	468	234
5th Nov. 1963	v_{c_1}	198	198
5th Nov. 1963	v_{c_2}	394	197
4th Nov. 1964	v_{c_1}	202	202
4th Nov. 1964	v_{c_3}	615	205
4th Nov. 1964	v_{c_1}	207	207

Average critical velocity for negative ions = 2.12 ± 0.16 m/sec.

Negative Ion Critical Velocities

TABLE II

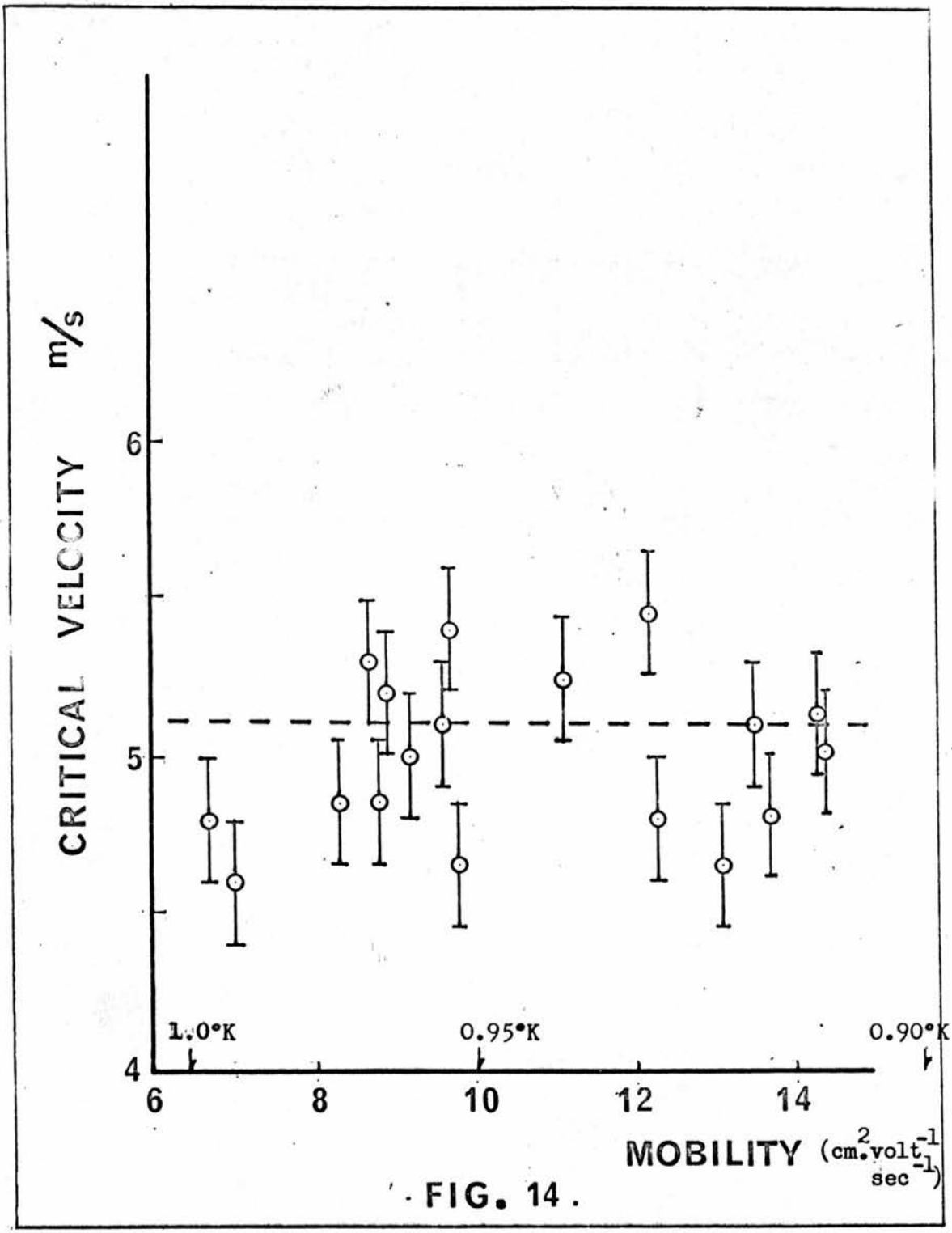
CRITICAL VELOCITY m/s
6
5
4
1.0°K
0.95°K
0.90°K
6
8
10
12
14
MOBILITY (cm.^{2}volt^{-1} sec^{-1})

FIG. 14.

distinct. The average value from these results was

$$\bar{v}_c^+ = 5.15 \text{ m/sec.}$$

and the root mean square deviation from this = $\pm$ 0.21 m/sec.

These results include some taken in earlier runs where the temperature control technique was not fully developed. Excluding these eleven early runs, the mean critical velocity from the remaining nineteen runs was

$$\bar{v}_c^+ = 5.21 \pm 0.08 \text{ m/sec.}$$

The lower r.m.s. deviation is an indication of the improvement in the method used for these later runs.

Negative Ions

Due to a lack of evidence for the velocity of the first discontinuity for negative ions, all the clearly defined discontinuities are considered and the values of v_{c_1} found by calculating $\frac{v_{c_2}}{2}$, $\frac{v_{c_3}}{3}$, etc. The relevant data is shown in Table II. This method is justified when the discontinuity is shown to be truly periodic (P. 71.)

The critical velocity for negative ions obtained in this way is

$$\bar{v}_c^- = 2.12 \pm 0.16 \text{ m/sec.}$$

The author has observed only three clear examples of the first discontinuity for negative ions. These occurred at 1.98 m/sec., 2.02 m/sec. and 2.07 m/sec.

Temperature Independence of Critical Velocity

The author confirmed Careri's observation of the temperature independence of the critical velocity within the narrow range 0.9 - 1.0°K.

This is demonstrated in Fig. 14 .....

which shows an even distribution of the values of v_c against $\mu(T)$. In most of the runs, therefore, the absolute value of the temperature was not accurately known but was, nevertheless, kept constant to within a millidegree. N.B. The error bars in Fig. 14 represent the uncertainty in the measurement of $\hat{\alpha}$ given critical velocity. Factors other than experimental observation must, therefore, account for the small distribution about $\bar{v}_c$.

Other Variables

In order to investigate the nature of the discontinuities the effect of varying the available parameters was sought.

At one time it was thought that the mobility steps might be due to a surface effect. The ions, on approaching the collector, might be trapped on vortex lines or rings attached to the electrode and the resulting space-charge could then retard those ions following behind. Surface contamination might also have the same effect. If this were true, the direction in which the frequency was changed during individual determinations of the drift velocity should affect the final result.

For instance, if the velocity of the ions at a given field is determined by measuring the current at successively higher values of frequency, the collector will receive current until the cut-off frequency is reached. Under these conditions the collector surface could have a space charge attached and this would appear as a reduction in the measured cut-off frequency. If, however, the measurements are made starting at high frequencies, then at the point when the cut-off frequency is reached, the collector should be 'clean' of charge. The ion current density is sufficiently small such that an appreciable space charge would require a time comparable to the measuring time to build up. Several runs were performed where velocities were measured by increasing the frequency and others decreasing the frequency and no consistent

effect was observed.

The amount of current collected may also precondition the collecting electrode's surface. Again, several runs showed that restricting the current arriving at the collector had no effect on the results.

Likewise, the direction in which the applied fields were altered and the rapidity, within reason, with which readings were taken, did not affect the measured velocities.

The possibility that macroscopic flow patterns, as observed in classical electrolytes,[55] were set up by the moving ions in He II and were affecting the critical velocity, was examined by varying the transverse diameter of the grid-collector space. This was done by inserting a plug into the existing space, thus reducing the volume of the drift space.* It was thought that this might alter the size of the discontinuity. In fact the observations were that, at low E_{gs}, the discontinuity was of the same magnitude but occurred at a lower velocity, 325 cm/sec. At high grid-source fields, the critical velocity was again 5.12 m/sec. This point is worthy of further investigation, as at first sight it suggests that the critical velocity is connected with macroscopic flow. For this reason heaters were put into the two halves of the cell to provide n-fluid flow. (See P. 76)

Vibration

Tapping the dewar during a series of measurements usually reduced the current arriving at the collector; the current would recover almost immediately the vibration ceased. No other consistent effect was observed.

* by approximately 50%

Grid-Collector Separation (L) cm.	Average Discontinuity Size $\Delta\mu$ %	No. of Examples
1.0	7.5 ± 1.6*	2
0.55	6.4 ± 2.0	19
0.41	8.3 ± 2.3	3
0.3	7.8 ± 2.6	5
0.2	6.1 ± 3.3	1

Variation of Discontinuity Size

with the Length of Ion Flight Path

TABLE III

* For calculation of the probable errors in $\Delta\mu$, see Appendix 3.

Variation of Electrode Separation

(P. 54-58)

The dependence of discontinuity size on grid-source field suggested that the effect producing the reduction in mobility either decayed with time or occurred only once in the early stages of the flight of each ion. In this way the reduction in mobility would be only temporary and when $E_{gs} > E_c$, the ion having undergone the dissipative process before reaching the grid, appears to have a 'normal' mobility in the grid collector space. If this were true and $E_{gs} < E_c$ so that the reduction in mobility was initiated as the ion entered the grid-collector space, then varying the grid-collector spacing should affect the apparent size of the mobility drop.* If the collector is placed close to the grid, the dissipative process should have a large effect on the total drift time, whereas if the collector is a long way from the grid, the process will have decayed and the overall effect will be less. Table III shows the results from thirty measurements of average step size for five different values of grid-collector spacing from 0.2 - 1.0 cm. It can be seen that there is no significant variation of step size. The accuracy of step size determination is rather poor and consequently there may be a small dependence which would not be evident from these results. The model which suggests that the drop in mobility is solely due to a dissipative process which acts only once over the first part of the ion's flight path, is precluded since this model would predict an increase in step size inversely proportional to the grid-collector spacing. This is definitely not observed.

---

* See P. 179, Section 12.

The Reduction in Mobility at Successive Discontinuities

The percentage drop in mobility for positive ions at successive discontinuities is

v	$\frac{\Delta\mu}{\mu}$
v_{c_1}	$6.5\% \pm 1.5$
v_{c_2}	7.5%
v_{c_3}	7.5%

This means that within the limits of accuracy of the experiment, the three discontinuities are of equal size.

The Periodicity of the Discontinuities

The author's apparatus was only capable of observing the first three discontinuities with ease. Higher fields could be obtained by making the distance between the grid and collector very small but this led to inaccurate measurements of velocity.

The values obtained for the first three discontinuities for positive ions are:-

$\ddot{v}_{c_1}$ = 5.15 ± 0.21 m/sec. from 30 examples (P. 63)
(5.21 ± 0.08) m/sec. from 19 examples

$\ddot{v}_{c_2}$ = 10.35 ± 0.9 m/sec. from 12 examples

$\ddot{v}_{c_3}$ = 15.25 ± 0.05 m/sec. from 4 examples

These are exactly periodic within the accuracy of the experiment.

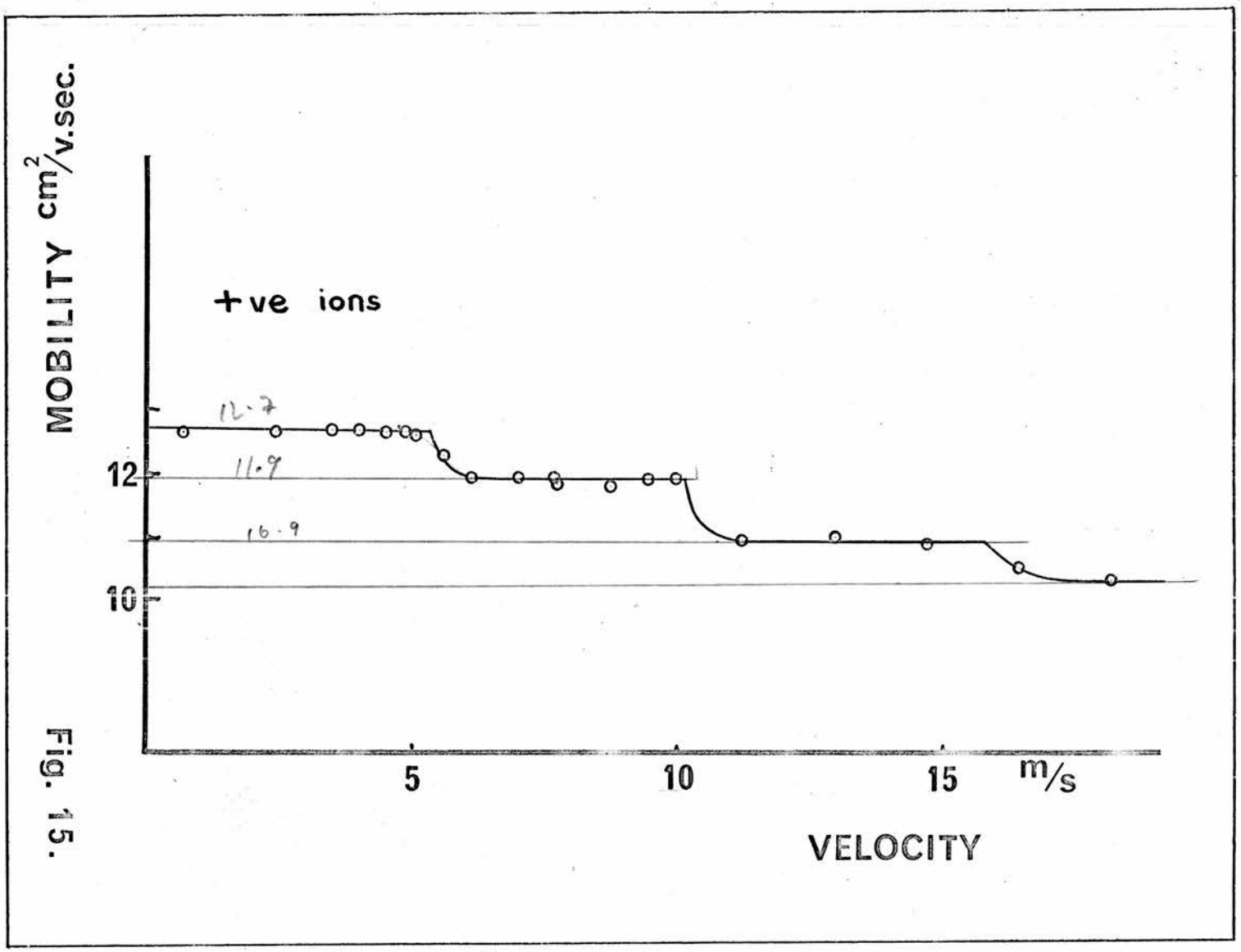

Fig. 15.

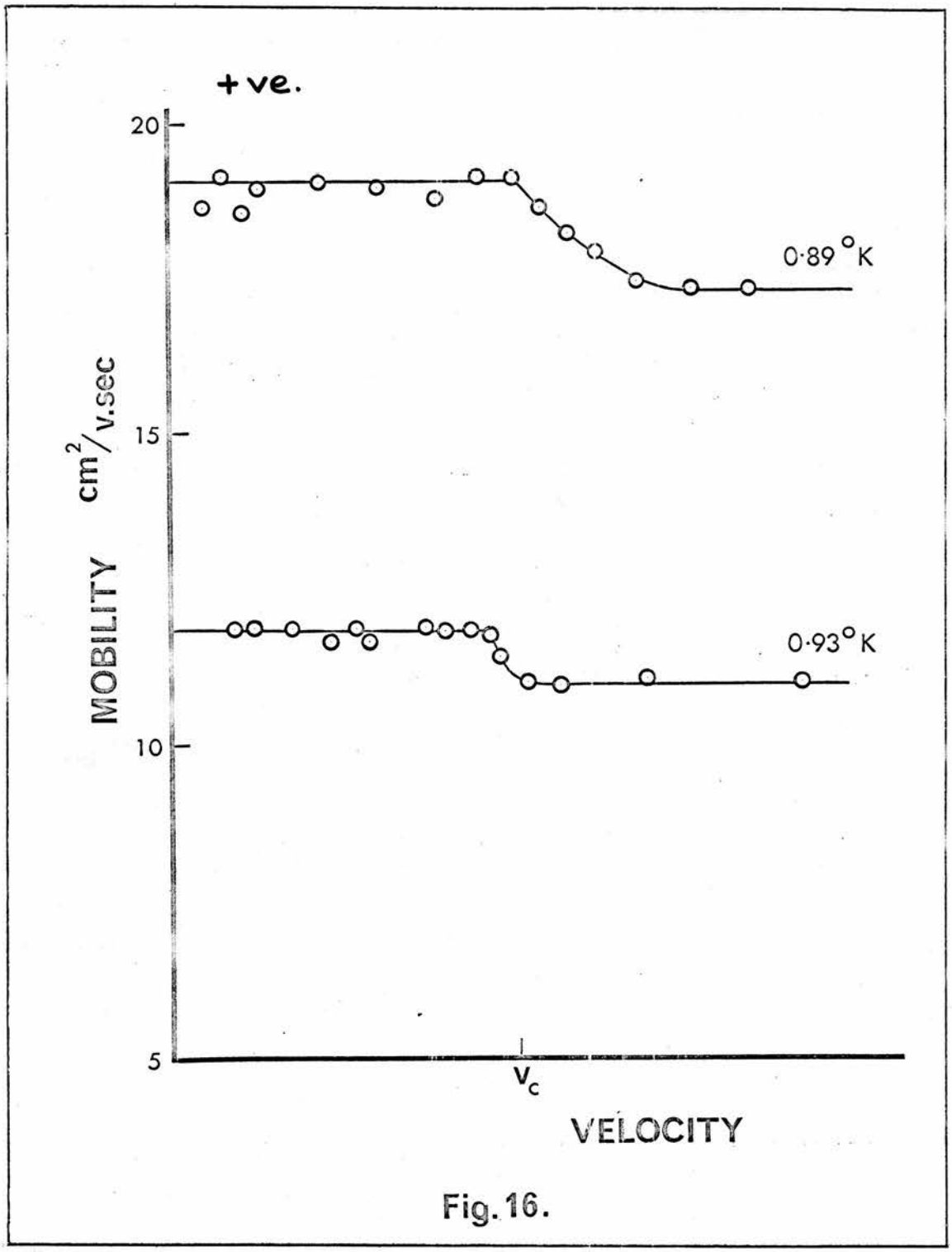

Fig. 16.

The corresponding values for negative ions are:-

v_{c_1} = 2.02 ± 0.04 m/sec. from 3 examples

v_{c_2} = 4.16 ± 0.3 m/sec. from 2 examples

v_{c_3} = 6.36 ± 0.3 m/sec. from 3 examples

Again true periodicity is observed.

A good example of a run in which three consecutive discontinuities were observed is shown in Fig. 15.

The Shape of the Discontinuity

At temperatures 0.96 - 1.0°K the discontinuity was usually fairly abrupt. The value of the mobility fell to its new level within 30 cm/sec. of the critical velocity. At temperatures below 0.93°K the change was more gradual. This is illustrated in Fig. 16, where the mobility is plotted at two different temperatures.

Anomolous Behaviour

On a very few occasions, when conditions favoured the appearance of a step, no discontinuity was observed. This was attributed to Careri's 'metastability,'[2] where disturbances in the fluid prevent the process of mobility loss from occurring.

In about twelve runs steps were observed midway between two critical velocities. The effect was not reproducible and 'metastability' is again held responsible.

Biassing the Applied Square Wave Potential

The mobility determinations were performed by applying a square wave potential to the grid, keeping the collector constant at earth potential.

See Fig. 1 facing P. 34.

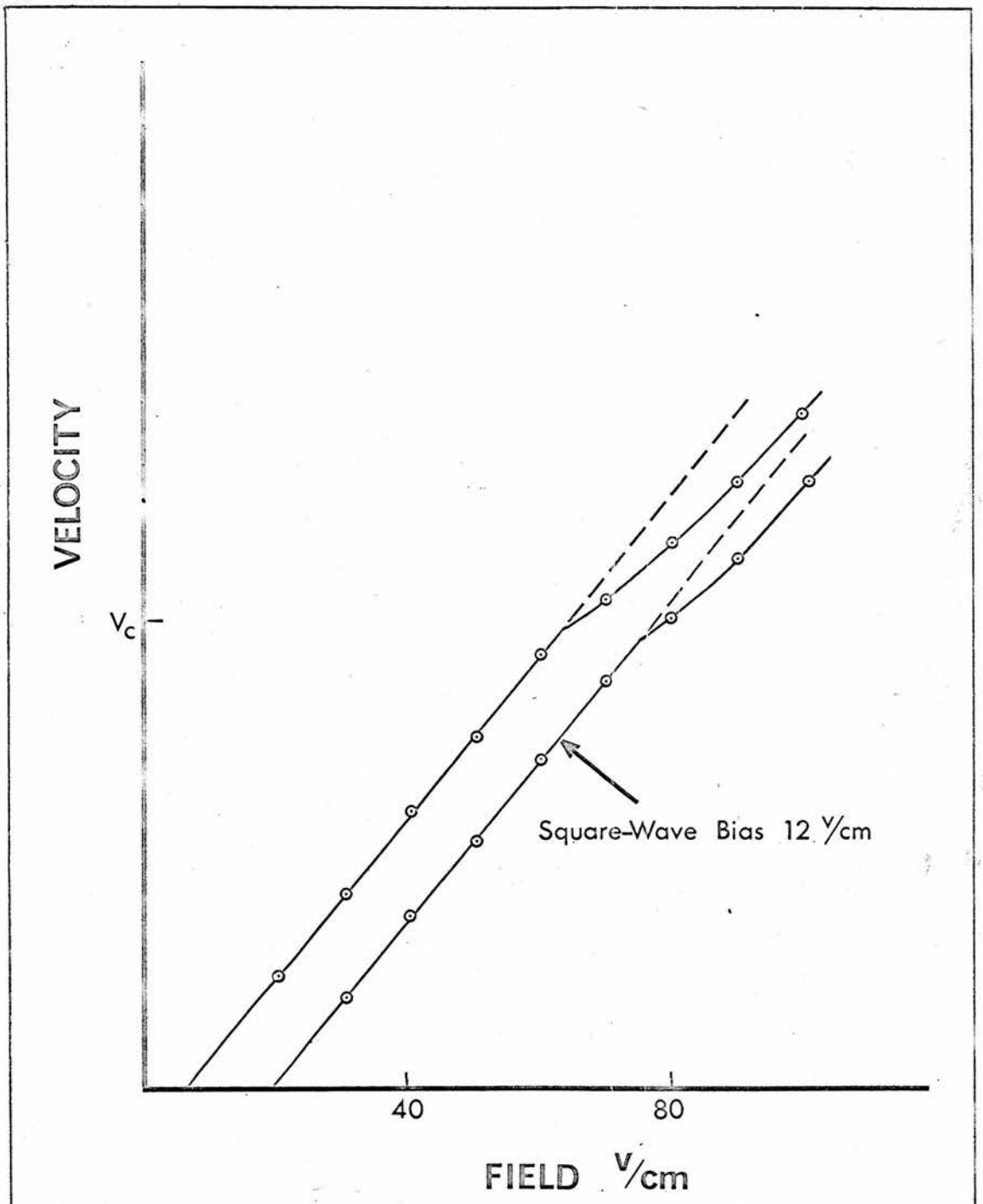

Fig. 17.

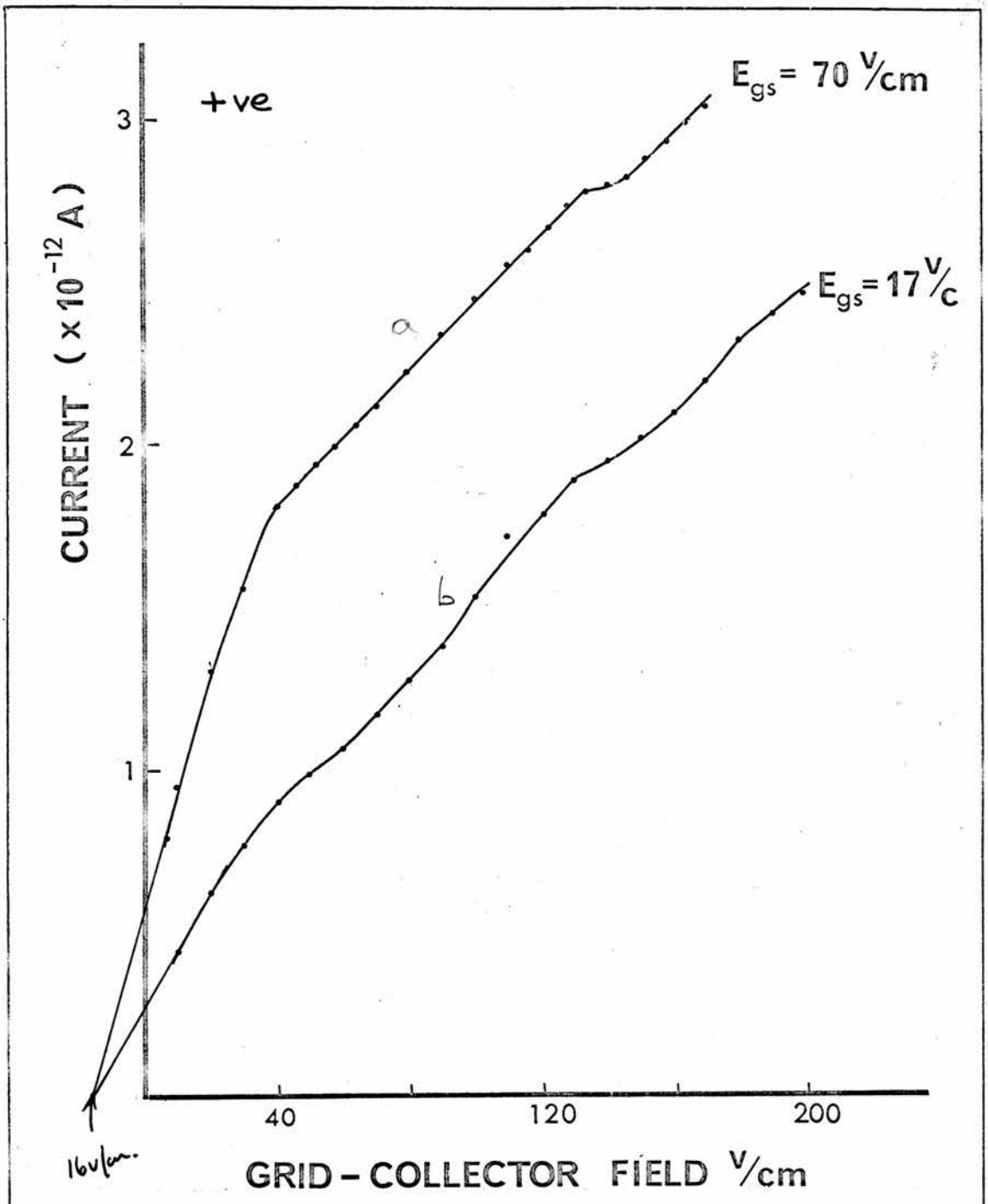
+ve
3
2
1
CURRENT (x 10^-12 A)
E_gs = 70 V/cm
E_gs = 17 V/c
a
b
40
120
200
16 v/cm.
GRID – COLLECTOR FIELD V/cm

Fig. 18.

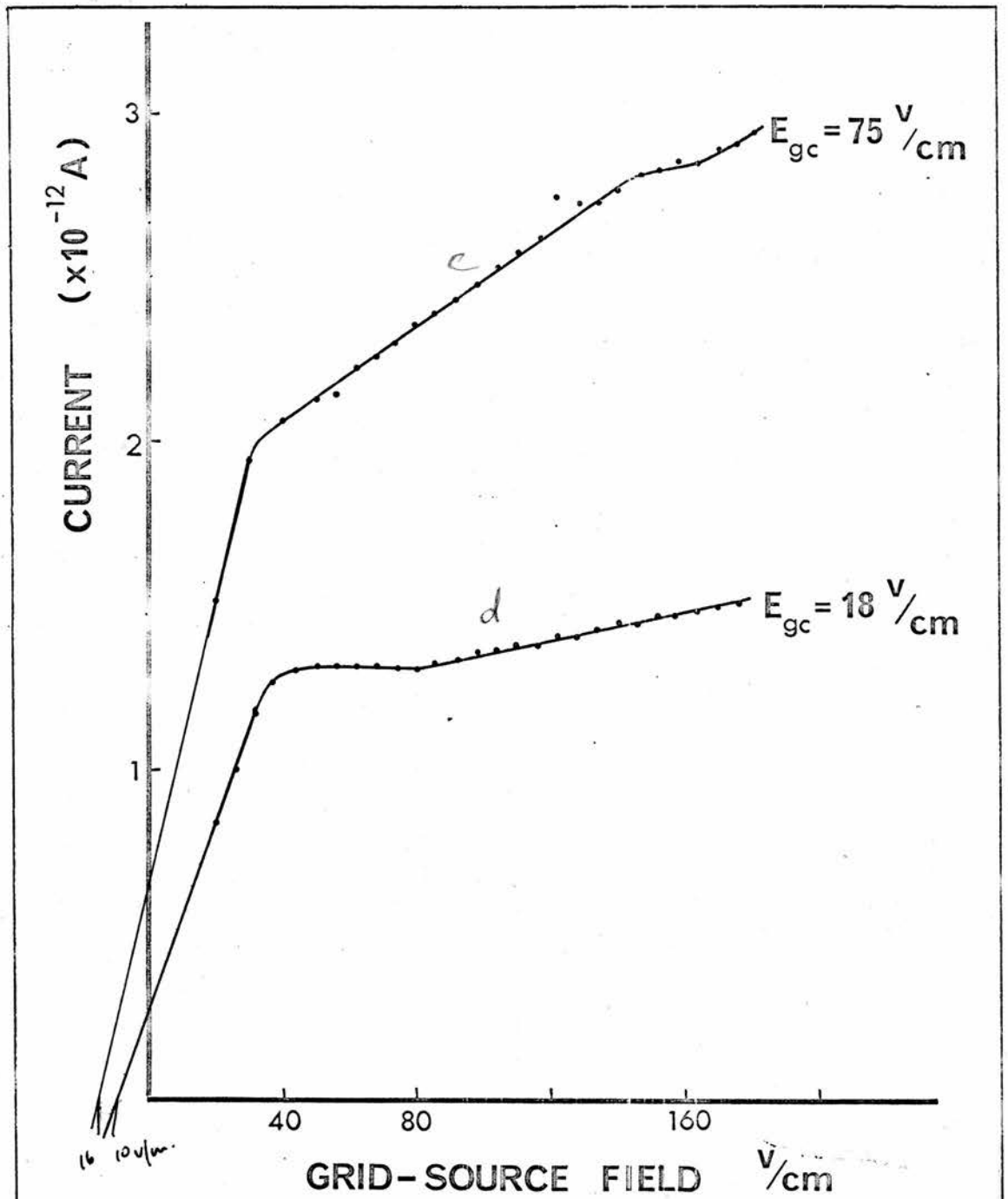
CURRENT (x10^{-12}A)
3
2
1
E_{gc} = 75 V/cm
c
d
E_{gc} = 18 V/cm
40
80
160
16 10 v/m.
GRID-SOURCE FIELD V/cm

Fig. 19.

For most of the runs the forward and reverse fields in the measuring space were equal in magnitude, but of different duration. The effect of deliberately biassing the square wave so that the reverse field, that driving ions from collector to grid, was larger than the forward field, was sought. This situation is of interest because, by adjusting the peak-to-peak size of the square wave, it would be possible to have the ions travelling at $v > v_c$ in the reverse direction while still travelling at $v < v_c$ in the forward direction. Fig. 17 shows that, in fact, this variation had no effect on the discontinuity position or magnitude. The opposite situation of a higher forward field was not feasible since this led to indistinct cut-off frequencies.

The D. C. Characteristics of the Triode Cell

The electrodes were connected to constant voltage sources. The current collected was measured under D. C. operation for the following circumstances:-

	Grid Source Field	Grid Collector Field
(a)	High	Variable
(b)	Low	Variable
(c)	Variable	High
(d)	Variable	Low

The results are shown graphically in Figs. 18 and 19.

In cases (a), (b) and (c), the current rose relatively steadily with increasing field, except for a discontinuity at $\sim$ 135-140 v/cm.

This discontinuity appeared very like that observed in the velocity field curves; in this case the current fell below the line of increasing

current. A field of 135 v/cm. is equivalent to a velocity of 1100 cm/sec. at the temperature (0.97°K) of this experiment. The drop in current then could be attributed to a reduction in mobility at the $v = v_{c_2}$ and subsequent loss due to spreading of the beam. There was no evidence for a discontinuity at a field equivalent to 500 cm/sec. in (a), (b) or (c). However, in case (d), the current having initially reached a plateau began to rise again quite distinctly at 77 v/cm. and continued to rise linearly without any discontinuity at 120 v/cm. This last result is consistent with Gaeta's[30] ionic recombination measurements where he observes a rise in current at fields above the critical value. The velocity at 77 v/cm. would be 570 cm/sec.

Heat Induced n-Fluid Flow

Heaters were cemented into the grid-source space behind the grid and into the grid-collector space in the 'moat' round the collector. Varying heat inputs were applied to these in order to provide n-fluid flow through the grid and in the measuring space. The effect on the ion velocity was examined. The following experiments were performed:-

I Heater in grid-collector space.

(a) The velocity-field curves were determined for

(i) No heat
(ii) 3 mW to heater
(iii) 10 mW to heater
(iv) 100 mW to heater

To ascertain the effect of an increasing n-fluid flow against the ion current

(b) Keeping grid-collector field constant, velocity of the ions versus heat input was determined for

(i) $E_{gc} > E_c$ $E_{gs} < E_c$
(ii) $E_{gc} < E_c$

To see if ions under a supercritical field had a greater interaction with the n-fluid flow

II Heater in grid-source space.

(a) The velocity-field curves for

(i)	No heat	$E_{gs} < E_c$	To ascertain the effect of an increasing n-fluid flow in the direction of the ion current
(ii)	5 mW to heater		
(iii)	10 mW to heater		
(iv)	15 mW to heater		

(b) Grid-collector field constant.

The velocity of the ions versus the heat input was determined for

(i)	$E_{gc} < E_c$	$E_{gs} < E_c$	To investigate the possible effect of an increased interaction between the ions travelling at critical velocities, and the n-fluid
(ii)	$E_{gc} > E_c$	$E_{gs} < E_c$	
(iii)	$E_{gc} < E_c$	$E_{gs} > E_c$	
(iv)	$E_{gc} > E_c$	$E_{gs} > E_c$	

(c) With fixed grid-collector field E_{gc}, the velocity of the ions was measured versus grid-source field E_{gs} for

(i)	No Heat	$E_{gc} > E_c$	To look for a connection between the variation of discontinuity size with E_{gs} and macroscopic flow patterns
(ii)	12 mW applied to heater		
(iii)	10 mW applied to heater		

The above experiments were performed on positive ions only except for II(b) for which positive and negative ions were used.

The main features of the results are as follows:-

(i) The apparent critical velocity is affected only slightly by the n-fluid flow. (Figs.22, 24, 25)

(ii) Apparent ion velocities are relatively unaffected by n-fluid flow towards the ion source. (Fig. 24)

(iii) Apparent ion velocities are enhanced when n-fluid flow is towards

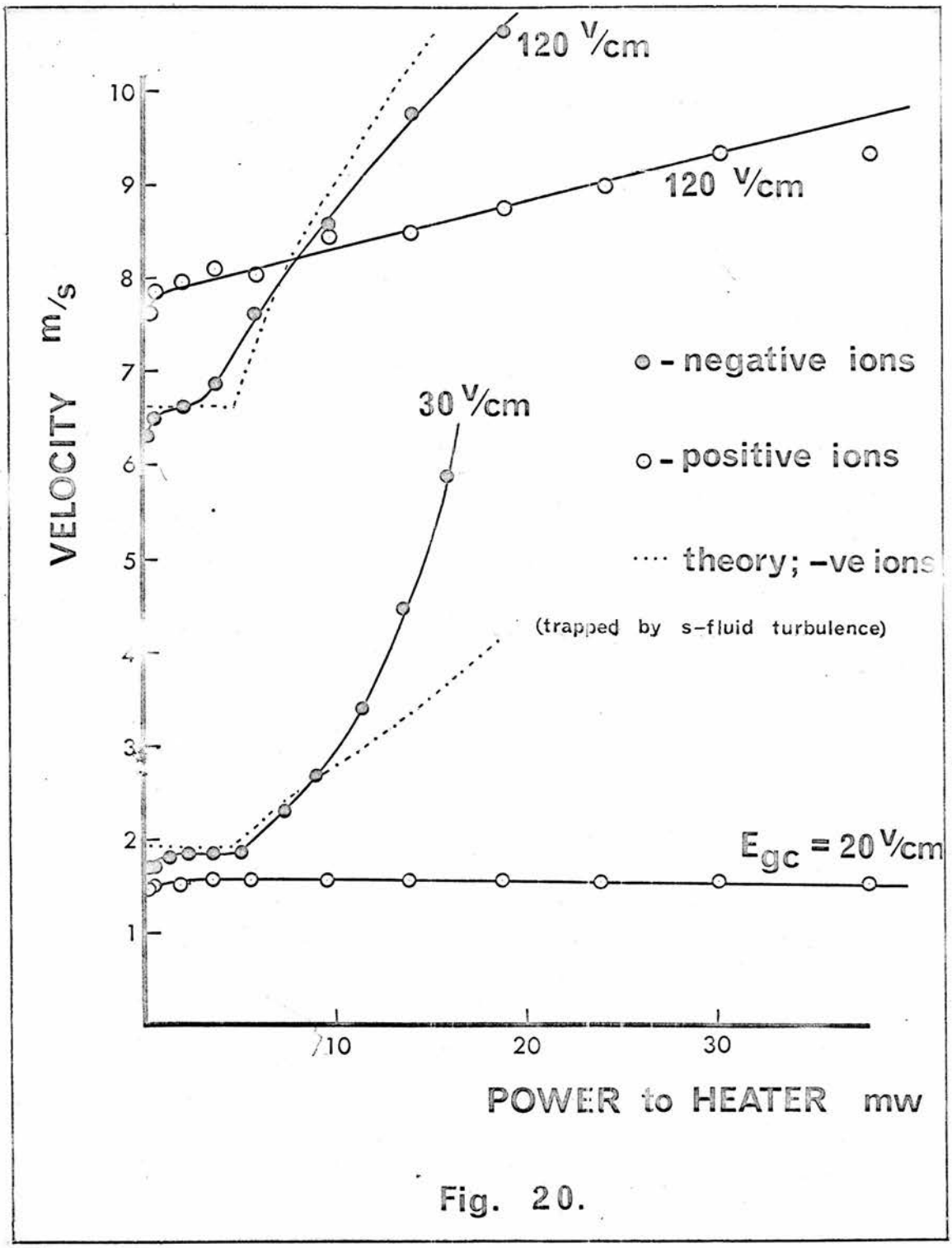
120 V/cm
120 V/cm
30 V/cm
o - negative ions
o - positive ions
···· theory; -ve ions
(trapped by s-fluid turbulence)
E_{gc} = 20 V/cm
VELOCITY m/s
POWER to HEATER mw
10
9
8
7
6
5
4
3
2
1
10
20
30

Fig. 20.

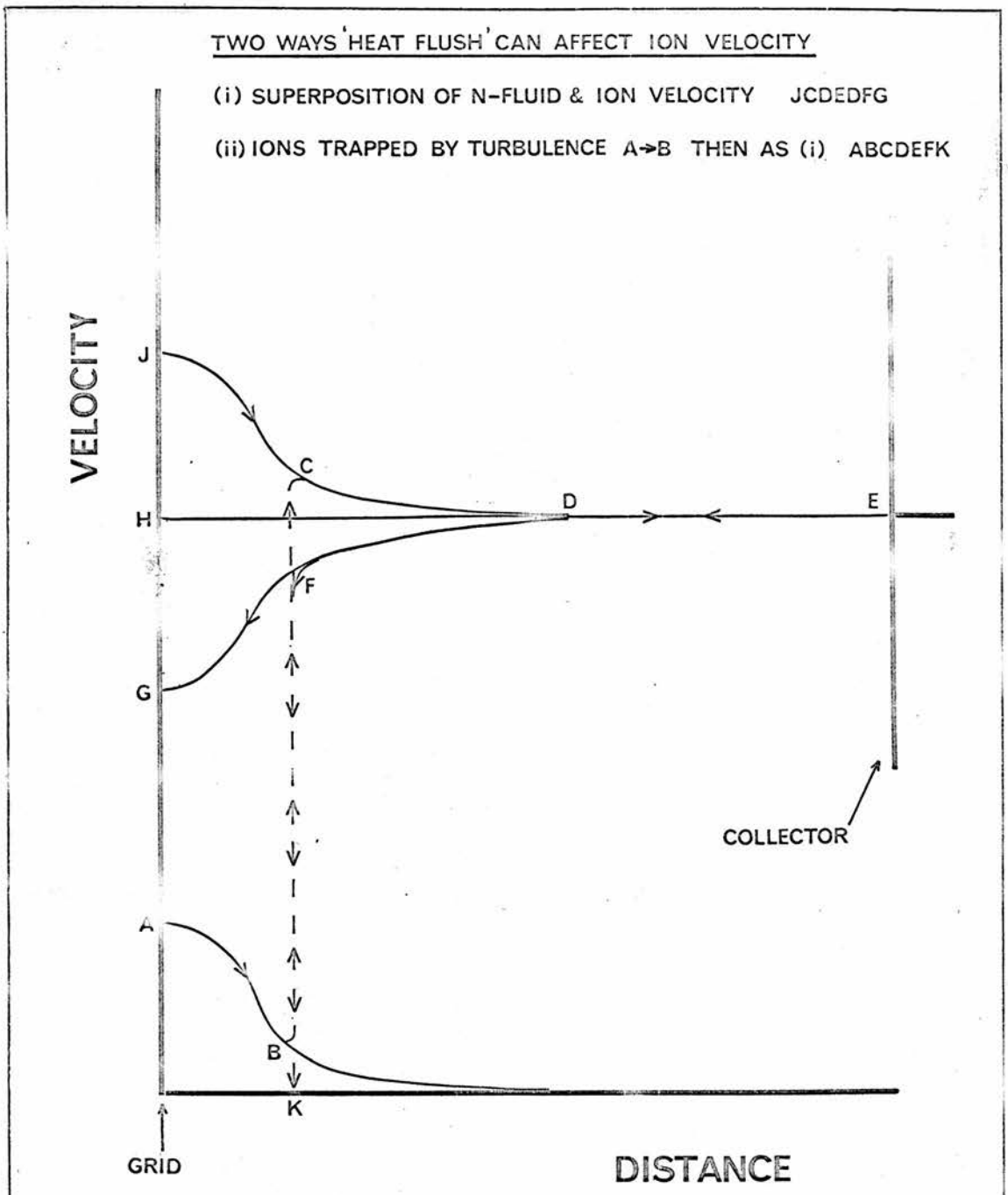
TWO WAYS 'HEAT FLUSH' CAN AFFECT ION VELOCITY
(i) SUPERPOSITION OF N-FLUID & ION VELOCITY JCDEDFG
(ii) IONS TRAPPED BY TURBULENCE A→B THEN AS (i) ABCDEFK
VELOCITY
J
C
H
D
E
F
G
COLLECTOR
A
B
K
GRID
DISTANCE

Fig. 21.

the collector. (Fig.20)

(iv) Negative ions are more sensitive than positive ions to the effects of forward n-fluid flow (i.e. towards collector.) (Fig.20)

(v) The apparent increase in ion velocity is greater than the maximum velocity of n-fluid flow at the grid. (Fig. 20)

(vi) Positive ion velocity-field curves for constant moderate heat inputs ($\leqslant$ 15 mW) have the same form as the curves for no-heat except the former has a greater slope. (Fig.22)

In order to explain these results, consider first Section (v) of the results, as illustrated in Fig. 20. A simple superposition of the n-fluid velocity onto the ion velocity is not satisfactory.

The argument runs as follows:-

Consider the situation where the applied frequency is too high to allow ions to reach the collector. When there is no nett n-fluid flow, the ion merely makes an excursion into the grid-collector space. The (See P.46) slightly longer pulse of the reverse field allows the ion plenty of time to return to the grid. In a given field an ion has a velocity relative to the surrounding n-fluid, then if the n-fluid is made to flow, the ion's velocity in that field will be changed by the vector addition of the n-fluid velocity. Now if n-fluid is made to flow through the grid towards the collector, the velocity of an ion entering the measuring (JCD, Fig.21) space will be enhanced. Moreover, on its return trip to the grid, the (DFG, Fig.21) ion will be retarded by the n-fluid flow. Fig. 21 shows how the velocity of an ion might be affected.* If the n-fluid flow is sufficiently great, an ion which just fails to reach the collector during the forward

---

* N.B. The shape of the velocity distribution curve near the grid is governed by the n-fluid velocity profile as given by equation 2(b), P.83b

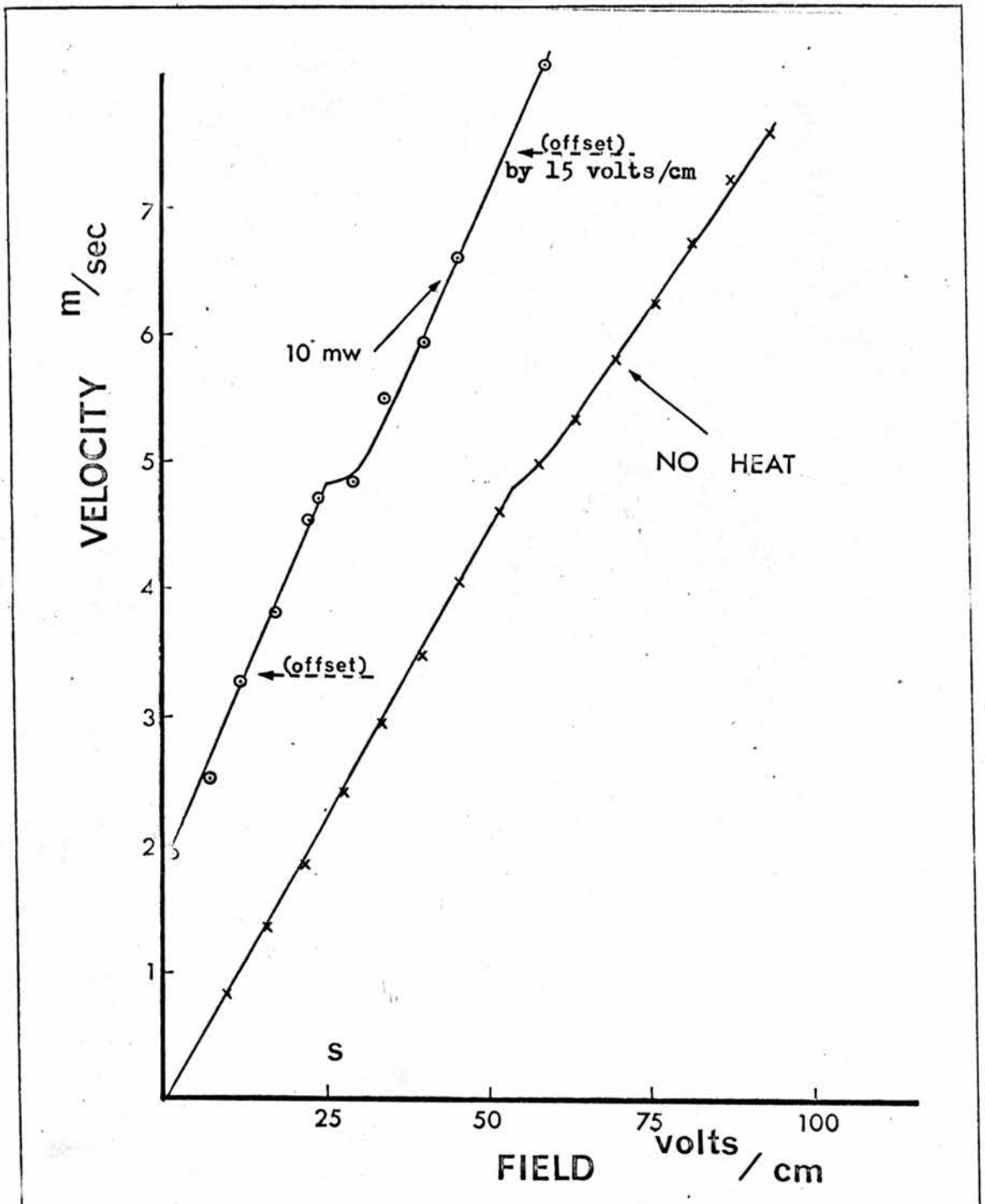
VELOCITY m/sec
7
6
5
4
3
2
1
(offset)
by 15 volts/cm
10 mw
NO HEAT
(offset)
S
25
50
75
100
FIELD volts / cm

Fig. 22.

pulse will not reach the grid during the reverse pulse. This means that, at the beginning of the next forward pulse, it will start from a point within the measuring space and, therefore, may now be able to reach the collector during the next pulse. In this way the effective flight path of ions actually arriving at the collector is shortened. Experimentally, this appears as a higher cut-off frequency which would be interpreted naively, as an increase in ion velocity. In this way it is possible to observe apparent ion velocities in excess of their true velocities by an amount greater than the n-fluid velocity. At frequencies beyond 'cut-off,' the ion, after many cycles, reaches an equilibrium situation where the excess forward velocity is balanced by the extra flight time in the reverse direction, due to the inequality of the pulse lengths. Space charge effects would give a distribution of ions about the point to which they return. The true distance the ion has travelled in the positive pulse, before arriving at the collector, would then be the distance from the collector to this equilibrium return point somewhere in the measuring space. If this velocity superposition theory were true however, the effect on the apparent ion velocity would be greatest at low fields where the ion velocity due to the field is low and that due to the n-fluid flow relatively high. At high fields, the effect should be negligible. This is not observed. Velocity-field curves for steady n-fluid flow show a constant percentage enhancement of velocity to the highest fields used, (Fig. 22.) The results when n-fluid flows through the grid towards the collector, are almost identical with those which would have been obtained if the grid-collector space had been shortened by a constant amount. It is, therefore, postulated that ions are trapped as

(See P.46)

NORMAL-FLUID VELOCITY DISTRIBUTION ACROSS THE GRID-COLLECTOR SPACE

(For derivation of the distribution see page 83a)

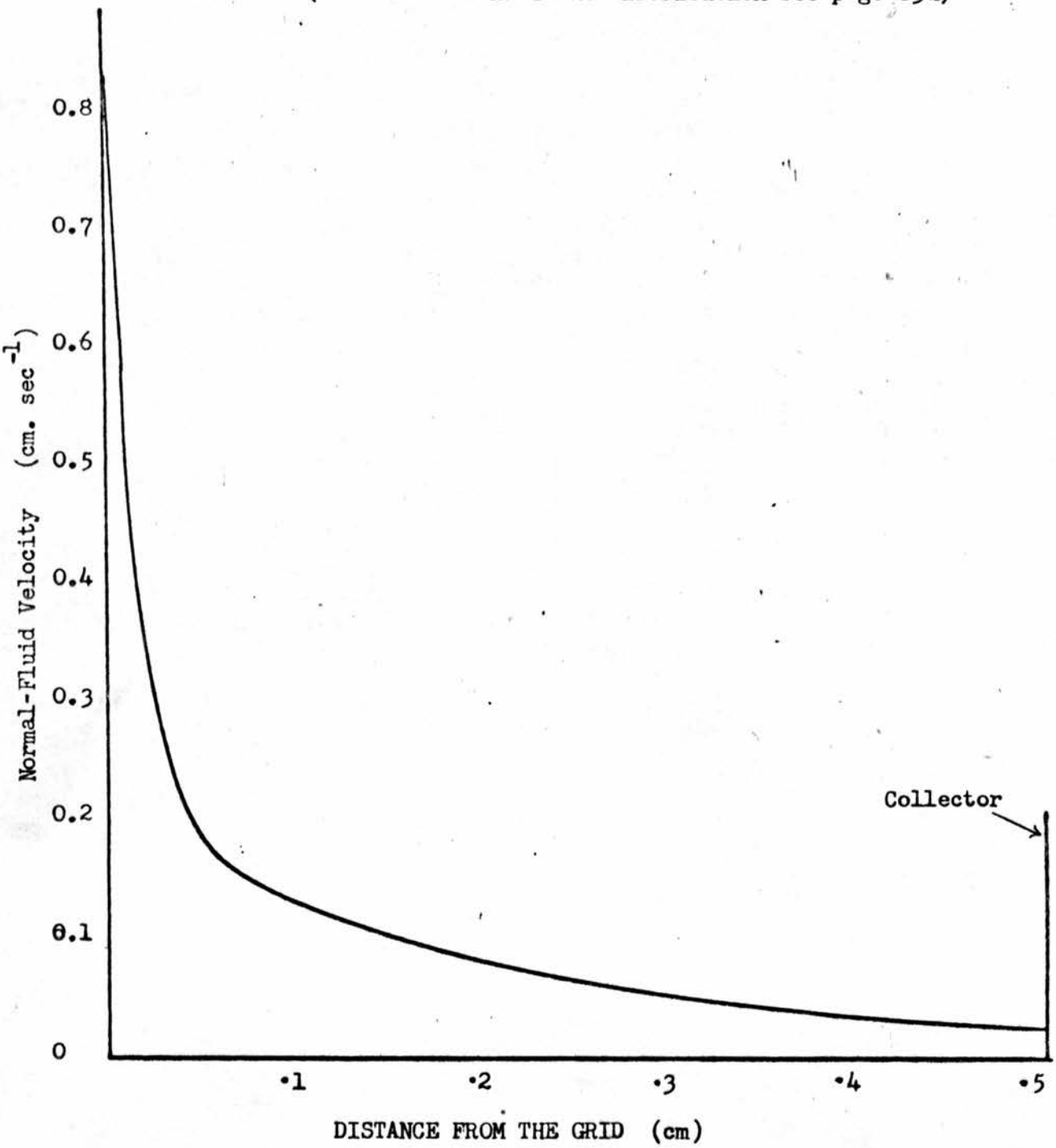

FIG.23

they pass through the region of maximum turbulence close to the grid, and are released at a definite point within the measuring space, (i.e. Points B and C in Fig. 21.) The possible effect of this trapping on the ion velocity is also shown in Fig. 21. At the point B where the ion ceases to be trapped, its velocity increases to the value which it would have on the superposition theory. There is no 'a priori' reason why the point F at which the ion, on its return journey to the grid, becomes trapped. should occur at the same point in the measuring space, i.e. B, F, C need not be a straight line. The effect of this trapping on apparent ion velocity is now calculated. It is first necessary to estimate the extent of the turbulent region in the measuring space.

Velocity Distribution in the Measuring Space

In order to determine the possible effect of turbulence on the ion velocity, it is necessary to know the velocity distribution of the normal fluid within the measuring space. The volume of n-fluid leaving the heater per second is given by

$$V_n = \frac{\dot{Q}}{\rho S T} \text{ cm}^3/\text{sec}. \quad \text{---------- 2(a)}$$

for non-turbulent flow

where $\dot{Q}$ = heat input

ρ = bulk liquid density

S = entropy

T = temperature ($^\circ$K)

For turbulent flow some of the heat goes into the creation of vortices.

Some of the n-fluid will be lost by heat conduction through the walls of the grid-source space. By considering the relative thermal conductivity of the cell walls, an estimated 30% of the total n-fluid produced actually passes through the grid holes. The velocity distribution of the n-fluid as it spreads into the measuring space will be given by

$$v_n(L) = \frac{0.3\dot{Q}}{A(L).\rho ST} \qquad \text{---------- 2(b)}$$

where L = distance from grid

A(L) = area through which n-fluid is passing distance L from grid.

This effective area has been calculated on the assumption that n-fluid passing through the grid spreads into the measuring space with an equal velocity in all directions, rather as a spherical wave might propagate. If the total radius of the grid is G, then the area of flow a distance L from the grid, is given by revolving the curve in the figure through π about the axis of the cell.

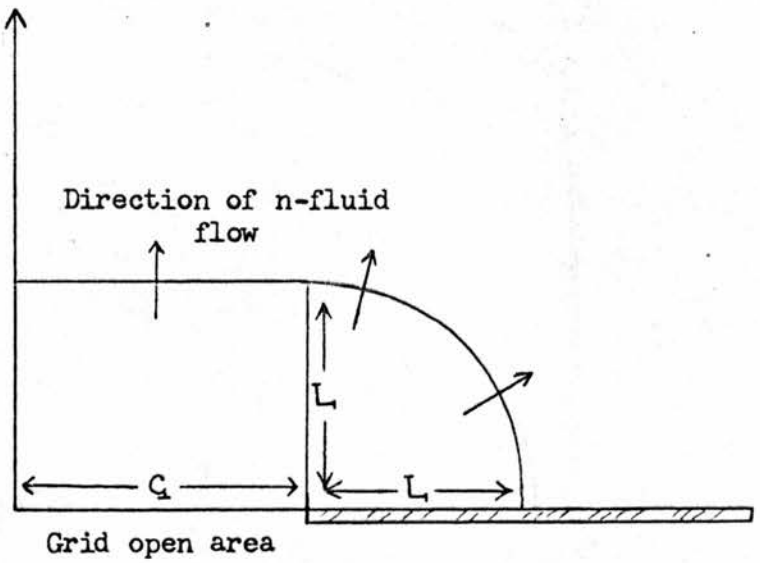

This gives $A(L) = \pi^2 LG + 2\pi L^2 + \pi G^2$ ——————— 2(c)

This is for $L \gg g$ = the radius of the holes in the grid

For $L \ll g$

$$A(L) = (\pi^2 Lg + 2\pi L^2 + \pi g^2) N \quad \text{——————} \quad 2(d)$$

where N = Number of holes in the grid.

The values for $v_n(L)$ are calculated from equation 2(b) for varying L from 0 - 0.5 cm.

These are plotted in Fig. 23.

Conduction of heat by the collector accounts for the flow of n-fluid into the collector. The magnitude of n-fluid flow here may be slightly different from that obtained from the graph. However this should have a small affect on the major portion of the curve away from the collector. The general velocity distribution curve is plotted assuming non-turbulent flow. When turbulence exists, the velocity distribution in the turbulent region will be altered, but this does not affect the argument which follows.

The Onset of Turbulence

It is necessary to establish whether turbulence begins in the measuring space or in the grid hole and whether this occurs at an n-fluid or a superfluid critical velocity.

The n-fluid critical velocity is given by

$$v_{n_c} = \frac{R_e \eta_n}{\rho d} \quad \text{(Ref. Van Alphen [53])} \quad \text{——————} \quad 2(e)$$

where R_e = Reynolds No. ≈ 1700

η_n = n-fluid viscosity

ρ = total fluid density

d = characteristic length

In the grid-hole $d = 0.08$ cm. and $v_{n_c}^H = 4.6$ cm/sec.

In the measuring space $d \approx 0.5$cm. $v_{n_c}^{GC} \approx 0.7$ cm/sec. } $0.95^\circ K$

There will be a transition region close to the grid where the critical velocity falls off rapidly from $v_{n_c}^{H}$ to $v_{n_c}^{GC}$. It is evident from a comparison of the n-fluid velocity distribution curve with the values of $v_{n_c}^{H}$ and v_{n}^{GC} that turbulence begins at, or close to, the grid. Therefore, for the onset of n-fluid turbulence there is a critical heat input $\approx \frac{v_{n_c}^{H}}{v_{n_G}}$ mW.

where v_{n_G} = velocity of n-fluid at grid/mW $\approx$ 1 cm/sec.

$\therefore$ critical heat input $\approx$ 4.6 mW.

The experimental curve of apparent negative ion velocities (Fig. 20) begins to rise sharply above a heat input of $\sim$ 5 mW in support of this mechanism.

The superfluid critical velocity is given by

$$v_{s_c} = \frac{C}{d^{1/4}} \quad \text{(Van Alphen)}^{53} \qquad \text{---------- (2f)}$$

where d = characteristic length

$C \approx 1$ (cm/sec.)$^{5/4}$

From this $v_{s_c}^{H} \approx 2$ cm/sec. in the grid-hole

and $v_{s_c}^{GC} \approx 1.2$ cm/sec. in the grid-collector space.

The superfluid velocity at any point is given by

$$v_s = \frac{\rho_n}{\rho_s} v_n \qquad \text{---------- (2g)}$$

At 0.95°K $\frac{\rho_n}{\rho_s} \approx 5 \times 10^{-3}$

The superfluid velocity distribution is therefore identical in form but different in magnitude to that for the n-fluid.

For the superfluid to reach a velocity v_{s_c} = 1 cm/sec. at 0.95°K, a counterflow of n-fluid with velocity 200 cm/sec. is required. A heat input of 200 mW is necessary to provide this n-fluid velocity. It is, therefore, obvious that at these temperatures, turbulence is initiated in the n-fluid.

The n-fluid turbulence may then entrain the s-fluid, producing vorticity in the whole of the fluid.

Turbulent Region

At the critical heat input $\sim$ 5 mW (see above), the n-fluid turbulence is initiated at the grid. For higher heat inputs the fluid in the measuring space is assumed turbulent to the point where the n-fluid velocity distribution curve passes through the critical n-fluid velocity $\approx$0.73 cm-sec.$^{-1}$ For the present purposes it is assumed that in the turbulent situation, an insignificant amount of heat is used to create turbulence, so that the velocity distribution outside the turbulent region is unaffected. The distance d_c from the grid over which turbulence exists, can then be found graphically for varying heat inputs. (from Fig. 23)

The effect of this turbulence close to the grid on the ion velocities, can be explained by ion trapping. The difference in the effect on positive and negative ions at different applied fields can be explained by considering the variation in trapping diameter as given by Donnelly [33, 47], for the different situations.

The Effect of Turbulence on Ion Velocities

The easiest way to see how turbulence affects the measured apparent ion velocities is to consider theevents occurring during a single reverse pulse of the applied square wave. Those ions which did not arrive at the collector during the previous forward pulse now begin to return towards the grid. At some point d_c from the grid, the ions enter the turbulent region and travel on towards the grid for a certain distance equal to an appropriate mean-free-path λ and are then trapped by a vortex line. The ion remains trapped for a time long compared to the period of the applied square wave. The trapped time can be obtained from the graph by Donnelly[47] giving the Probability of Escape for each species of ion. The trapped ions produce a space charge reducing the reverse field over the length λ, thus increasing the effective trapping diameter and producing even more trapping in the region. The effect avalanches into the trapping of a large number of the ions a distance λ inside the turbulent region. Further ions are stopped at this point by the reverse field produced by the trapped charge and probably fail to be trapped themselves because all trapping sites are occupied. At the beginning of the next forward pulse then, ions begin moving towards the collector from a point $(d_c - \lambda)$ inside the grid-collector space. The trapped charge also increases the forward field. The free ions therefore reach the collector in a shorter time due to:

(i) The reduced path length $= L_o - d_c + \lambda = L_{eff}$

where L_o = grid-collector separation

(ii) The increased field due to trapped charge

It is postulated that near to the grid there is a high density of trapped ions reducing the forward field to almost zero. The effective field in the region of free flight of the ion will then be

$$E_{eff} = E_o \cdot \frac{L_o}{L_o - d_c + \lambda} \qquad \text{---------- (2h)}$$

where E_o = Field for zero heat input

and the flight time of ions over the distance $L - d_c + \lambda$ will be

$$t_{eff} = \frac{(L_o - d_c + \lambda)^2}{\mu E_o \cdot L_o} \qquad \text{---------- (2i)}$$

The apparent ion velocity

$$= \frac{\text{Grid-Collector Separation}}{\text{Apparent Flight Time}} = \frac{L_o}{t_{eff}}$$

$$= \frac{\mu E_o L_o^2}{(L_o - d_c + \lambda)^2} \qquad \text{---------- (2j)}$$

The Ion Mean-Free-Path Between Trapping on a Vortex Line

It can easily be shown (See Appendix 4) that the mean-free-path λ for an ion in a regular array of vortex lines of density 'n' cm^{-2} and trapping diameter σ is $\lambda = \frac{1}{n\sigma}$. In the present experiment the turbulence is considered to be a regular array of vortex lines spreading slowly into the grid-collector space. The density n (L) of vortex lines is a function of the distance from the grid. Assuming the vortex lines spread out uniformly from the grid $n(L) = n_g \left(\frac{g}{\pi L}\right)$ ---------- (2k)

where g = grid-hole diameter

L = distance from grid

n_g = density of vortex lines at grid

The mean-free-path between trapping is then also a function of L.

$$\lambda(L) = \frac{1}{n(L)\sigma} = \frac{1}{n_G \sigma} \left(\frac{\pi L}{G}\right) \qquad (2l)$$

The value of n_G, the vortex line density at the grid, is considered constant independent of heat input. At higher heat inputs the turbulence spreads more rapidly into the grid-collector space and the vortex line lattice maintains approximately the same spacing.

The average mean-free-path $\bar{\lambda}$ from

$L = d_c$ to $L = d_c - \bar{\lambda}$ is

$$\bar{\lambda}(L) = \frac{1}{n_G \sigma} \frac{\int_{d_c - \bar{\lambda}}^{d_c} \left(\frac{\pi L}{G}\right) dL}{\bar{\lambda}} \qquad (2m)$$

Integrating gives

$$\bar{\lambda}(L) = \frac{1}{n_G \sigma}\left(\frac{\pi d_c}{G} - \frac{\pi \bar{\lambda}}{2G}\right) \qquad (2n)$$

and $$\frac{\bar{\lambda}}{d_c} = \frac{k/\sigma}{1 + k/2\sigma} \quad \text{where} \quad k = \frac{\pi}{G n_G} \qquad (2p)$$

A comparison between the values of trapping diameter σ can be obtained from the various results of Donnelly.[47] Since only one mean-free-path between trapping is considered here, the term e^{-Pt} related to the probability of escape need not be considered. The comparative (not absolute) values of trapping diameters obtained from Donnelly's results are:

Negative ion	120 V/cm.	10	} arbitrary units.
Negative ion	30 V/cm.	4	
Positive ion	120 V/cm.	3.1	
Positive ion	20 V-cm.	0.9 ?	

Because of the large uncertainties in the absolute values of n and σ the method can only be used to compare the effects of turbulence on positive and negative ions and to predict the dependence of the apparent ion velocity on heat input.

As a typical starting point the apparent velocity of positive ions at 120 V/cm. for a heat input of 10 mW was 833 cm.sec.$^{-1}$, while for zero heat input the ion velocity was 750 cm.sec.$^{-1}$. This result substituted in equation (2j) yields $\bar{\lambda}$ which is taken with the graphically determined value of d_c to give the ration $\frac{\bar{\lambda}}{d_c}$ which is then substituted into equation (2p) to obtain a value for $\frac{k}{\sigma}$. Other values of $\frac{k}{\sigma}$ for different fields and for negative ions are obtained by substituting the appropriate value of σ.

Using these values of $\frac{k}{\sigma}$, and performing the above calculations in reverse, the apparent ion velocities are obtained. The calculated velocities shown in Fig. (20) agree reasonably well with the experimental results, both with regard to the different behaviour of positive and negative ions and for the field dependence of each ion.

N.B. PAGES 84 – 86 inc OF ORIGINAL THESIS REMOVED.

Velocity of n-fluid through grid	Velocity of ions v_i cm/sec.	Δv_i	Critical Velocity v_c cm/sec.	Δv_c
0	500 ± 5	0	520 ± 5	0
20 3·3 cm/sec	532	32 ± 10	530	10 ± 10
48 8·0	556	56	565	45
80 13·3	560	60	570	50
100 16·7	576	76	535	15

Runs October 8th, October 15th, October 13th, December 22nd, 1964.

where $\Delta v_i = v_i - 500$ cm/sec.

$\Delta v_c = v_c - 520$ cm/sec.

Effect of n-fluid Flow on Ion Velocity and on Ion Critical Velocity

TABLE IV

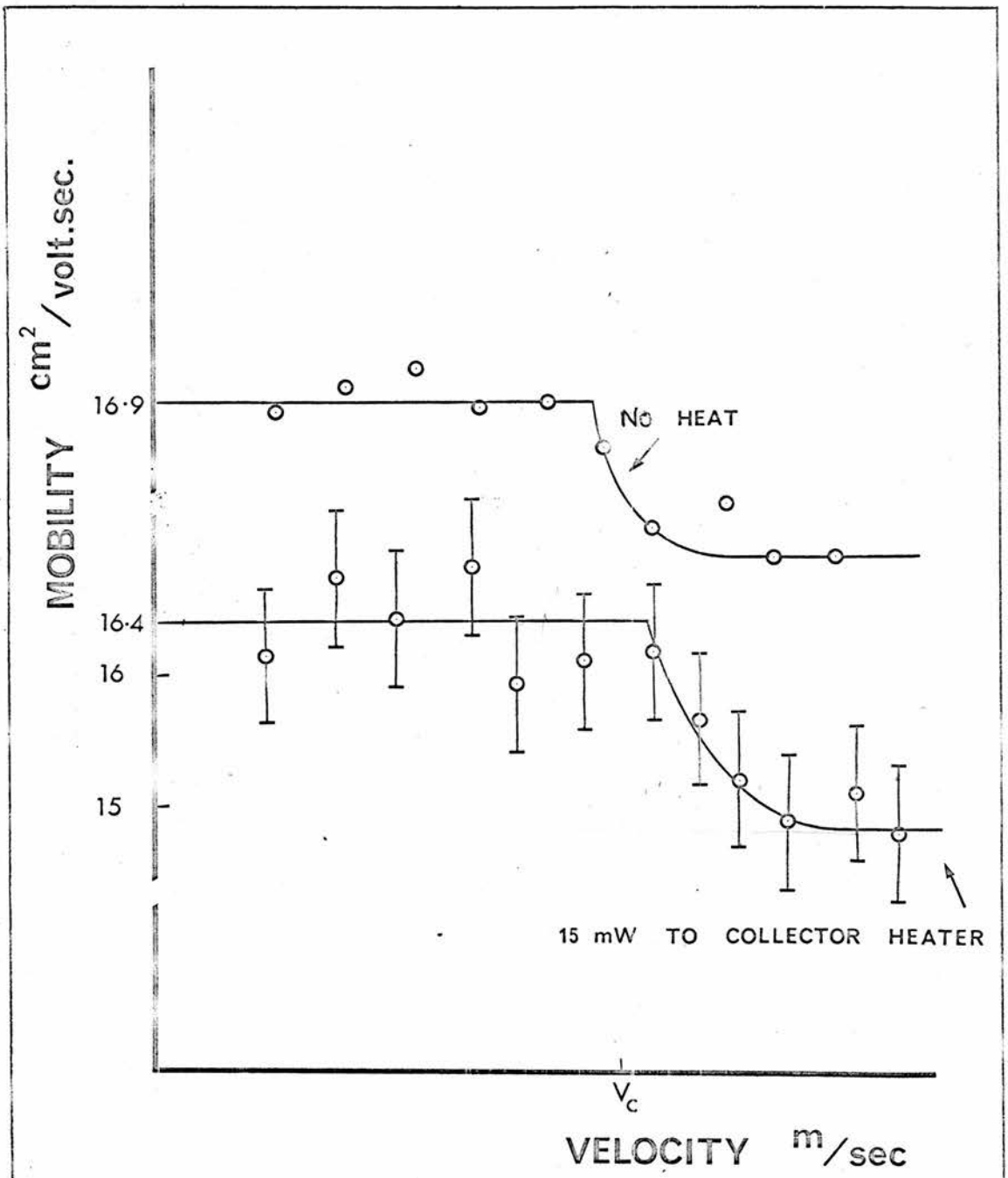
MOBILITY cm²/volt.sec.
16·9
16·4
16
15
No HEAT
15 mW TO COLLECTOR HEATER
Vc
VELOCITY m/sec

Fig. 24.

The Effect of Trapping on the Ion Critical Velocity

When n-fluid flowed towards the source, four runs showed no consistent change in the critical velocity for positive ions. Fig. 24 shows a noticeable change in v_c. However two runs showed a decrease in v_c, and two runs showed an increase in v_c. When n-fluid flowed towards the collector, a slight enhancement of the critical velocity less than the enhancement of ion drift velocity, was observed in five out of six runs, (Fig. 25 and Table IV.) These results are explained in the following way:-

The trapped ions close to the grid constitute a space charge which enhances the field in that region of the measuring space where the ions move freely. The measured flight time of the ions will then be affected in two ways.

(a) Trapping shortens the effective flight path, thus reducing the measured flight time and giving an apparent velocity increase.

(b) Trapping causes a space charge to build up close to the grid which enhances the field and shortens the measured flight time. This produces a real increase in ion velocity.

When translated to the velocity-field curves (a) enhances the apparent critical velocity at constant field and (b) enables the ion to reach the critical velocity at a lower applied field than if no trapping occurred. This explains the experimental observation (i) that the increase in critical velocity for a given heat input was less than the apparent increase in drift velocity. Table IV shows the comparison between the apparent increase in ion drift velocity and critical velocity enhancement.

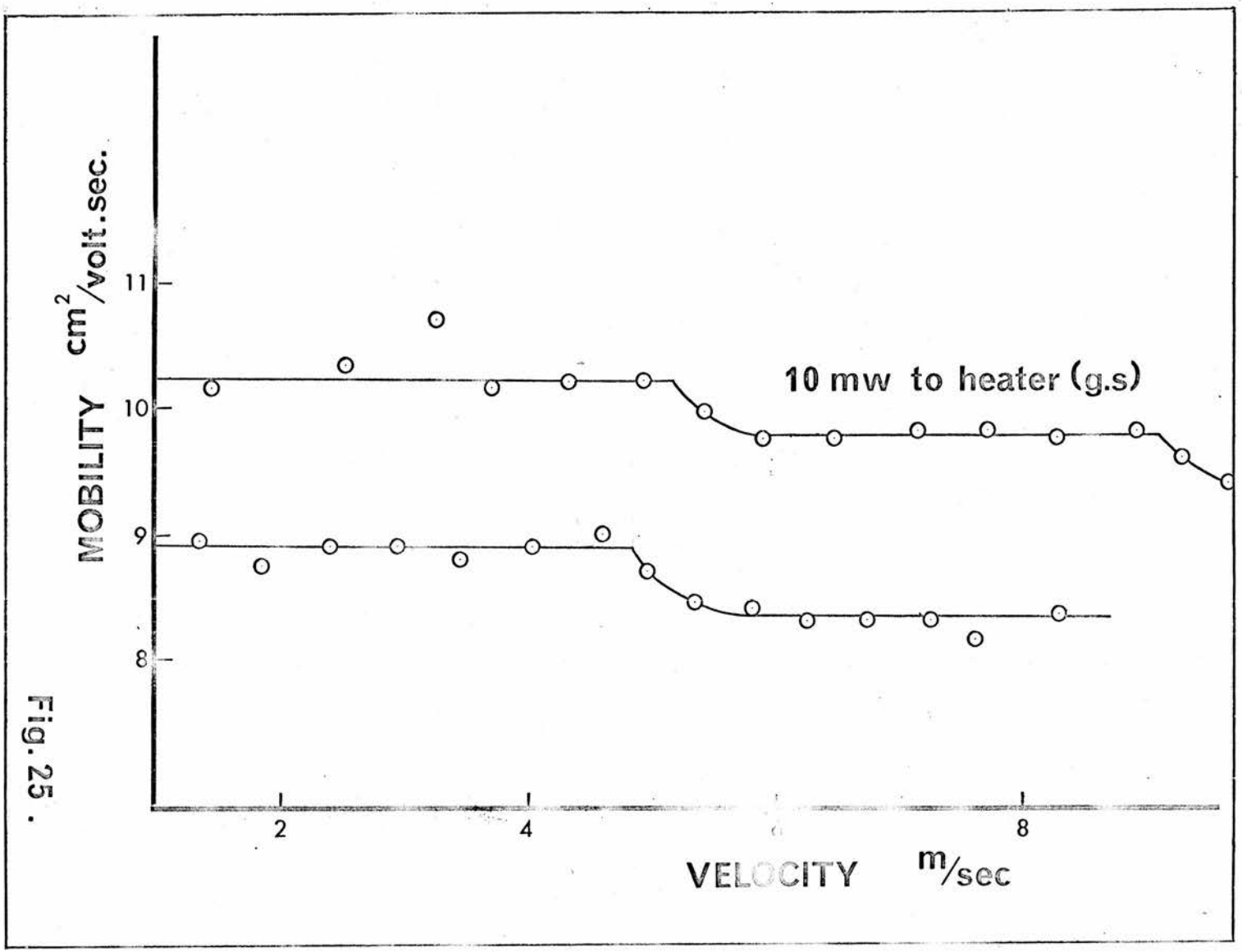
MOBILITY cm²/volt.sec.
11
10
9
8
10 mw to heater (g.s)
2
4
8
VELOCITY m/sec

Fig. 25 .

n-fluid Flow towards the Source

n-fluid flowing in the opposite direction to the ions had only a small effect on either the drift velocity or the critical velocity of the ions. It is assumed that classical turbulence occurs in the form of vortex rings formed in the grid holes. This turbulence is then carried into the grid-source space. In the grid-source region there is a steady electric field accelerating ions towards the grid, therefore trapping of the ions will merely delay their arrival at the grid, and produce a space charge close to the grid. This would reduce the amount of current arriving at the grid but would not affect the velocity of the ions in the measuring space.

Effect of Very Low Heat Inputs

On all the velocity-heat input curves for n-fluid flow towards the collector, there was an initial rapid increase in ion velocity levelling off to a steady dependence for heat inputs in excess of 5 mW. This initial increase is attributed to a straight-forward enhancement of ion velocity by n-fluid flow through the grid.

PAGE 92. REMOVED.

DISCUSSION

The periodic discontinuities in the drift velocity of ions in an electric field have not, at present, been explained satisfactorily. Careri[1] suggested initially that at the critical velocity, an ion creates a vortex ring in its wake. The vortex ring would have the dimensions of the ion and one quantum of circulation. Subsequent discontinuities correspond to vortex rings of the same dimensions as the first but having successive quanta of circulations. There are two main criticisms of this mechanism. They are:

(i) The kinetic energy of an ion at the critical velocity is insufficient to create a vortex ring of the dimensions of the ion. The energy of a vortex ring of radius 'r' and core radius 'a' is given by the classical hydrodynamic equation[31]

$$E = \frac{1}{2} \rho \kappa^2 r \left(\beta - \frac{7}{4}\right) \qquad \text{----------} \qquad (3)$$

where ρ = bulk liquid density

κ = circulation

$\beta = \log_e \frac{8r}{a}$

The radius of the positive ion is given by Kuper[11] to be 6.3Å. A vortex ring of radius 6.3Å and core radius 1Å has an energy of $= 10^{-14}$ ergs. This is a factor 10^2 more than the kinetic energy of the positive ion at 5 m/sec. In fact, the ion has insufficient energy to create a roton which, according to Feynmann[6] may be considered to be the smallest

conceivable vortex ring.

(ii) This mechanism does not predict the observed difference in the critical velocities for positive and negative ions.

The radius of a negative ion = 12.1Å; this is almost double that of the positive ion and is demonstrated by its lower mobility. Thus, the larger negative ion requires more energy to create a vortex ring in its wake. If the effective masses of the positive and negative ions are comparable, the negative ion would require more energy and therefore a higher velocity to create a vortex ring in its wake. This is contrary to experimental evidence. The critical velocity for positive ions is = 5 m/sec. and for negative ions = 2.1 m/sec.

Careri avoided the first of these difficulties by suggesting that the ions co-operated in the formation of vortex rings; several ions being involved in the creation of one vortex ring. The situation is analogous to the creation of a smoke ring by a fast moving stream of gas. On a phenomenological basis, one would expect a co-operative phenomenon to depend on the separation of the ions. The experiments in Rome were performed at different ion densities, and those at St. Andrews at a further different value, without affecting the position or magnitude of the discontinuity and, therefore, suggest that a co-operative phenomenon is not the answer.

The discontinuities occur at a well defined drift velocity and any proposed mechanism must explain why the drift velocity and not the instantaneous velocity of the ions is significant.

Careri suggested that the process by which an ion created a vortex

ring and therefore lost mobility, required a time very much longer than the time for one free path of the ion and thus the average velocity over several mean free paths is important. This point will be dealt with more fully later. (See appendix 5 and P. 121)

If it is assumed that the kinetic energy due to the ions drift velocity is dissipated at the discontinuity and goes into some definite energy state such as a vortex ring, then there is clearly another difficulty which must be accommodated in any new theory. The kinetic energy of the ion increases classically with the square of the velocity and here the vortex ring theory is successful in that the energy of a ring of given dimensions also increases as the square of the circulation (Equation 3.) This suggests, at first sight, that any new system of energy states must show a dependence on the square of some quantity. This is shown later to be an unnecessary condition, (Page 109).

The giant discontinuity in the drift velocity of the positive ions at = 28 m/sec. observed by Careri[2], has now been ascribed by him to the creation of a vortex ring which then remains bound to the ion. The hyperbolic fall/of velocity for fields greater than that at which the ion attains 28 m/sec., (i.e. $vE \approx$ constant) is consistent with this picture and comparable to the hyperbolic dependence of drift velocity on energy of ions at $0.3^{\circ}K$ observed by Rayfield and Reif.[7] Moreover the energy of the ion at this velocity is sufficient to create a roton. That the giant discontinuity at 28 m/sec. corresponds to the creation of a roton by the ion, tends to emphasize the improbability of the discontinuity at 5 m/sec. being explained by the same mechanism.

To summarise the present position - the vortex ring theory of Careri does not account successfully for the periodic discontinuities, because the ion has insufficient energy to create the smallest vortex ring and does not explain the difference in critical velocities for positive and negative ions. Any new theory must satisfy the energy conditions, explain the periodicity of the discontinuities and the difference between the critical velocities for positive and negative ions.

Huang and Olinto[42] have overcome some of these difficulties by postulating that at the critical velocity an ion feeds energy from the field into turbulence until a vortex ring of unit circulation is created. Their theory does not predict an absolute critical velocity but does account for the difference between positive and negative ion critical velocities. A detailed review and criticism appears in the literature survey, Page 168 .

Model Proposed

The model proposed here, which the author claims satisfies these conditions, is based on the concept of a vibrating ion. The ion is excited by collision, at its critical velocity, into a vibrational state and subsequently emits a phonon.

The drop in mobility at the critical velocity corresponds to the loss of the kinetic energy of the ion and a gain of vibrational energy.

Franck-Hertz Analogue

The process is analogous to the classical Franck-Hertz process where inelastic electron-molecule collisions excite vibrational energy states

in the molecule which then decay by photon emission. In the Franck-Hertz experiment*, when the electric field is increased, the current traversing the cell increases until the electrons acquire sufficient energy to excite the first vibrational state of the molecules. The electrons are stopped when they excite a molecule and this manifests itself as a drop in current across the cell. A further drop in current is observed when the electron has sufficient energy to excite two molecules in successive collisions, i.e. there is twice the probability of excitation. Similarly the second discontinuity for the ions occurs when the ion has sufficient momentum to be excited at two successive collisions. (See Fig. 28)

Positive and negative ions differ in size and structure and therefore their vibrational energy levels are different. This gives the required difference in critical velocity.

Calculation of Fundamental Vibrational Frequencies

The fundamental frequency of oscillation of an ion may be calculated in three different ways. The ion can be considered as (i) a solid sphere of known dimensions and bulk modulus, or as (ii) a liquid drop where surface tension is the governing parameter, or as (iii) a sound resonator.

(i) From a dimensional argument, the frequency of vibration of a solid sphere of radius R and bulk modulus K and density ρ is

$$\gamma = \frac{X}{R}\left(\frac{K}{\rho}\right)^{\frac{1}{2}} \qquad \text{.....} \qquad (4)$$

where X = constant ~ 1

* See for Example 'Principles of Modern Physics' French, A. P. (Wiley) P. 119

taken to be 11

The radius of the positive ion is/6.3Å and the bulk modulus[8] of the solid 0.7×10^{9} dynes cm^{-2}. The value for the density is somewhat difficult to choose as, due to electrostriction, the atoms composing the ion are probably more closely packed than in the normal solid. The density of the core of the ion suggested by the diagram in 'Atkins'[9] paper would be of the order of 2.5 $gm.cm^{-3}$. The ratio Effective Mass to Apparent Volume, gives a density of ~ 0.7 $gm.cm^{-3}$ for the positive ion. This, however, gives an average density for the whole ion; the core may be considerably denser than this. Substituting the value $\rho = 2$ into equation (4), the fundamental frequency of vibration is 3×10^{11} c/s.

(ii) The ion can also be treated as a liquid drop in the same way that vibrational states are calculated for the nucleus. The nucleus is treated as a spherical harmonic oscillator with collective modes of motion. The equation giving the frequency of vibration[10] is

$$\gamma = \left[\frac{4\pi\sigma}{3M}\, \ell(\ell - 1)(\ell + 2)\right]^{\frac{1}{2}} \text{ ---------} \qquad (5)$$

where M is the mass of the drop and σ the surface tension. The mode $\ell = 1$ corresponds to displacement of the drop as a whole and hence $\gamma = 0$ for this value. $\ell = 2$ corresponds to the fundamental mode of vibration. Substituting values for $\sigma = 0.35$ ergs/cm. and $M^{+} = 100\ m_{He}$ gives a fundamental frequency of vibration of $\underline{1.2 \times 10^{11}\ c/s}$. The value of surface tension is not necessarily appropriate for an ion.

(iii) The third method for estimating the fundamental frequency of vibration, is to treat the ion as a spherical acoustic resonator. Then for the fundamental frequency the wavelength is equal to the circumference of the ion. The vibration is, in fact, a wave on the surface of the ion. The frequency may be obtained from this, using the equation $c = \gamma\lambda$, where c = the velocity of sound in the ion and λ = wavelength. The velocity of sound in the ion is taken as $\simeq$ velocity of sound in the bulk liquid; in the ion the sound velocity may be higher than this. The vibrational frequencies obtained from this model are $\gamma^{+} = 0.6 \times 10^{11}$ c/s. and $\gamma^{-} = 0.32 \times 10^{11}$ c/s. The particular value of this model is that although the absolute values of the vibrational frequencies are not reliable, the comparison between the frequencies of vibration for the positive and negative ions is directly connected to their sizes and, therefore, probably correct. If the velocity of sound in solid helium^{43} is substituted, the vibrational frequencies obtained are

$$\gamma^{+} = 3 \times 10^{11} \text{ c/s. and } \gamma^{-} = 1.6 \times 10^{11} \text{ c/s.}$$

These three methods are not entirely independent since, for instance, the velocity of sound depends on the density and the bulk modulus of the liquid. The range of values for the fundamental vibrational frequency of the positive ion from the three different models is $0.6 \longrightarrow 3 \times 10^{11}$ c/s. The uncertainty in the values of the surface tension, velocity of sound, bulk modulus and density, accounts for the variation in the frequencies obtained. The energies of the lowest vibrational states for the positive and negative ions is then

$$E^{+} = h\gamma^{+} = 4 \longrightarrow 20 \times 10^{-16} \text{ ergs.}$$
$$E^{-} = h\gamma^{-} = 2.1 \longrightarrow 10 \times 10^{-16} \text{ ergs.} \qquad \text{--------- (6)}$$

Where h = Planck constant

Multiplying the frequencies obtained by Planck's constant to obtain the energy, is justified only if it is understood that the values obtained are the lowest energies possible. For example, the energy of a vibrating tuning fork is considerably in excess of the product of Planck's constant and the frequency. However, neither the tuning fork nor the vibrating ion can have energy less than $h\gamma$.

The lower energy values obtained from the acoustic resonator model agree best with the available energies.

For comparison, it is interesting to compare Kuper's[11] calculations for the fundamental frequency for radial pulsations of the 'bubble' model of the negative ion. He does this by finding the 'potential' term in the Hamiltonian for the oscillations. This is of the form $\frac{1}{2} \underline{m} \gamma^2 x^2$, where γ is the frequency, x the amplitude of oscillation and $\underline{m}$ the total mass of the vibrating atoms. We need the coefficient of x^2 in the Taylor expansion of the bubble energy E. Now the pressure at the ion

$$p = \frac{\delta E}{\delta V} = \frac{1}{4\pi r^2} \cdot \frac{\delta E}{\delta r} \qquad \text{---------- (7)}$$

$$\therefore \frac{\delta E}{\delta r} = 4\pi r^2 p(r)$$

In the paper quoted, Kuper lists three contributions to the pressure at the ion; they are

(i) Pressure due to van der Waals' attractions

$$p_{v.d.W} = -38 \left(1 - \frac{d^2}{r^2}\right) \qquad \text{(8)}$$

where d is the mean interatomic distance = 3.6Å.

(ii) Electrostatic interaction gives a pressure

$$p_{e.s.} = \frac{5.2 \times 10^4}{r^4} \text{ atm. Å}^4 \qquad \text{(9)}$$

and

(iii) There is an outward pressure due to the kinetic energy of the electron

$$p_{kin.} = \frac{7.9 \times 10^6}{r^5} \text{ atm. Å}^5 \qquad \text{(10)}$$

The pressure at the bubble wall is then

$$p_o = p_{kin} - p_{v.d.W} - p_{e.s.} \qquad \text{(11)}$$

Substituting the value of p_o in Equation 11 and differentiating with respect to r, gives

$$\frac{\delta^2 E}{\delta r^2} = 10^3 r + \frac{3 \times 10^8}{r^4} - \frac{13 \times 10^5}{r^3} \qquad \text{(12)}$$

The equilibrium value for r_- = 12.1Å, calculated by Kuper[11], gives

$$\frac{\delta^2 E}{\delta r^2} = 2.5 \times 10^4 \text{ atm.Å} = 2.5 \times 10^2 \text{ dynes cm}^{-1}$$

'Intrinsic' energy Δ of a roton = 12.3×10^{-16} ergs.

Kinetic energy of a roton at $1^{\circ}K = \frac{1}{2}kT$ = 0.7×10^{-16} ergs.

This value for the kinetic energy of a roton is the most probable value at temperature T. *

	Positive Ion $\times 10^{+16}$ ergs.	Negative Ion $\times 10^{+16}$ ergs.
Energy of vortex ring of same diameter as ion with a core radius = 1Å	96	240
Energy of fundamental modeof vibration of ion		
(i) Spherical harmonic oscillator	20	(40)
(ii) Liquid drop model	⟵ (7.9) ⟶	
(iii) Acoustic resonator	4.0	2.1
(iv) Kupers' radially pulsating 'bubble'		4.0
Kinetic energy of ion at v_c for effective mass = 100 m_{He} 1	0.87	0.19

TABLE V

(40) in brackets because formulae for frequency of oscillation of spherical harmonic oscillator is for a solid sphere in contrast to the negative ions bubble structure.

(ii) 7.9 may apply to the positive ion or the negative ion, but not both.

This gives

$$\gamma^2 = \frac{1}{m} \frac{\delta^2 E}{\delta r^2} \sim 4 \times 10^{23} \ c^2 \ \text{sec.}^{-2}$$

for $m = 100 \ m_{He}$.

This gives $\gamma_- = 6 \times 10^{11}$ c/s. which is an order of magnitude higher than the estimate from the acoustic resonator model. This result is expected since radial pulsations would have a higher frequency than surface waves.

The energies of excitation obtained from the three models proposed are between 5 and 30 times less than the energy of a vortex ring of the dimensions of the ion, and therefore, make the excitation of vibrational states a more probable process than the creation of a vortex ring. Table V shows how the energies from the various models compare with the energies of vortex rings, rotons and the kinetic energy of the ion, due to its drift velocity. The kinetic energy of the ion is still low but is at least of the same order as the vibrational energy necessary.

Excitation Processes

The collision processes by which the ion could be excited into a vibrational energy state have been studies with regard to the conservation of energy and momentum. The processes which have been considered are:-

(i) ion + roton $\longrightarrow$ vibrating ion $\longrightarrow$ phonon + ion

(ii) ion + phonon $\longrightarrow$ roton + ion

(iii) ion + phonon $\longrightarrow$ phonon + ion

(iv) ion + thermal roton $\longrightarrow$ stationary roton + vibrating ion

$\longrightarrow$ ion + phonon

It will be shown that (iv) is the most probable process.

(i) Ion + roton → vibrating ion → ion + phonon

In this collision the ion destroys the roton, takes up its energy into a vibrational state and then decays by the emission of a phonon of the same frequency as the vibrating ion. For the positive ion, where $m^{+}_{eff} = 100\ m_{He}$, the energy and momentum conservation equations at the first discontinuity are:

$$\tfrac{1}{2}mv_c^2 + (\Delta + \tfrac{1}{2}kT^{*}) \rightarrow E_v + \tfrac{1}{2}mv'^2 \rightarrow E_p + \tfrac{1}{2}mv''^2 \quad \text{..... (13)}$$

$$mv_c - (p_o + p) \rightarrow mv' \rightarrow \frac{E_p}{u} + mv'' \quad \text{..... (14)}$$

where E_v is the energy of vibration, E_p the emitted phonon energy, u the velocity of first sound in the liquid. The energy, and hence the frequency of the emitted phonon, can be calculated from these equations. $E_p \sim \Delta = 13 \times 10^{-16}$ ergs. since $\tfrac{1}{2}mv_c^2 \ll \Delta$ and $u_1 \gg v''$. This gives a vibrational energy $\sim 14 \times 10^{-16}$ ergs. and frequency 2×10^{11} c/s. This corresponds to a wavelength of 12Å, a length comparable to the positive ion diameter.

The main criticisms of this process are:

(a) The fundamental vibrational states for the positive and negative ions would have approximately equal energies. This would imply equal vibrational frequencies for the two ions, a situation which is difficult to correlate to their different sizes and structures.

(b) Since $\tfrac{1}{2}mv_c^2 \ll \Delta$, the process could presumably occur when a slower moving ion collides with a slightly more energetic roton. This would result in an indistinct discontinuity, in contrast with the observed sharp discontinuity.

---

*Average roton thermal energy. (Rice - Proc. 9th Int. Conference on Low Temp. Phys. P.89)

(c) At discontinuities beyond the first, the value of $E_v = \frac{1}{2}mv^2 + \Delta$ are far from periodic. The observed periodicity must then be a direct result of momentum conservation only. An ion going at $2v_c$ has enough momentum to perform the above process twice in succession. This, however, requires that at the first discontinuity, the ion be brought to rest $v'' = 0$ at an inelastic collision. This condition does not fit the energy momentum equations (13, 14) unless the effective masses are adjusted.

(ii) Ion + phonon $\rightarrow$ roton + ion

This process is the reverse of (i). Here an ion absorbs a phonon and then has enough energy to create a roton. The phonon would need to be of the same frequency as the fundamental frequency of vibration of the ion. The first discontinuity occurs when the energy-momentum conservation equations are satisfied

$$\frac{1}{2}mv_c^2 + E_p = \Delta + \frac{1}{2}mv'^2 \qquad \text{(15)}$$

$$(0.9 + 11.4 = 12.3 + 0.04) \times 10^{-16} \text{ ergs.}$$

$$mv_c + \frac{E_p}{u_1} = p_o + mv' \qquad \text{(16)}$$

$$(3.33 - 0.48 = 2.1 + 0.75) \times 10^{-19} \text{ grm.cm/sec.}$$

This process shows the same inconsistency as its converse (i).

To satisfy energy, momentum and periodicity conditions, and to give the observed critical velocities for positive and negative ions

$$v' = 0, \quad m^+_{eff.} = 80\, m_{He} \quad \text{and} \quad m^-_{eff.} = 160\, m_{He}$$

See Page 119 for a discussion of the meaning of the effective mass.

The absorbed phonons are of nearly equal energy and therefore equal frequencies, which does not agree with the difference in fundamental frequencies of vibration for positive and negative ions. Periodicity is obtained in the same way as (i). In discontinuities beyond the first there is a small amount of energy in excess of that needed to create a roton. This could go to the kinetic energy of translation of the roton.

(iii) Ion + phonon $\longrightarrow$ phonon + Ion

This process is not simple scattering, but the conversion of a phonon of one wavelength into a phonon of a different wavelength. The incident and emitted phonon need not be of the same frequency. Because of the Doppler Effect a phonon, approaching the ion head-on, would appear to have a higher frequency than its frequency in the laboratory frame. This means that the ion could absorb a phonon having a frequency slightly less than its fundamental vibrational frequency. If the ion then re-emits the phonon forwards, this phonon will appear to a stationary observer to have a frequency slightly higher than the vibrational frequency and, overall, the ion will have lost energy. There is an upper limit to the allowed frequency for phonons, corresponding to the Debye cut-off wavelength. At the critical velocity, phonons with the maximum frequency are just capable of being absorbed. The momentum of such a high energy phonon is sufficient to 'stop' the ion when it is re-emitted in a forward direction. However, it would seem rather a coincidence that, at the critical velocity, the ion should have momentum equal to twice the phonon momentum and that the appropriate energies should be correct. Moreover, at velocities above the critical velocity, the ions can interact with an

increasing number of phonons and this would suggest a monotonically decreasing mobility beyond the critical velocity. Also, at $1^{o}K$, there can be very few phonons with energy near the Debye cut-off. The calculation of v_c for the ions is as shown

Frequency of phonon at Debye cut-off wavelength = 4.25×10^{11} c/s

Phonon Energy = 28×10^{-16} ergs. Momentum = 1.15×10^{-19} dyne.sec.

Apparent frequency of phonon to ion travelling at 5 m/s when two approach head-on = $\frac{245}{240} \times 4.25 \times 10^{11} = 4.34 \times 10^{11}$ c/s

N.B. Phonon velocity = 240 m/sec.

Frequency of emitted phonon $\frac{245}{240} \times 4.34 \times 10^{11}$ c/s = 4.43×10^{11} c/s.

Energy loss by ion = $h(4.43 - 4.25) \times 10^{11} = 1.2 \times 10^{-16}$ ergs.

Momentum loss by ion = 2.3×10^{-19} dyne.sec.

Energy conservation equation:

$$\tfrac{1}{2}mv_c^2 - \tfrac{1}{2}mv'^2 = 1.2 \times 10^{-16} \text{ ergs.}$$

Momentum conservation:

$$mv_c - mv' = 2.3 \times 10^{-19} \text{ dyne.sec.}$$

If $m_{eff} = 100\ m_{He}$ is substituted in these equations a critical velocity of 680 cm/sec. is predicted. This result must, of course, be fed back to the point where the apparent frequencies of absorbed and emitted phonons were calculated. If this is done repeatedly, the predicted ion critical velocity $\approx$ 10 m/sec.

(iv) Ion + thermal roton $\longrightarrow$ vibrating ion + roton $\longrightarrow$ ion + phonon

In this process the roton is not destroyed but merely dethermalised by the colliding ion. It is shown later/that the maximum energy becomes P.109 available for the excitation of vibrational states when the ion makes a head-on collision with a roton in which the rotons momentum p_o is reversed in direction. At the critical velocity, the kinetic energy of the ion and the thermal energy of the roton are sufficient to excite the fundamental vibrational mode of the ion. Subsequently the ion emits a phonon. If the energy momentum equations are calculated for the emission of a phonon when a roton and ion collide, it is found that the instantaneous emission of a phonon, without the vibrating ion intermediate state, is possible for the positive ion, but not for the negative ion because, in this case, in order to satisfy conservation laws, the recoil velocity of the ion would be greater than its initial velocity. Although there is no 'a priori' reason why this should not be so, the maximum amount of energy cannot be obtained from the system when this occurs. When a positive ion of mass = 100 m_{He} collides at 5 m/sec. with a roton, the phonon emitted in the forward direction has a wavelength of $\sim$ 100Å.

Since (iv) is the most likely process, the dynamics of ion-roton collisions will now be discussed.

The Dynamics of Ion-Roton Collisions

In order to find the critical velocity at which excitation of the ion can occur, it is necessary to determine the collision conditions which make available the maximum amount of energy. A 'head-on' collision with a roton in which the momentum of the roton is reversed, allows the

maximum loss of momentum by the ion and, provided the ion momentum $mv > 2p_o$, the maximum loss of kinetic energy. Conservation of momentum gives:

$$mv - 2p_o = mv' \quad \text{---------- (17)}$$

Where mv, mv' = ion momentum before and after collision

p_o = roton 'intrinsic' momentum

Since the maximum amount of energy available at a collision is required, the kinetic energy, $\frac{1}{2}$ kT, of the roton must be taken into account. If this is capable of being absorbed into the excitation, then the total energy available is

$$E = \frac{1}{2} m(v^2 - v'^2) + (\tfrac{1}{2}) kT \quad \text{---------- (18)}$$

Substituting from (17)

$$E = 2p_o v + (\tfrac{1}{2}) kT - \frac{2p_o^2}{m} \quad \text{---------- (19)}$$

The mass of the positive and negative ions is $\sim 100\ m_{He}$. This gives $\frac{2p_o^2}{m} \approx (\frac{1}{2})$ kT, where $\frac{2p_o^2}{m} = 1.2 \times 10^{-16}$ ergs. and $\frac{1}{2}$ kT $= 0.7 \times 10^{-16}$ ergs. This result is purely coincidental and implies that the maximum energy available is approximately proportional to the incident velocity of the ion. The first discontinuity will occur when $2p_o v = E_o$, the energy of the fundamental mode of vibration. Subsequent discontinuities will occur at integer multiples of the first critical velocity and correspond to the higher modes of vibration. The velocity separation of the discontinuities is thus predicted from the dynamics of ion-roton collisions, but the 'strict' periodicity is then purely a coincidence of the near equality of $\frac{2p_o^2}{m}$ and $(\frac{1}{2})$

The experiments have been performed at temperatures in the range 0.85°K - 1.0°K and no measurable change in v_c observed. This is to be

ℓ	$\ell(\ell - 1)(\ell + 2)^{\frac{1}{2}}$	Normalised Energy Available from Inelastic Collisions with Rotons	
		-ve ions	+ve ions
2	2.8	3.5	2.5
3	5.5	5.3	5.7
4	8.5	8.3	8.1
5	11.8	11.8	12.2
6	15.5	15.4	15.5
7	19.5	18.9	-

Comparison of Energy Available with Energy Necessary for the Excitation of Vibrational States

TABLE VI

expected since $\frac{2p_o^2}{m} - (\frac{1}{2})\ kT \ll 2p_o v_c$ for this range of temperatures, particularly in the case of the positive ions where $v_c = 5.2$ m/s.

For the negative ions both mv_{c_1} and $mv_{c_2} < 2p_o$ and for the positive ions $mv_{c_1} < 2p_o$. Under these conditions a head-on collision of the type described would result in the ion being scattered backwards with a finite velocity, while the maximum amount of kinetic energy can be obtained from the ion if it is brought to rest by an oblique collision with a roton. In this case the energy available is simply:

$$\tfrac{1}{2}mv_c^2 + \tfrac{1}{2}\ kT \qquad \text{.....} \qquad (20)$$

Table VI shows how the energy available increases with increasing velocity for both positive and negative ions. The values are normalised to show the comparison with the values of $\ell(\ell - 1)(\ell + 2)^{\frac{1}{2}}$, the suggested sequence of vibrational energy states for $\ell = 2, 3, 4, \ldots\ldots$ The sequence of energy values fit well for the first six steps, but diverge somewhat thereafter.

The Giant Discontinuity

The giant discontinuity observed by Careri[2] for both positive and negative ions at a critical drift velocity of 25 - 30 m/s. is also explained well by this process. The energy available in a head-on collision with a roton, where the roton's momentum p_o is reversed, is almost exactly equal to the 'creation' energy Δ for a roton. The momentum and energy equations are:

$$mv - 2p_o = mv' + p_o \qquad \text{.....} \qquad (21)$$

(p_o: created roton)

$$E^* = \tfrac{1}{2}m(v^2 \,..\, v'^2) + \tfrac{1}{2}\,kT = 13 \times 10^{-16} \text{ ergs.} = \Delta \text{ -- (22)}$$

for $m_{eff} = 100\ m_{He}$ and $v_c^* = 28$ m/s.

Equal effective masses for positive and negative ions and the creation of one roton in each case, predicts the same critical velocity for the giant discontinuity as observed.

Reif and Rayfield[13] worked at lower temperatures, 0.3 - 0.6°K, where the mean free path of the ions between collisions with rotons is long, compared to their patch across the cell. It is not surprising then that they were able to observe velocities in excess of 30 m/s. up to 50 m/s., without the appearance of a giant discontinuity, since the creation of a roton at an ion velocity of 30 m/s. requires a collision with another roton. At 58 m/s. energy-momentum considerations make it possible for the ion to create a roton by itself.

Since rotons provide the main scattering centres for the ions, their particular properties will now be discussed.

Collisions with rotons

The mobility of the ions is derived mainly from scattering by rotons. It is therefore important to consider the effect of the following points:

(α) Density of rotons

(β) The effective mass of rotons in collisions

(γ) Variation of roton density with temperature

(δ) The thermal velocity of rotons

(ε) The analogy of a roton collision with a vortex ring collision.

(α) According to Atkins[14], the effective number density of rotons is

$$N_r = \frac{2\omega^{\frac{1}{2}} p_o^2 (kT)^{\frac{1}{2}} e^{-\Delta/kT}}{(2\pi)^{\frac{3}{2}} \hbar^3} \qquad \text{(23)}$$

where ω = effective mass for transport properties from neutron scattering data, p_o = momentum of a stationary roton and Δ = energy of stationary roton, i.e. roton at minimum of energy-momentum curve. At 1^oK the density of rotons is 0.9×10^{19} per cm. ^{3}.

The mean free path of ions between collisions with rotons is given by[15]

$$\lambda_{ir} = \frac{v_i}{\pi \theta^2 N_r (v_i^2 + v_r^2)^{\frac{1}{2}}} \qquad \text{(24)}$$

where θ = mean collision diameter

Substituting the value of N_r calculated above, the theoretical ion-roton scattering cross-section for the positive ion, and the thermal velocity of the rotons ($\sim$ 7200 cm/sec.) gives

$$\lambda_{ir}^+ = \frac{v_i}{21.6} \text{ Å} = 23\text{Å} \text{ at } v_i = 5 \text{ m/sec.}$$

It is better, because of the dependence of λ_i on v_i, to give a mean free time τ^+ between collisions.

$$\tau^+ = \frac{\lambda_{ir}}{v_i} = 4.6 \times 10^{-10} \text{ sec.} \qquad \text{(25)}$$

If this value is now substituted in the mobility equation derived from kinetic theory[16],

$$\mu = 0.815 \frac{e\lambda}{m_i v_i} \left(\frac{m_i + m_r}{m_r} \right)^{\frac{1}{2}} \qquad \text{(26)}$$

where m_r = mass of roton (See (β) P. 114)

the mobility of positive ions derived for 1°K is ~18 cm.^{2}sec.$^{-1}$volt^{-1}. This is a factor 3 higher than the observed mobility at these temperatures. The discrepancy can be attributed to two sources. Firstly the theoretical ion cross-section is taken as the actual physical cross-section of the ion; it is quite probable that the ion's influence on approaching rotons, extends well beyond its hard-core boundary. In order to account for the factor of 3, the positive ion radius would have to be 13Å. Alternatively the use of a simple kinetic theory equation which takes no account of the shortening of the mean-free-path due to the attractive forces, can affect the result.

(β) In the previous calculations the effective mass of the roton was taken as 0.26 m_{He}, a value obtained from neutron scattering experiments[17]. This assumes that only the thermal momentum of the roton is active in any collision and that p_o, the intrinsic momentum, is dormant. If, however, this is not true for ion-roton collisions and, in fact, the ion does interact with the velocity field of the roton such that p_o is affected, then a different effective mass $m^* = \frac{p_o^2}{2\Delta}$ should be considered. Then $m^* = 2.4\ m_{He}$. Substituting this value in equation (26) together with the mean-free-time calculated from the theoretical cross-section, gives $\mu_+ = 6.1$. This agrees well with the experimentally measured $\mu_+ = 5.9$ cm.^{2}sec.$^{-1}$volt^{-1}. (Ref. 3)

The corresponding calculation performed for negative ions gives $\tau = 2 \times 10^{-10}$ sec. and $\mu_- = 2.8$ cm.^{2}sec.$^{-1}$volt^{-1} compared to the experimentally determined value of $\mu_- = 3.6$ cm.^{2}sec.$^{-1}$volt^{-1}. (Ref. 3)

It is, of course, necessary to justify the use of different effective masses for ion and neutron scattering. It is difficult to produce any quantitative argument in favour of this, but it is postulated that fast small neutrons interact less easily with the intrinsic momentum p_o of a roton than a large slow moving ion. The neutron wavelengths $\lambda \sim 4\text{Å}$ used for the scattering experiments, are of the same dimensions as a roton, while both positive and negative ions are much larger. The analogy of a roton as a vortex ring helps to illustrate how the size of the incident particles influences the result of the collision.

(γ) Equations (23), (24), (26) predict that $\mu \propto \frac{e^{\Delta}}{T}$. Near $1^{\circ}K$ the exponential term is predominant. This agrees with the experimentally observed logarithmic dependence of mobility on temperature.

(δ) The condition necessary for the above equations to hold is that the ion velocity $\bar{v}_i \ll \bar{v}_r$ the thermal velocity of the rotons.

Now $\bar{v}_r = (2kT/\pi\omega)^{\frac{1}{2}}$, where ω is the effective mass of a roton. At $1^{\circ}K$ $\bar{v}_r \sim 7300$ cm/sec., therefore under the experimental conditions employed, $v_i \ll v_r$.

(ε) In calculating the mobility of the ions, rotons have been treated as ordinary particles. The excitation spectrum of liquid helium suggests that this is not entirely justified. Rotons correspond to the excitations near the minimum of the E-p curve and they have two properties, due to this position, which distinguishes them from ordinary particles.

(i) At the minimum rotons have zero velocity, since $\frac{\delta E}{\delta p} = 0$, but a finite momentum. The minimum occurs at an energy $\Delta = 8.9^{\circ}K$ and momentum

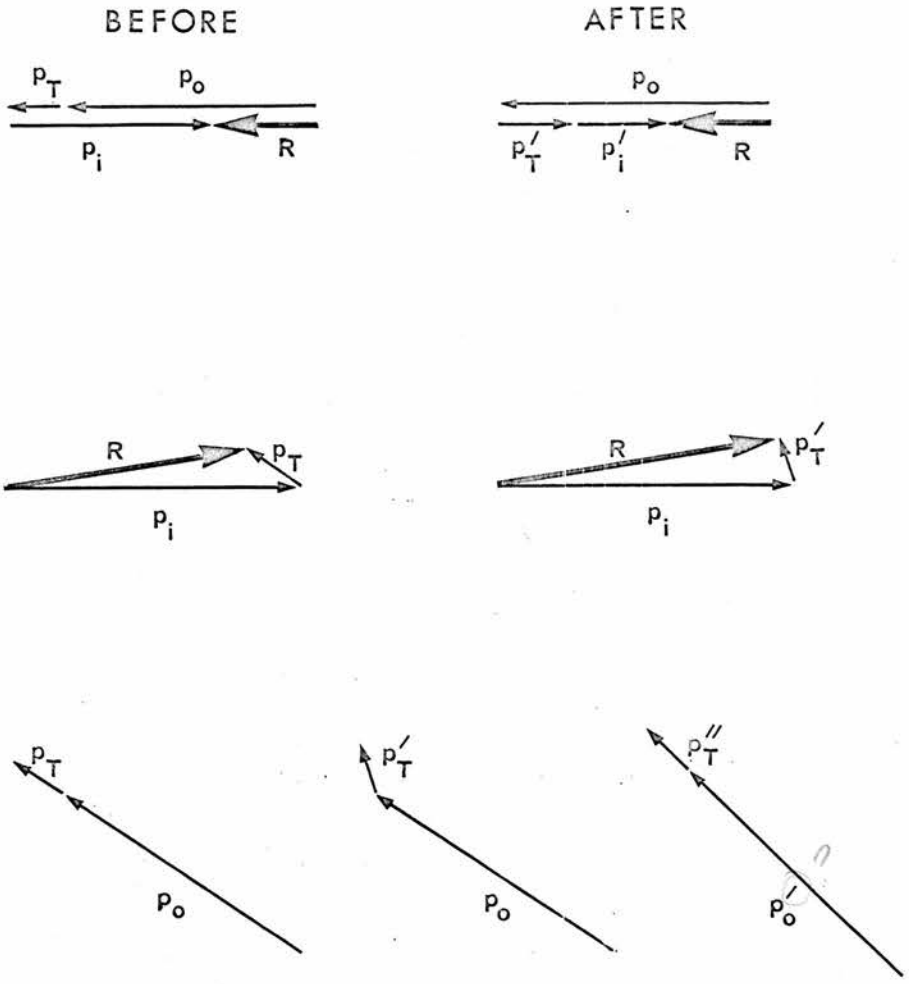

Ion-Roton Collisions at Subcritical Velocities

Fig. 26.

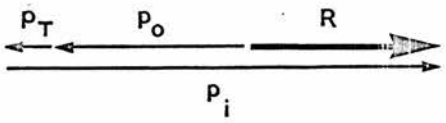

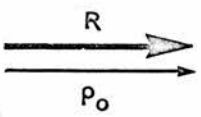

$p_T = 0$

$p_i' = 0$

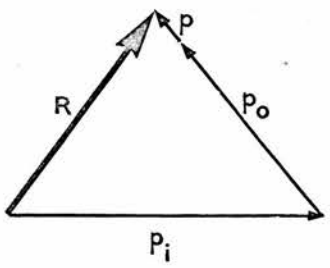

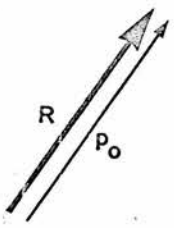

$p_T = 0$

$p_i' = 0$

Momenta for Exciting Collisions

Fig. 27.

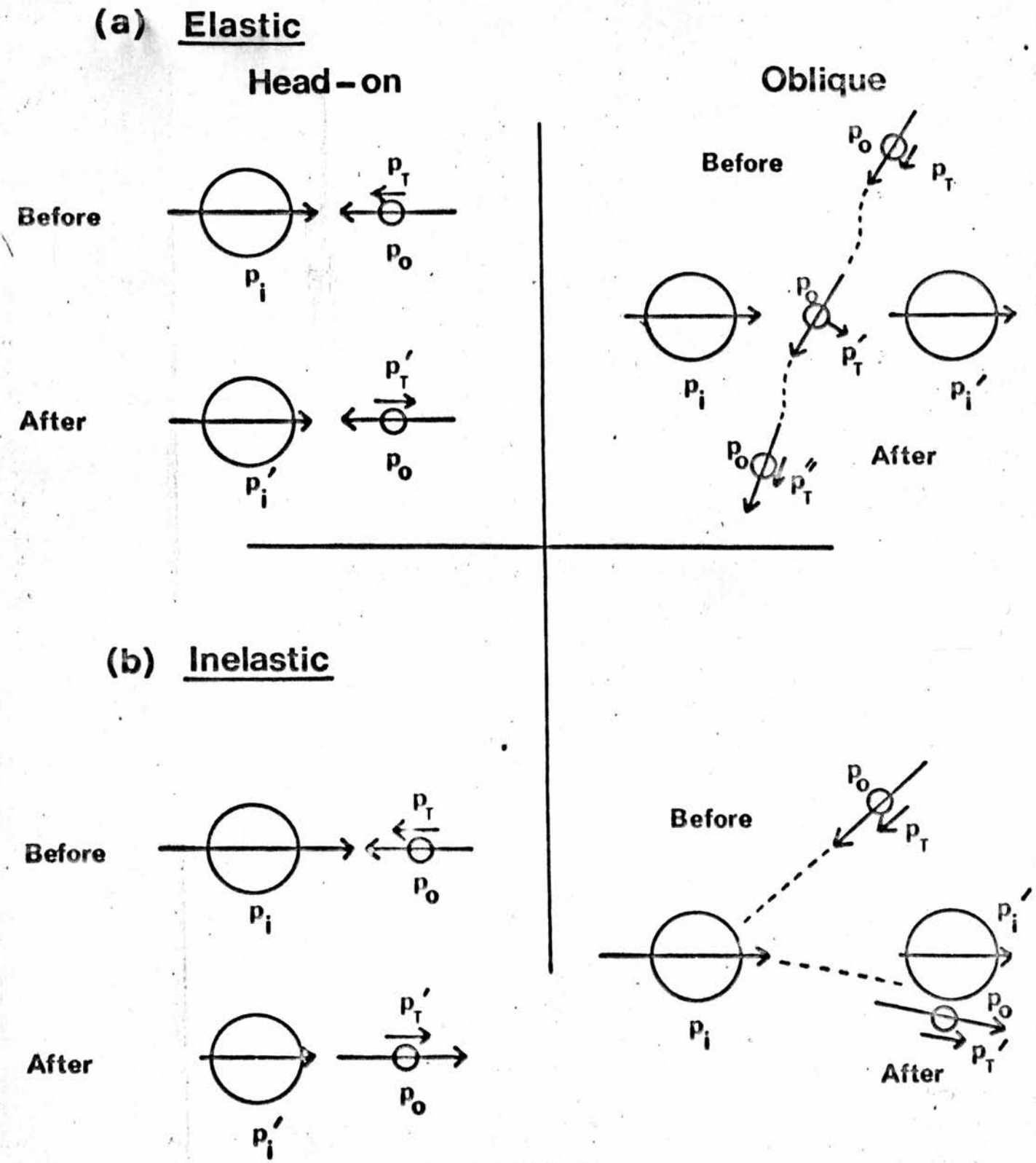

FIG. 27(a)

Momenta changes in Ion-proton collisions shown schematically.

(8.9 + 1.0°K)

$p_o \sim 1.95 \text{Å}^{-1}$. At 1°K rotons with energies up to 10°K are excited, i.e. / Rotons at the minimum are in 'stable' equilibrium since changes in either direction involve an increase in energy.

(ii) The momentum p_o is that due to the rotational motion only. It is / postulated that roton also have momentum due to their thermal velocity and that this 'thermal' momentum p_T can be parallel or anti-parallel to the 'rotational' momentum. When they are parallel the total momentum p is greater than p_o, which corresponds to the right of the minimum, and when they are anti-parallel the total momentum is less than p_o and the rotons are to the left of the minimum. In the latter case the velocity $\frac{\delta E}{\delta p}$, is negative, which means that the direction of the velocity and total momentum are opposed. In this respect, rotons differ from a classical vortex ring, which always has its velocity and momentum in the same direction. When a heavy particle and a vortex ring collide, the vortex ring expands and gives up its momentum to the particle but the vortex ring cannot be 'reflected' in the opposite direction.

When an ion collides head-on with a roton at subcritical velocities, it is possible for the roton to rebound elastically with velocity reversed but with the original direction of p_o unchanged. (See Fig. 26)

The author postulates that at subcritical velocities ions colliding obliquely with rotons interact predominantly with the 'thermal' momentum p_T of the roton, reversing its direction relative to p_o. In these collisions p_o is only slightly affected. However, in an inelastic collision the ion interacts with $p_o + p_T$ (Fig. 27). and (Fig. 27(a))

At a critical velocity the ion 'absorbs' the thermal energy of the roton. The details of this process are not clear, particularly as there is no classical couterpart for comparison.

In order to collide 'head-on' the ion momentum must be antiparallel to the 'thermal' momentum of the roton and, in order to be excited into a vibrational state, the ion's momentum and the roton's intrinsic momentum p_o must be opposed. Therefore, only those rotons whose intrinsic and thermal momenta are parallel, are capable of colliding inelastically with the ion.

In all the previous calculations, the velocity of the ions at collisions has been equated to the measured drift velocity of the ion. (See Appendix 5) This would not normally be justifiable. In a gas at room temperature for instance, the mass of an ion is comparable to that of the scattering molecules and, secondly, the velocity of drift for moderate electric fields is small compared to the thermal velocity of the ions. Under these circumstances the drifting ion would trace a very erratic path. In liquid helium at $1^{o}K$ for the fields considered, the ions are very heavy compared to the effective mass of the scattering rotons, even if $m^* = 2.4\, m_{He}$ and their drift velocity is approximately equal to their thermal velocity. Moreover, the velocity of the ions is small compared to the average thermal velocity of the rotons.

Effective Mass of Helium Ions

The effective mass of a positive helium ion for transport properties has three components, Kuper[11]:

(a) Displacement mass. This is the difference between the

total and excess mass within the spherical ion

$$m_D = \frac{4}{3} \pi \rho_o r_+^3 \qquad \text{(27)}$$

(b) Electrostrictive mass. This is the excess mass, as calculated by Atkins, due to the electrostatic attraction of the charge $m_e = 40\ m_{He}$

(c) 'Hydrodynamic' Mass $m_H = \frac{1}{2} \cdot \frac{4}{3} \pi \rho_o r_+^3$ caused by the necessity to displace atoms as the ion moves.

Substituting $\rho_o = 0.14$ gm/cm^3 and $r_+ = 6.3$Å gives effective mass for +ve ions $= 74\ m_{He}$, a figure which is lower than that given by Kuper ($100\ m_{He}$). The calculations have been checked and seem to be correct. For the negative bubble model, the displacement mass is absent and the effective mass is just the sum of the hydrodynamic and electrostrictive masses. These are $81\ m_{He}$ and $17\ m_{He}$ respectively for $r_- = 12.1$Å and $\rho_o = 0.14$ grm/cm. The 'thermal' velocity of a positive ion of mass $= 75\ m_{He}$ is ~900 cm/sec. at 1°K. In all other calculations the effective ion mass has been taken equal to $100\ m_{He}$.

In order to ascertain the error in assuming that the drift velocity and instantaneous velocity of the ions is the same, the expected persistence of velocity of an ion when it collides with a roton is calculated. Jeans[19] has calculated the persistence of velocities for collisions of elastic spheres of different initial velocities and equal mass, and then extended the result to include different masses. The positive ion has a critical velocity of ~ 5 m/sec. whilst the thermal velocity of the rotons = 70 m/sec. If these particles had equal masses, the ratio of the average component of velocity of the ion in the forward

direction to its initial velocity would be

$$\left(\frac{\alpha}{c}\right)_{\text{equal mass}} = 0.333$$

∴ Average ion velocity after collision = 0.333 x 5 m/sec., = 1.7 m/sec.
The actual persistence of velocity is given by

$$\left(\frac{\alpha}{c}\right)_m = \frac{m_i - m_r}{m_i + m_r} + \frac{2m_r}{m_i + m_r}\left(\frac{\alpha}{c}\right)_{\substack{\text{equal}\\ \text{masses}}} \quad \text{----} \quad (28)$$

where m_i = mass of ion = 100 m_{He}

m_r = mass of roton = 0.25 m_{He} if the neutron scattering figure is taken or m_r = 2.4 m_{He} if the effective momentum p_o is taken into consideration.

For the positive ion near its critical velocity, the persistence of velocity when scattered by rotons of mass 0.25 m_{He} is = 0.997. When scattered by rotons of effective mass 2.4 m_{He} the persistence of velocity is 0.97 Thus, in non-exciting collisions, the ion will lose on average between 0.3% and 3% of its velocity in the forward direction. The drift velocity is then approximately constant with small perturbations superimposed on it due to collisions.

The same result is obviously obtained for the negative ion. It appears then that the original assumption that the instantaneous velocity and drift velocity are approximately equal, was justified.

The above calculation however, only gives the average persistence of velocity. The range of values of velocity after impact might be sufficiently large to invalidate the argument. For the 'light' roton $m = 0.25\ m_{He}$ the maximum loss of velocity by the ion in a head-on

collision is 4%, but for a thermal roton of effective mass $m = 24\ m_{He}$ the ion could be stopped by the impact. (See also Appendix 5)

Discontinuity Size

An explanation for critical velocities has just been given, the next most important consideration is to explain the size of the discontinuity. The average drop in mobility at the first discontinuity at 0.95°K for positive ions is 7% taken from twenty examples; seven from the published results of Careri, and the rest from the author's own observations.

(see also Appendix 5)

As has been shown in the previous section, /the ion continues steadily towards the collector with only minor fluctuations in its velocity v_t, unless it collides with a roton in such a way as to excite vibration. It then drops to a velocity $v_t - v_c$ and must accelerate through the roton sea to its terminal velocity v_t again. (See Fig. 28) The magnitude of the discontinuity depends on the relative number of exciting collisions to normal elastic collisions. One inelastic exciting collision in every 150 ordinary collisions would give an apparent drop in mobility of the right order. The mean-free-path at $v = v_c^+$ between exciting collisions would then be = 2000Å compared to 14Å for the ion-roton mean-free-path. This would mean that any given ion makes very many inelastic collisions in traversing the cell but few compared to the number of elastic collisions it undergoes. It is suggested that the reason only one in 150 collisions are exciting ones is that the conditions for excitation are very stringent. It may be that the collisions must occur at well defined angles of incidence. The correct ratio is obtained

if only those collisions which lie within $\sim 2^{\circ}$ of a given angle of incidence are effective. In collisions which do not satisfy these conditions, normal conservation laws hold and the ion and roton are deflected. The discontinuity size should not depend on roton density very sensitively since the ratio of collisions within the specified angle of incidence necessary for excitation to all other angles of incidence, will remain the same. The magnitude of the discontinuity varies little with temperature. At the lowest temperature investigated, the discontinuity size shows a slight decline. The author attributes this decline to the decrease in the number of rotons of sufficient energy to excite the vibrational states. Below $0.9^{\circ}K$, rotons having the required energy are situated on that section of the Maxwell Distribution curve where $\frac{dn(E)}{dE}$ is negative. Further lowering of the temperature should result in a marked decrease in the discontinuity size, however one is then in a region where the discontinuity is less distinct, so this may not be easy to demonstrate.

The Shape of the Discontinuity

Above $0.95^{\circ}K$ the discontinuity is sharp, well defined and complete when at a velocity only slightly in excess of v_c, e.g. $1.1v_c$. Below $0.9^{\circ}K$ however, the discontinuity remains distinct, but the drop in mobility is more gradual, becoming complete at $v = 1.5v_c$. In considering in detail the shape of the discontinuity, the motion of the ion while accelerating and while travelling at the terminal drift velocity, must be considered separately for both (i) head-on and (ii) oblique exciting collisions with rotons.

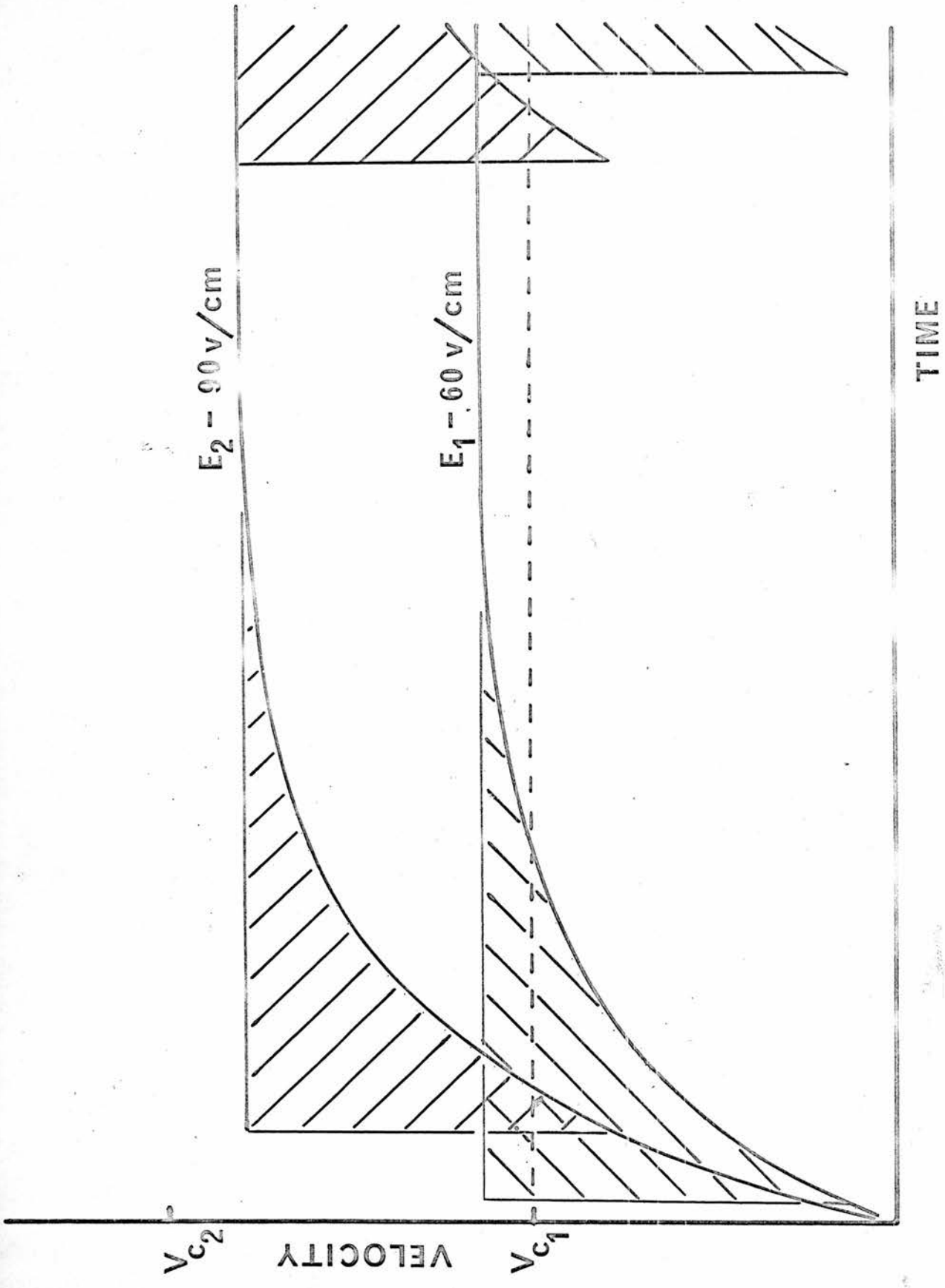

Fig. 28.

The Drift Velocity of an Ion under a Field $E \geq E_{c_2}$

AB = Drop in velocity at excitation of 1st. vibrational state.

CD = " " " " " " 2nd. " "

EF = " " " " " " 1st. " "

Shaded areas = Distance lost by ion due to inelastic collisions.

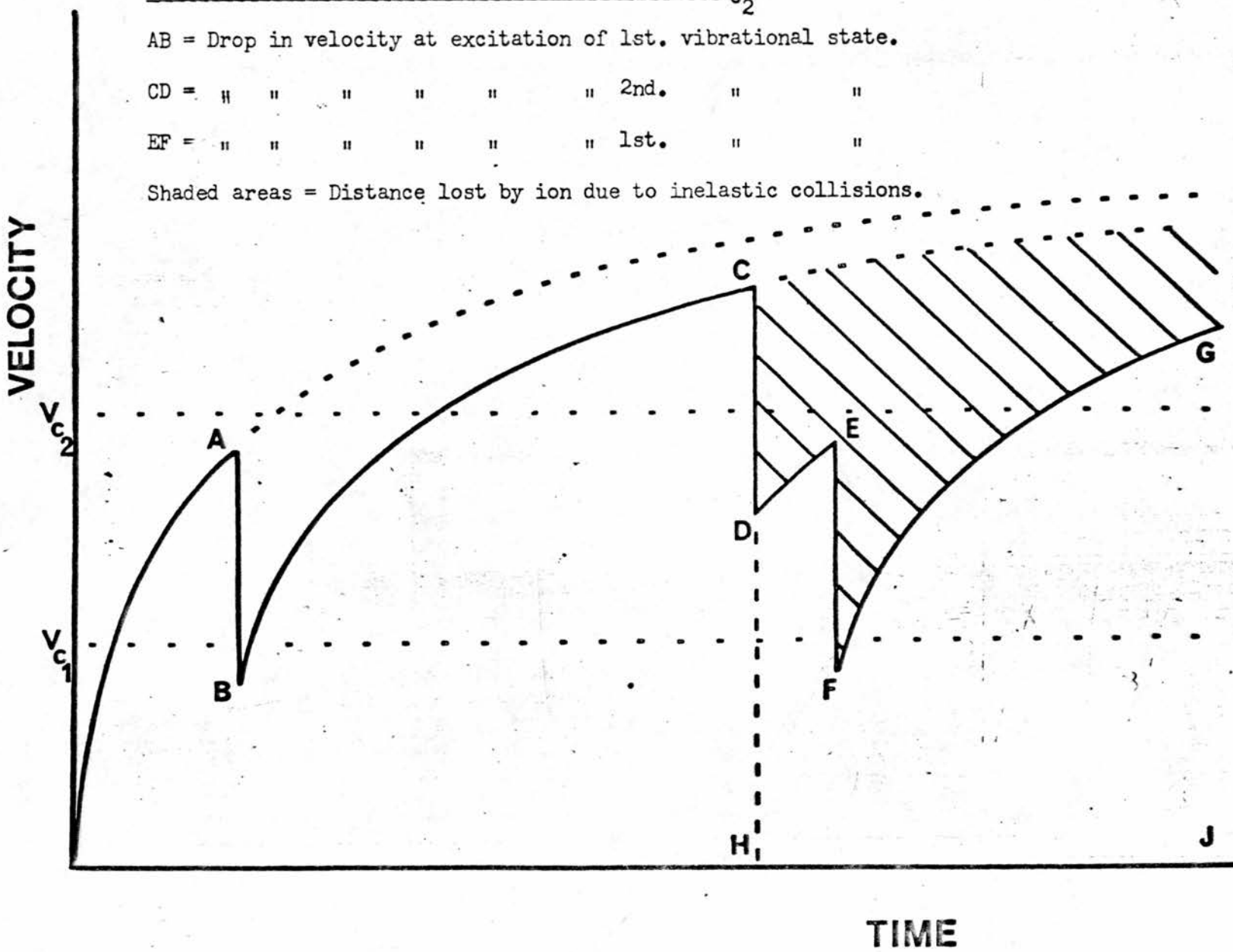

FIG. 28(a)

(i) Head-on Collisions

These provide the maximum energy for excitation when $mv > 2p_o$.

(a) Accelerating Region

For the purpose of calculation, the ion is considered as a classical particle accelerating in a viscous medium. The time required for the ion to accelerate from velocity v_o to v_c is given by *

$$t_c = \frac{1}{B} \log_e \left(\frac{v_c}{v_d - v_c} \right) \quad \text{(See Appendix 6)} \qquad (29)$$

where v_d = terminal drift velocity acquired in the field E and

$$B = \frac{e}{m \mu}$$

The distance covered by the ion while accelerating from $v_o \longrightarrow v_c$ is

$$S_c = \frac{1}{B} \left[v_d \left(1 + \log_e \frac{v_c}{v_d - v_c}\right) - 2v_c \right] \quad \text{(See Appendix 6)} \qquad (30)$$

The ion continues to accelerate beyond the critical velocity v_c until it either reaches the terminal drift velocity v_d or undergoes an inelastic collision with a roton.

The velocity of an ion against time is shown in Fig. 28. The area below the curve represents the distance travelled by the ion towards the collector. The shaded portions correspond to the distance lost by the ion due to an inelastic collision. The area of the shaded portion relative to the area below the line of constant drift velocity, gives the drop in mobility. (See also Fig. 28a for $E > E_{c_2}$)

---

* v_o = ion velocity immediately after an inelastic collision.

These shaded portions are of approximately equal area independent of the drift velocity, so for a constant drop in mobility the average distance travelled by an ion between inelastic collisions, must be constant.

(b) Terminal Drift Velocity

The time for which an ion travels with its terminal drift velocity before making an inelastic collision, must then be inversely proportional to the drift velocity, if the above condition for constant discontinuity size is to be satisfied. Since the time between all collisions, elastic and inelastic, is a constant, the fraction of collisions which are inelastic must be proportional to the drift velocity of the ion; the faster the ion goes, the more probable is an inelastic collision. This can come about in the following way:-

The ion must collide within a certain small angle of head-on with the roton in order to be excited. The faster the ion goes, the more readily will this condition be satisfied since then the velocity of any given roton relative to the ion subtends a smaller angle with the forward direction of motion of the ion. As the velocity of the ion increases, the rotons appear to approach more nearly from ahead. Since the ion velocity is small relative to the roton velocity, the small angle of incidence within which an inelastic collision is possible, is directly proportional to the ion velocity. Thus as the velocity of the ion increases, the number of exciting collisions increases proportionally and at each collision the ion loses on average approximately the same distance towards the collector. (because the shaded areas are equal, Fig. 28)

To a first approximation the distance S_E for which an ion travels

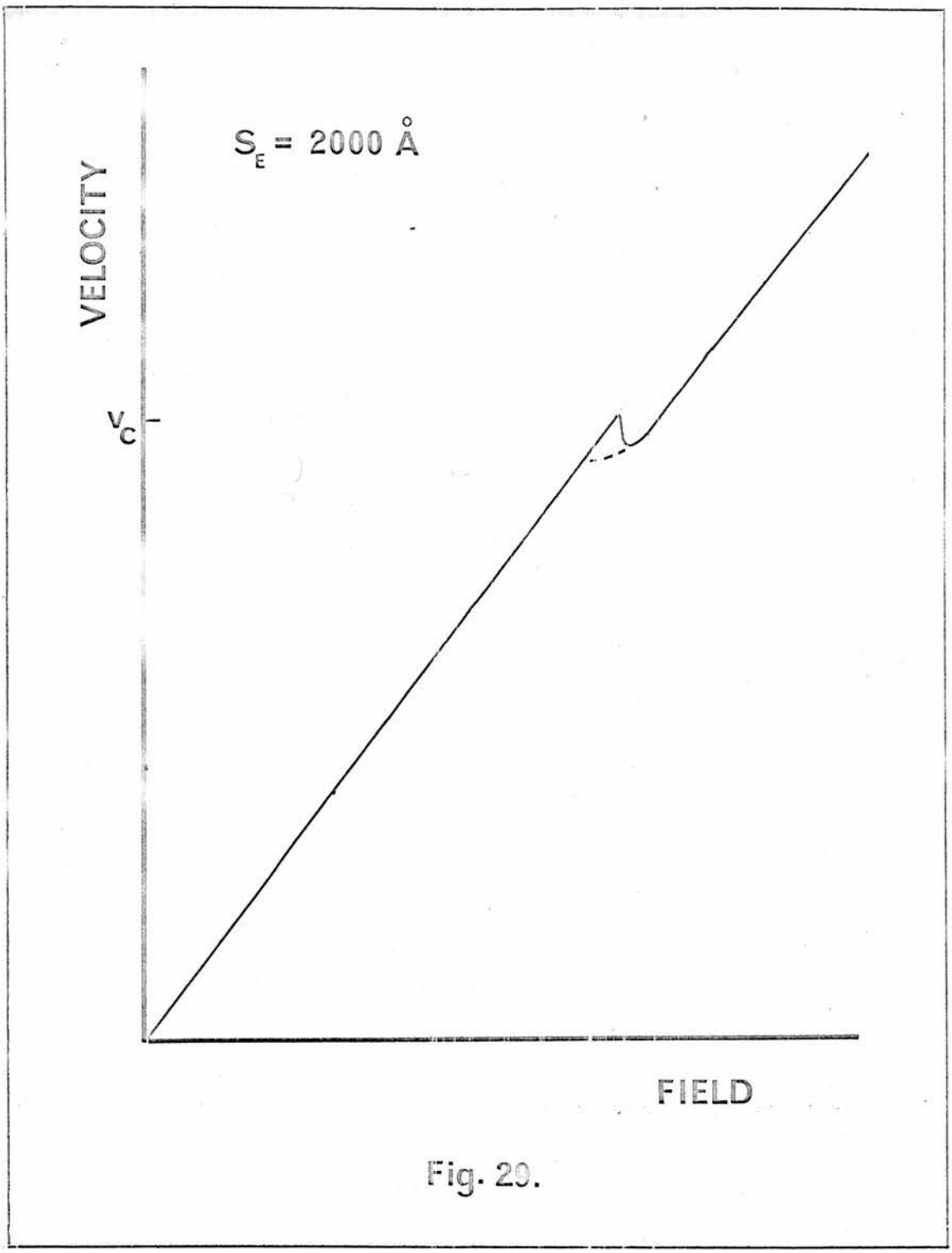

Fig. 20.

with a velocity $v > v_c$, is a constant. The equation of motion is

$$S_E = \frac{v_c - v_d}{B}(1 - Ee^{-Bt_E}) + v_d t_E \qquad \text{(31)}$$

(See appendix 6)

which may be solved for t_E = time for which ion travels at velocity $v > v_c$.

The average drift velocity $\bar{v}$ for the flight of an ion across the cell will be

$$\bar{v} = \frac{S_E + S_c}{t_E + t_c} \qquad \text{(32)}$$

If $\mu = 10$ and $S_E = 2000$Å is substituted into these equations, a discontinuity of 9% occurs at the critical velocity. The theoretical curve is shown in Fig. 29. This compares well with the experimental curve except in one important detail. At a field just in excess of E_c, the critical field, the mean drift velocity is less than v_c. It would, however, require measurements at very closely spaced fields to detect this drop and it seems likely that even under these circumstances, the effect might be obscured by fluctuations in ion velocities due to thermal motion.

(ii) Oblique Collisions

The first positive ion discontinuity and the first and second discontinuities for the negative ion cannot however be due to head-on collisions. As explained elsewhere (Page 111), when $mv < 2p_o$, the maximum energy is available at an oblique collision with a roton.

The ion is stopped by the appropriate oblique collision and its

kinetic energy goes into the vibrational energy state. For an ion travelling at a given velocity $< \frac{2p_o}{m}$ there is a particular angle of incidence for which this process can occur. At the critical velocity this process is the only one capable of supplying sufficient energy to excite the vibrational state; however, when the ion is travelling at velocity $v > v_c$, there is a range of angles of incidence for which collisions will provide the vibrational energy. It is easy to show that for $v > v_c$ the range of allowed angles of incidence is approximately proportional to $(v - v_c)$ and that the average collision is one in which the ion loses momentum mv_c. Consequently, for $v > v_c$, the ion on average will not be stopped by these exciting collisions but merely lose momentum mv_c. The constant drop in mobility observed is thus explained for the case where oblique collisions are responsible for the loss of ion velocity at the critical velocity.

The mobility μ does not, however, drop to its new level when v is just greater than v_c; it does not reach its new value until $v = 1.1v_c$ at $1.0^{\circ}K$. At lower temperatures the change is even more gradual.

Once the ion has $v > v_c$ it is capable of making inelastic collisions, so the mean-free-path before the ion makes an inelastic collision must be measured from the time at which the ion acquires $v = v_c$. As the field is increased the ion reaches the critical velocity earlier and, therefore, the next inelastic collision will occur sooner. For high fields then, the ion will make a higher proportion of inelastic collisions and the mobility will be reduced further as a consequence.

For fields which give the ion drift velocity just greater than v_c, the

Damping Factor = Resistance retardation for unit velocity

$$= \frac{a\eta}{m} = 3 \times 10^{9}$$

where a = radius of ion

η = n-fluid viscocity

m = ion mass

Time for the vibration to be damped to half its initial amplitude

$$= -\frac{2}{k} \log_e \frac{1}{2} \approx 3 \times 10^{-10} \text{ sec.}$$

drop in mobility is small because the ion spends a large proportion of its flight time at velocities $v < v_c$ where it cannot make inelastic collisions. (AB in Fig. 28)

The drop in mobility is less abrupt at temperatures < 0.92°K. At these lower temperatures two effects can alter the shape of the mobility curve. Firstly the persistence of velocity of the ions will be greater since the velocity of the impinging rotons is reduced. Also the mean-free-time between collisions is considerably increased. The first of these effects is small since v_r depends weakly on T. The increase in mean-free-path, however, means that the field necessary to maintain a given terminal velocity is very much reduced. Thus, after an exciting collision, the ion has much less acceleration, and it travels further before acquiring $v = v_c$. This means that the effect which resulted in the smooth shape of the discontinuity, is more marked at the lower temperatures.

Relaxation Time for the Emission of a Phonon by the Excited Ion

It is important to know how long the ion remains in an excited state after making an inelastic collision. The decay time for the vibrating ion in a viscous medium is calculated. The damping may be considered as the result of internal friction within the ion or, alternatively, as the probability of phonon emission at the succeeding ion-roton collisions. In this latter case it seems likely that the probability of emission of a phonon is high. ~ 1. The damping factor Λ for an ion of mass $m = 100\ m_{He}$ in liquid He of viscosity ~ 30 micropoise,[56] is of the order of $10^9 \longrightarrow 10^{10}$. The decay time for the vibration is then approximately 3×10^{-10} sec. This is of the order of the time between successive collisions with rotons and is much less than the time between successive excitations. Thus it is likely from this calculation, that the ion will emit its phonon or phonons before the next possible exciting collision.

(see opposite)

The Variation of Discontinuity Size with Grid-Source Field

The extent of the drop in mobility above the critical velocity was found to depend on the magnitude of the grid-source field Egs. When Egs became supercritical the size of the discontinuity at v_c for positive ions changed from a 6 $\rightarrow$ 10% drop in mobility to $\leq$ 3%. Elsewhere[20], this has been ascribed to the production of an n-fluid 'wind,' through the grid towards the collector, by the ions in the source-grid space. A process of elimination suggested that this mechanism was probably the only one which fitted the results qualitatively. The argument went as follows:-

(See P. 54)

The events in the source-grid space can affect either the ion or the background fluid, or both. The velocity of the ion may be changed by a single event or by a continuous process, or both.

For example, suppose the ion at $v = v_c$ creates a bound vortex ring in its wake. The observed drop in mobility can be due to a loss of velocity at the creation process and to the increased scattering cross-section of the ion-vortex ring combination. If the creation occurs in the source-grid space, then a smaller drop in mobility due only to the bound vortex ring would be observed in the grid-collector space. The immediate criticism of this process is that even if the ion were stopped at the creation of a vortex ring, the effect on the average drift velocity across the cell would be immeasurably small. It would be necessary to postulate that during the creation process, the ion travelled at $v = v_c$ for a significant proportion of its flight path across the cell. Even if, in this way, the single event could account for the observed

change in the mobility yet another difficulty is apparent; the extent of the effect on the average drift velocity would then depend on the total distance travelled by the ion - the shorter the total distance travelled, the greater the effect of the creation process. Variation of the grid-collector spacing shows no such dependence.

When $E_{gs} < E_c$ the discontinuity remains approximately constant; when $E_{gs} > E_c$ the discontinuity, although small, tends to decrease slightly with decreasing grid-collector spacing.

Another possibility is that an ion, when initially excited, exhibits an enlarged scattering cross-section which then decays towards its original value, or alternatively the same effect would be observed if a large vortex ring were created behind the ion which then shrank as the ion accelerated. This would result in a large initial drop in velocity by the ion but a slow recovery to some final velocity, which is nevertheless lower than the terminal velocity the ion would have acquired had it not undergone the critical phenomenon. If the initial loss of forward velocity occurs in the source-grid space, then the ion will already have acquired its new terminal velocity when it enters the grid-collector space. It has been shown on Page 129 that the decay time of a vibrating ion is very much too small to be effective in this process. The decay of a vortex ring in the wake of an ion, could be a much slower process and the ion velocity may not recover for a significant part of its flight across the cell. However, this model again predicts a dependence of discontinuity size on the electrode spacings which is not confirmed by experiment.

None of the above suggestions wholly explain the experimental observations and, therefore, the processes which might effect the background fluid were considered. It is postulated that ions in the source-grid space set up a flow of n-fluid towards the grid and that some of this is carried through into the grid-collector space. The production of this n-fluid 'wind' is closely connected with the previously described model of a vibrating ion. In an exciting collision the ion tends to polarise the roton momentum along its own direction of travel. The roton may remain bound to the ion for a short time in which case it will be further constrained to move in the direction of the ion. Now the roton-roton mean-free-path = 1000Å (Atkins, Page 109) is long compared to the ion-roton mean-free-path. Thus ion-roton collisions increase the forward polarisation of the rotons such that after a period of continuous passage of the ions, a flow of n-fluid corresponding to the preferential direction of the roton momenta, is set up along the axis of the source-grid space. This flow of n-fluid is carried into the measuring space through the grid. There the preferential orientation of roton momenta towards the collector will render them incapable of exciting the forward moving ions. Moreover ions returning to the grid during the reverse cycle of the applied square wave potential, encounter a higher proportion of rotons approaching from head-on. It is possible then that, as in the case of heat induced n-fluid flow, the ions do not reach the grid on their return flight and the effective flight path of the ions is shortened. Phonon-roton collisions tend to destroy this polarisation. Equilibrium will be maintained when the polarising and depolarising influences

Momentum before collision L.H.S.

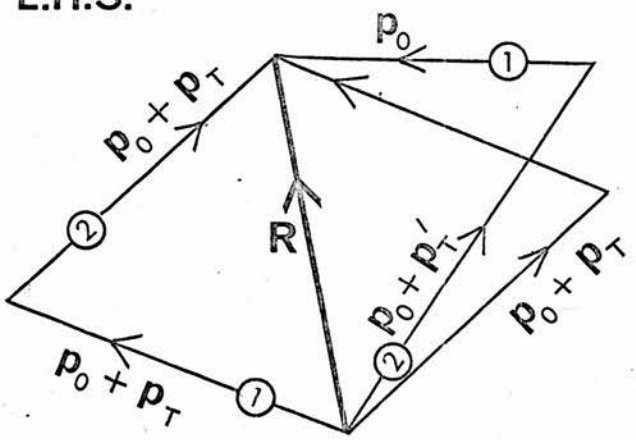

Range of possible momenta after collision R.H.S.

Fig. 30.

balance. The low ion density in comparison to the roton density, would suggest that the effect is microscopic; however factors which support the concept of a significant ion induced n-fluid flow are:-

(a) Heat flush results for varying fields, explained previously. (P.77-8, results (iii) and (v))

(b) The experimental observation of flow patterns in electrolytic tanks.[46]

(c) The ion density though still small, is higher in the source-grid space than the grid-collector space.

(d) Each ion, at any instant, affects a large number of helium atoms.

(e) Conservation of energy and momentum in roton-roton collisions predicts that a roton will 'inherit' the direction of travel of the colliding roton. The form of the excitation spectrum predicts that rotons with momentum differing from p_o by a large amount, require an energy much higher than Δ and therefore at 1°K few of them exist in the liquid. The spectrum also predicts that when two rotons with momenta $\sim p_o$ collide the magnitude of their momenta is very little altered from p_o, since again this would require a relatively large amount of energy. Therefore the momentum diagram (Fig. 30) describing such a collision, will be approximately an equilateral parallelogram of side p_o. The exchange of thermal energy in the collision gives a slight variation in initial and final momenta. Fig. 30, a typical momentum diagram, shows how the maximum deviation from an equilateral parallelogram occurs when, during the collision, one roton loses all of its thermal energy to the other roton,

giving final momenta p_o and $p_o + p'_T$. Most collisions, however, will be represented by a more regular diagram, this means that the final momenta differ very little in magnitude or direction from the momenta before the collision. Therefore an individual roton emerges from the collision either with its initial momentum or with the momentum of the colliding roton. This is what the author means by saying that the roton 'inherits' the direction of travel of the colliding roton. Thus, in this way, a preferred direction is maintained through the liquid. Rotons can be considered as possessing 'gyroscopic' stability. In this way polarisation of rotons near the grid in the grid-collector space explains the variation in discontinuity size with source grid field. When $E_{gs} > E_c$ exciting collisions in the source-grid space are a source of rotons polarised in the forward direction. The polarisation of rotons in the region of the grid reduces the probability of a forward moving ion being excited and increases the probability of one moving in the reverse direction being excited. These effects combine to give an apparent reduced drop in mobility. If the grid-collector .....

space is reduced the magnitude of the discontinuity should be decreased still further.

An attempt is made here to calculate the extent and effect of any n-fluid 'wind' in the measuring space.

To determine how far into the measuring space the polarisation of rotons extends, the flight of one roton is considered. Suppose an ion in the grid-source space collides inelastically with a roton. Immediately after the collision the roton will travel directly towards the collector, having 'intrinsic' momentum p_o and thermal momentum p_T polarised in the forward direction of ion motion. Subsequent collisions with rotons, phonons and ions, will tend to destroy their polarisation. Since, under the conditions of the experiment, the roton density is greater than the phonon or ion density, roton-roton collisions only will be considered. In estimating the effect of the many collisions experienced by the original roton, concepts from Kinetic Theory have been used. This will give only an 'order of magnitude' calculation.

The original roton is considered to have the most probable velocity = 60 m/sec. at $1^{\circ}K$ and to collide with rotons of average velocity = 73 m/sec. It can easily be shown that an average collision involves the original forward moving roton with another incident at an angle of 82° to the forward direction. Under such circumstances the original roton is deflected, on average, only 0.7° from its original course. The small deflection is a result of the invariance of the 'intrinsic' momentum p_o, mentioned earlier (P. 134). Using the principle of random walk, the deflection θ after 'n' collisions will be, on average:

$$\theta = n^{\frac{1}{2}}(0.7^\circ)$$

For a deflection of $\frac{\pi}{2}$, (a deflection of $\frac{\pi}{2}$ would remove completely the polarisation of the roton in the forward direction.) the original roton must undergo $\sim 2 \times 10^4$ collisions. The roton-roton mean-free-path is $\sim 1000\text{Å}$. Therefore, the distance the roton travels before being completely depolarised is ~ 2 mm. In other words, the above calculations show that a roton could travel a distance comparable to the electrode spacings before being able to excite vibration in a forward-moving ion. In order to estimate the effect on the ion beam, it is necessary to calculate the proportion of 'polarised' rotons in the measuring space. The number of rotons normally arriving at the grid polarised within 1° of the grid-collector direction, is $= 0.5 \times 10^{15}$/sec. Assuming a constant current of 10^{-10} amps in the grid source space, $\sim 10^9$ ions/sec. arrive at the grid.

If the ion velocity in the grid-source space $v > v_c$, each ion will polarise, by inelastic collisions, 10^5 rotons on its journey from the source. Many of these rotons would normally be scattered before reaching the grid. There are two effects which counteract the scattering process:-

(i) The directional stability of the rotons described above

(ii) Every ion-roton collision, inelastic or elastic, tends to direct rotons along the path of the ion. The continuous passage of ions in one direction in the grid-source space increases the proportion of rotons moving towards the grid.

The number of rotons polarised by inelastic collisions with ions, arriving at the grid $\sim 10^{14}$/sec. compared to 5×10^{14}/sec. arriving due to the normal velocity distribution of the rotons. Therefore, in the region of the grid, the discontinuity size should be reduced by 20% from 8% to 6.5%

by increasing the grid-source field to a supercritical value. Even close to the grid where the effect would be greatest, the predicted change in discontinuity size of 1.5% is small compared to the 5% observed when the grid-source field E_{gs} was made supercritical $E_{gs} > E_c$. (See P. 54)

The effect of the roton polarisation will be reduced with distance from the grid and the overall effect on the discontinuity size would be very small. In order to predict an effect equal to that observed experimentally, it is estimated that the number of 'polarised' rotons arriving at the grid would have to increase from 5×10^{14}/sec. to $\sim 15 \times 10^{14}$/sec. when the grid-source field was made supercritical. Therefore the number of rotons polarised by inelastic ion-roton collisions is required to be $\sim 10^{15}$/sec. This is one order of magnitude higher than that calculated for the observed grid-source current. The discrepancy may be accommodated by postulating a greater effect on the rotons by the ions in the grid-source space. If the penetration of polarisation is ~ 2 mm. as suggested by the previous calculation, the observations could be explained by postulating that when $v_{gs} > v_c$, no inelastic collisions occur within 2 mm. of the grid. In this case the magnitude of the effect would agree well with experiment. Thus it can be seen that an effect which was expected to be immeasurably small, could in fact become large enough to have a measurable effect on the discontinuity size.

The idea of an ion produced n-fluid 'wind' explains qualitatively the observed dependence of discontinuity size with grid-source field. Quantitatively, the model predicts an effect one order of magnitude smaller than observed.

Ions moving at sub-critical velocities may also interact with the n-fluid 'wind' but this type of interaction will persist at supercritical velocities and hence no change in the discontinuity should be observed due to this.

Electric Field Penetration

When considering the above results it is important to assess the affect of field penetration at the grid, since at first sight, the results could be attributed to this. Verster[22] has calculated the field penetration factors in triodes for grids of different construction. The penetration factor D is defined by the equation

$$D = \frac{V_g}{V_a} \qquad \text{(33)}$$

where V_a is the potential on the anode and V_g is the potential required on the grid such that the region between the grid and the cathode should be predominantly field free. The majority of the author's experiments were performed using a grid made of a thin plate having circular holes (P.39-40 (See Appendix 2) drilled through it in a hexagonal pattern. Extrapolating Verster's Graph for the appropriate configuration and size of grid, gives a penetration factor of 5×10^{-5} when the 'anode' is 5 mm. from the grid. This means that penetration of the source-grid field into the measuring space and vice-versa, can be ignored. The experimental observations also confirm this result, that field penetration at the grid cannot explain the variation of discontinuity size. Field penetration would affect the

position from which the ion begins its transit to the collector. If $F_{gc} > F_{gs}$ the ion would start from the side of the grid nearest the source and if $E_{gc} < E_{gs}$ the ion would start from the side nearest the collector. Thus a discontinuity should occur in the velocity-field curves when E_{gc} becomes greater than E_{gs}. However, for constant $E_{gs} \neq E_c$ no discontinuity is observed at $E_{gc} = E_{gs}$.

LITERATURE SURVEY

Introduction

The early work on ions is described and compared with the author's present ideas.

The mobility of ions in liquid helium was first measured by Williams[23]. The method promised to be a useful tool in investigating the properties of liquid helium. Ions provide microscopic probes which are controllable by an applied electric or magnetic field. Their position, flight path and velocity, can be determined relatively easily. This renders them superior to measurements of the macroscopic properties of liquid He II, to the neutron bombardment measurements and He^3 diffusion measurements in determining the detailed properties of the liquid. The main difficulty in applying the ion results is in ascertaining the scattering cross-section and effective mass of the ion. Much theoretical and experimental work has aimed at a better knowledge of the dimensions of the ion. It soon became clear that the mobility of ions in liquid helium was very low, corresponding to a high collision cross-section.

Since the original experiments by Williams, the work on the motion of ions through liquid helium has been concentrated in two centres, Rome and Chicago. The survey here gives a comparison of the basic experiment in each centre followed by a report of the two different series of experiments performed subsequently.

Williams used a simple diode and observed the flight of a single ion

across the cell. During the ion's flight the current induced in the collecting electrode is passed through a resistor and the resulting potential difference recorded on an oscilloscope. The time of flight is calculated from the shape of the oscilloscope trace. Williams also did measurements for liquid Argon and found that positive ion mobility was approximately constant, while the negative ion (electron) mobility obeyed a law of the form.

$$\mu_e = \frac{1}{A + BE} \qquad (34)$$

where A and B are constant and E is the electric field strength. The results in liquid helium can be summarised as follows:-

1. Above the λ point.
   (a) Mobility very weakly dependent on field
   (b) Mobility sensitive to diode spacing
   (c) Positive ion mobility = 5 x negative ion mobility
   Typical value of mobility, $\mu^- = 0.025$; $\mu^+ = 0.125$ cm.^{2}/volt.sec.
2. Below the λ point.
   (a) Field dependent mobility - decreasing with increasing field
   (b) Temperature dependent mobility - increasing with decreasing temperature.

Williams finds no satisfactory explanation of these phenomena observed below the λ point; the region of prime interest here.

Williams' results were for relatively high fields and widely separated field strengths. Meyer and Reif and Careri subsequently investigated mobilities in much greater detail.

Meyer and Reif[3,18] used a shutter method where pulses of ions were admitted to a drift space across which they travel under a constant applied field. The gating frequency which allows these ions to pass through the second shutter is measured and gives the velocity of the ion. This method is potentially far more accurate than the pulse method used by Williams.

The first experiments were performed at comparatively low fields, i.e. up to 200 v/cm. only and temperatures down to 1.2°K. Later the measurements were extended to higher fields and lower temperatures. The preliminary results showed that the mobility was constant in the range of fields measured and that there was a strong temperature dependence. The rise in mobility with decreasing temperature suggested $\mu \propto \rho_n^{-1}$. Putting $\rho_n = e^{-\Delta/kT}$ gives $\mu \propto e^{\Delta/kT}$. If this equation is accepted then the slope of a plot of $\log_e \mu$ against T^{-1} gives $\frac{\Delta}{k} = 8.3°K$. To quote Meyer and Reif, "This value of $\frac{\Delta}{k}$ lies within the spread of values for $\frac{\Delta}{k}$ deduced from measurements of ρ_n by different methods."

Careri[25] had already performed an experiment on the 'heat flush' of ions to determine the effect of excitations on moving ions. The ions are constrained to move across a rectangular cell, the two opposite walls of which form a simple diode, while a heater at the bottom of the cell provides a flow of n-fluid perpendicular to the undisturbed direction of the ions. An array of electrodes on the collector side of the cell allows the drift of the ion with the n-fluid flow to be measured. The relative change in current $\frac{\Delta i}{i}$ received at the electrode opposite the source, was measured for varying heat inputs and from this the deflection of the ion

beam could be calculated for a given n-fluid velocity. Using known mobility values, Careri was able to show that the velocity superimposed on the ions due to the heat flow, was equal to the n-fluid velocity. Reversing the argument and assuming the superimposed ion velocity to be equal to the n-fluid velocity, the mobility can be obtained from the equation $\frac{\Delta i}{i} = \frac{Kv_n}{\mu E}$ where v_n = n-fluid velocity. In this way Careri was able to extend the measurements of mobility to lower temperatures, (0.95°K), than had been investigated previously.

Careri's results fitted well the exponential dependence of mobility on temperature described by Meyer and Reif.[3] Moreover the measurements at lower temperatures fitted the extrapolatiom of this dependence. Throughout these experiments, the heat input was kept sufficiently low ($\leq$ 10 mW/cm.^{2}) such that the superfluid flow was non-turbulent. Later experiments[26] showed the effect of turbulent flow.

In turbulent flow the negative ions were dragged in the direction of the heat current much more than in the non-turbulent region, also the total current collected decreased. These results were interpreted as a decrease in the mobility of the ions. In the light of more recent experiments (Douglass[32]) it seems likely that the apparent decrease in mobility could be attributed to trapping of the ion on vortices. The enhanced interaction between ion and n-fluid for the negative ions is consistent with the largereffect of heat flow on the negative ions observed by the present author.

The positive ions were affected less by the turbulent flow than by non-turbulent flow. Two possible explanations are given by Careri.

(i) The n-fluid velocity profile for turbulent flow is different from that expected for non-turbulent or laminar flow. A correction factor calculated by Careri for this effect describes approximately the observed behaviour.

(ii) Alternatively, it is suggested that in the turbulent case some of the heat goes into the production of the vorticity, and therefore the n-fluid velocity v_n is not as high as that predicted by the equation

$$v_n = \frac{\dot{q}}{\rho s T}$$

These ideas, applied to the author's heat flush experiments, would alter the n-fluid velocity profile in the measuring space. However the effect of n-fluid flow was shown not to be due to a simple superposition of ion and n-fluid velocity, but to trapping or some other mechanism which shortens the drift space. (See page 83) The n-fluid velocity profile should be modified for supercritical heat inputs

Careri derives the ion mobility using a treatment similar to that employed for calculating the diffusion coefficient of He^3 in He^4. The two systems are similar in that in neither case is there any significant interaction between the ions, or He^3 atoms. Assuming roton scattering to be the dominant process and using the Landau Kalatnikov expression for the roton density fields by simple kinetic theory, the expression

$$\mu = \frac{\pi^2}{2} \frac{e\hbar^3}{\sigma_{i\xi}\, m_\xi^{1/2}\, m^{1/2}\, p_o^2} = \frac{1}{kT} \exp\left(\frac{\Delta}{kT}\right) \quad \text{---------- (35)}$$

where $\sigma_{i\xi}$ = ion-roton cross-section, m_ξ = roton effective mass,

p_o = roton momentum

Careri gives for positive ions $\frac{\Delta}{k} = 7.3°K$

and for negative ions $\frac{\Delta}{k} = 6.9°K$

calculated from the slopes of the log.μ versus $\frac{1}{T}$ curves.

Careri also calculates values of the ion-roton mean-free-path and ion scattering cross-section for postulated values of the effective mass of 1 m_{He}, 10 m_{He} and 100 m_{He}.

Careri postulates a large ion-roton cross-section because of polarisation forces; suggests a bubble model for the negative ion and points out that ion-phonon collisions are unimportant even at $1^{o}K$.

Later Careri[1] measured the ion mobility by the time of flight method using a triode type cell. This method has been fully described elsewhere in this thesis. The applied field in this case was in the form of a square wave. This meant that the method was limited to comparatively low fields. However while the experiment lacked in the range of fields available, it gained in the accuracy with which it was possible to measure the ion velocity and, therefore, the field dependence of the mobility could be measured in much greater detail. This much greater accuracy led to the discovery of the periodic discontinuities in the field dependence of the mobility, the main subject of this thesis.

The most recent paper by Careri, Cunsolo and Mazzoldi[2], describes the full range of experiments and results performed by this method. The experiments were performed at temperatures in the range $0.80^{o}K$ - $1.02^{o}K$ with different ion sources and different cell dimensions. All the results at different temperatures plotted on a universal graph of measured drift velocity versus $\mu_{o}E$ where μ_{o} = zero field mobility, show conclusively that a discontinuity exists in the region of 5 m/sec. Statistical analysis yields a critical velocity of 5.15 ± 0.2 m/sec. for the positive ions and 2.43 ± 0.07 m/sec. for negative ions. Careri's

results also show that discontinuities occur at multiples of v_c up to at least $5v_c$. These discontinuities are more clearly defined in the upper half of the temperature range. The critical velocity for negative ions is found by finding the average separation of discontinuities at high velocities corresponding to $v > 3v_c$. To quote Careri, "Under no experimental conditions have we been able to observe the first discontinuity at 2.43 m/sec." The present author, by making E_{gs} sufficiently small, has observed the first discontinuity for negative ions.

The observed positive ion critical velocity agrees with the author's value, while Careri's value for $v_c = 2.43$ m/sec. is $\sim$10% higher.

At very high fields $\geq$300 v/cm. the occurrence of a giant discontinuity is reported.

Some runs are shown in which certain discontinuities appear to be missing and others where the drop in mobility does not occur till the velocity is noticeable greater than the appropriate critical velocity. These results are attributed to a form of 'metastability' and related to bath disturbances. An experiment is described in which this 'metastability' was induced by providing artifical bath disturbances

The average drop in mobility at the first discontinuity observed by Careri was 6%.

Careri then discusses these results. He suggests that the sharpness of the discontinuity is a results of a long relaxation time for the process giving the transition, compared to the thermal relaxation time. The independence of critical velocity and temperature suggests that the

process is not connected with the density of the excitations, while the different observed critical velocities for positive and negative ions lead to the conclusion that the process is characteristic of the ion-fluid system.

The tentative model put forward by Careri to explain these results is that the ions create quantised vortex rings which then remain closely bound to the ion in motion. A vortex ring of unit circulation having a radius of $\sim$100Å, is created at 5 m/sec. The extra dissipation due to roton scattering by the vortex ring, is calculated from the Lifshitz-Pitaevskii expression for the Gorter Mellink force, and would produce a mobility change of the order of magnitude observed.

Three uncertainties are mentioned in this model:-

(a) The validity of the equations of motion for vortex rings bound to an ion

(b) The stability of ion-vortex ring systems in motion

(c) The creation process for the vortex ring is obscure

The experiments and conclusions of Rayfield and Reif are compared with Careri's results.

Neither Williams nor Meyer and Reif have reported any discontinuities. Williams' apparatus was probably insufficiently accurate to reveal the effect and Meyer and Reif concentrated on different effects. It would be interesting to see if the discontinuities could be observed using a Meyer and Reif type velocity spectrometer. The author attempted this but, through lack of time, was unable to perfect the technique sufficiently to obtain accurate results.

The experiments giving the strongest evidence for vortex rings and giving the best agreement with theory, are those reported by Rayfield and Reif.[13] They used a velocity spectrometer to determine the velocity of ions under varying fields at 0.3 - 0.7°K. At these very low temperatures the mean-free path of an ion is longer than the cell dimensions. Consequently a very small field is necessary to accelerate the ions to velocities higher than their thermal velocities.

The results may be summarised as follows:-

(a) Having accelerated an ion to a certain velocity, it would continue to travel across a field-free region and, in fact, it was necessary to apply a retarding field to bring the ion to rest.

(b) The potential and not electric field was found to be the significant parameter in stopping charge carriers.

(c) Fractional energy loss of charge carrier traversing a field-free region was 5 - 10% per cm. depending on temperature.

(d) The velocity of the charge carriers in a field was very low and inversely proportional to the energy imparted to them from the field.

It is this last rather unique dependence of v upon E that leads to the assumption that the charge carriers are in fact ions bound to vortex rings. The Lamb[31] expressions for a vortex ring are

$$E = \frac{1}{2}\rho\kappa^2 R(\beta - \frac{7}{4}) \qquad \text{----------} \quad (36)$$

$$v = \frac{\kappa}{4\pi R}(\beta - \frac{1}{4}) \qquad \text{----------} \quad (37)$$

where ρ = density of bulk liquid

κ = circulation

$\beta = \ln. \frac{8R}{a}$

R = radius of vortex ring

a = radius of ring core

Eliminating r from these equations gives $v \propto \frac{1}{E}$

The experimental 'velocity-energy' curves fit a curve of vE = constant, extremely well.

Now $\beta = \ln.\frac{8R}{a}$; choosing a = 1Å and using experimental results, Rayfield and Reif obtain $\kappa = 10^{-3}$ cm^2/sec. This is in remarkable agreement with the predicted value $\frac{h}{m} = 0.998 \times 10^{-3}$. Thus they assume the charge carriers are vortex rings with a circulation of precisely one quantum.

Rayfield and Reif speculate that the ion moves freely as a classical particle around the core of the vortex ring. It was attracted there in the first place because, by Bernoulli, the core is a region of low pressure. They suggest that a vortex ring of the dimensions of the ion is created at $\sim$50 m/sec. whereupon the ion is captured and the charged vortex ring slows down.

To check that the charge carriers are vortex rings, Rayfield and Reif carried out an experiment in which they passed a beam of charge carriers

through a transverse electric field and measured their deflection from a straight-through path. The apparatus was something like a cathode-ray tube. Slits in the first three electrodes allowed a well collimated beam of charge carriers with a well defined energy, to be emitted into the drift space. Here they passed between a pair of electrodes applying a field perpendicular to the direction of motion of the ions. Rayfield and Reif derive the equation of motion for a vortex ring under these circumstances and show that $E \propto p$. This was verified experimentally. The deflection experiment then provides extra evidence that the charge carriers are indeed vortex rings.

The energy loss of a charged vortex ring was also measured. This was achieved in two ways. The first method involved the compensation of frictional losses by a known applied field. The second method was to supply the charge carrier with a known amount of energy, allow it to drift across a field-free region and then find what potential was necessary to stop it. In this way the energy loss in the field-free region is measured. The attenuation constant is calculated from these results. A graph of attenuation coefficient against $\frac{1}{T}$ agrees well with calculated coefficient when scattering due to rotons, He^3 impurities and phonons, is considered. The scattering cross-section for rotons and for He^3 impurities is determined.

Rayfield and Reif conclude that their experiments present strong evidence for the creation of vortex rings of unit circulation in liquid He II and that these vortex rings are bound to the ions.

The present author's model gives a method by which the vortex ring

is first created, and agrees with Rayfield and Reif's estimate of the creation velocity of ≃ 50 m/sec.

Having measured the ion mobility and its temperature dependence, the two groups concentrated on different aspects of the problem. Careri and his co-workers looked for a different method of detecting the discontinuities, of extending their measurements to higher fields and different experiments to elucidate the structure of the ions, while Meyer and Reif meanwhile extended their measurements to lower temperatures and higher fields.

The other methods by which discontinuities in the drift velocity of ions have been observed will be described next.

Careri[28,24] repeated the measurements of the mobility of the positive ions by the heat-flush method in order to establish the existence of a discontinuity at a critical drift velocity. While the apparatus and method were essentially the same as described previously, the experimental procedure was different. Here the beam displacement at different values of the field E was observed, keeping the heat input $\dot{q}$ and bath temperature T constant. Previously E and T were kept constant and $\dot{q}$ changed. Measurements were extended to superc·itical fields and the region near the critical field investigated in detail. The current changes at the collecting electrode are related to the mobility by the equation:

$$\frac{\Delta I}{I} = \frac{K v_n}{\mu E} \qquad \text{----------} \qquad (38)$$

Careri detected a discontinuity in the graph of $\frac{\Delta I}{IK}$ against $\frac{I}{E}$ and

showed that it corresponded to an ion velocity of 5.2 m/sec. in perfect agreement with the discontinuity found by the time of flight method. This heat-flush method was further elaborated and another grid inserted into the cell so that the time of flight of the ions could be measured simultaneously with the heat-flush effect. The results from this more elaborate apparatus are reported two years after the first detection of the discontinuity by the heat-flush method. In this later paper Careri[28] et al argues that the predominant interaction is of the ions with the n-fluid. The experimental results are presented in three sections.

(a) The effect of heat flow on mobility was investigated.

It is shown that the low field mobility is unaffected by the heat flow. The heat flow in this case was perpendicular to the direction of ion drift, in contrast to the experiment performed by the present author, where flow was parallel to the direction of ion drift. In this latter case also it was found that the heat flow had only a small effect on the ion mobility. Careri further observed the effect of heat flow on the high field mobility. With a fixed heat input, the mobility was determined at varying values of field strength. A discontinuity in mobility at a critical field corresponding to a critical velocity of = 5 m/sec. occurred as in the absence of heat flow. At this discontinuity the mobility dropped to a new lower value and remained constant until the field was such that the drift velocityh was = 7.5 m/sec. when the mobility increased again to its previous value. Careri does not attempt to explain this latter unexpected phenomenon and it is not explicable by the model of the vibrating ion. It may be that the

effect of the perpendicular n-fluid flow and of the forward moving ions combine to polarise the rotons in a direction which would make them incapable of undergoing inelastic collisions with the ions, hence removing the discontinuity. The author's results for ions travelling at supercritical velocities showed an increasing enhancement of velocity with increasing heat input and increasing velocity. Fig. 20 showshow the slopes $\frac{\delta v}{\delta \dot{q}}$ increase with increasing E. It is suggested that there is no real discontinuity at 7.5 m/sec but that above the critical velocity the mobility rises continuously with increasing field.

(b) Careri performed a particular run at constant temperature, constant heat input in which the angle of deflection of the ions was measured as a function of the applied field. A graph of tan.α, where α = angle of deflection against $\frac{1}{E}$, demonstrates that the data points lie on two straight lines which meet at the origin. From the value of the field at the change-over of points from one line to the other and using the known value of low-field mobility at this temperature, the critical velocity was calculated and shown to agree with previously determined values. The mobility could have been determined directly from the slope of the tan.α versus $\frac{1}{E}$ graph; this however gives high values because of heat leakage through the walls.

(c) Lastly a series of experiments were performed using the straight forward heat-flush method and the critical velocity observed at temperatures from 0.9 - 0.97°K.

Careri shows that the critical velocity is independent of temperature, ion density and apparatus geometry. From these results, the average

v_c = 4.96 m/sec. This value agrees, within the experimental error, with the critical velocity obtained by the 'time-of-flight' method.

The magnitude of the discontinuity observed by the heat-flush method was found to be approximately equal to that observed in the 'time-of-flight' method. From this Careri concludes that the new dissipation suffered by the ion beam at v_c is due mainly to an increase in its interaction with the normal fluid. A small interaction with the superfluid would be too small for observation. This conclusion does not conflict with the model of a vibrating ion, since the drop in mobility in this case is also ascribed to an increased interaction with the n-fluid.

These heat flush results therefore neither conflict with nor confirm the author's model.

Meanwhile Gaeta[30,27,29] performed a very simple experiment which also gave evidence of a discontinuity in the motion of the ions at a critical velocity. Gaeta used a simple diode cell, one electrode of which was coated with a radioactive material to give a source of ions. Initially he used Po^{210} and later the β-emitter Pm^{147}. An electric field was supplied between the electrodes, and the current traversing the cell measured. At a given temperature the current was measured for several values of the applied field, and the measurements repeated at different temperatures. Current was plotted against temperature for constant field. A sharp increase in current is observed in each graph below a certain value of temperature. By extrapolating the two parts of the curve, the temperature at which the current increase begins was

determined. This transition temperature depended on field strength. Gaeta showed that the product of the known mobility at the transition temperature and the field strength equalled approximately the critical velocity observed by Careri.

Recombination of the ions is the mechanism which controls the number of ions available to traverse the cell and be recorded as current. The rise in current observed below a certain temperature at constant field, must be related to a decrease in the effective recombination coefficient. Gaeta, using an earlier technique where two beams of ions of opposite sign travel across the cell in opposite directions, looked for a change in the recombination coefficient r. He observed a fall in r at the critical velocity but of insufficient extent to account for the rise in current observed above.

Clearly in the single beam experiment recombination takes place only within the range of the β-particles which produce the ions, since outside this range there are ions of one sign only. Ions escaping the vicinity of the radio-active source should be received eventually at the collecting electrode. Therefore events in the region where the ions are produced control the amount of current passed across the cell.

The recombination coefficient measured above is the volume coefficient r obeying the Langevin expression

$$r = 4\pi e(\mu_+ + \mu_-) \quad \text{----------} \quad (39)$$

where e = electronic charge.

Opposing recombination the diffusion of the ions away from the columns of high ion density, is also directly proportional to mobility of the ions.

The horizontal portion of the current vs $\frac{1}{r}$ curve is evidence that these two effects in equilibrium, render the current density independent of mobility.

It is likely that recombination in the region of the production of the ions will obey a different law. The α or β-particle produces columns of ions, each column being then a localised area of high ion density. Moreover these newly created ions are simple ionised atoms before the electrostriction forces have time to gather a shell of helium atoms about the charge to form a bubble-like negative ion or drop-like positive ion. The 'naked' ion most probably has a very much enhanced recombination coefficient. Recombination in the region of ion production must be high since only about one ion in a thousand escapes and reaches the collecting electrode.

In this way recombination in the region of ion production can have a stronger effect on the measured current than recombination in the drift space. This could explain why Gaeta observed an effect corresponding to a large change of recombination coefficient while he could only detect a small change in recombination coefficient in the drift space.

The author wishes to suggest some alternative tentative explanations for the observed increase in current at sufficiently low temperatures, as follows:-

For sufficiently high fields, the large number of ions in the source

region move at supercritical velocity. Positive and negative ions reach their respective critical velocities under approximately the same field by virtue of the difference in their mobilities.

An ion performing an inelastic collision reflects a roton in the forward direction of ion motion. In this way an ion travelling through the liquid at a supercritical velocity will be preceded by rotons moving in the same direction. In order that ions of opposite sign should collide, they must 'break through' this barrier of rotons. This could result in a reduced recombination coefficient.

An alternative solution would be to postulate that vibrating ions recombine with much greater difficulty because of energy conservation conditions. Ions only recombine if they come within a certain distance 'd' of each other. At this distance the electrostatic forces between ions of opposite sign prevail over thermal agitation. Thomson suggested that this distance

$$d = \frac{2e^2}{3kT}$$

For vibrating ions the denominator may be larger. This explanation suffers from the disadvantage that ions vibrate for a time less than the mean-free-time between ionic collisions. This would mean that the probability of two ions, both vibrating, approaching one another, is insignificantly small.

Another much more feasible solution is as follows:-

The incident radio-active particles have sufficient energy to create a succession of vortex rings in their wake. These vortex rings

will then continue to travel along the original direction of the particle while at the same time losing energy by interaction with the n fluid. The initial velocity of the vortex rings is governed by their diameter according to the equation

$$v = \frac{\hbar^2}{4\pi r}\left(\beta - \frac{1}{4}\right) \quad \text{(Lamb}^{31}\text{)} \qquad \ldots\ldots\ldots \qquad (40)$$

This means that a β-particle should create a ring travelling at 100 m/sec. Within a few mean-free-paths, however, the ring will have slowed down to ~100 cm/sec. and simultaneously grow in size.

In the temperature range of Gaeta's experiments, there is a finite probability of capture of negative ions by vortices (Donnelly.)

It is suggested that the probabilities of capture and escape are such that the ion will be retained by the β-particle created vortex ring for a time comparable to the ion-ion collision time. This time is very much shorter than the time a negative ion is trapped on a vortex line as measured by Douglass[32] and predicted by Donnelly[33].

One must now postulate that a trapped ion finds it difficult to recombine with a neighbouring ion of opposite sign. In order to recombine, the one ion must escape from the vortex or the other one penetrate it. This may be a more difficult process than the recombination of free ions. Moreover, while trapped the ion is dominated by the motion of the vortex ring. The experiments of Rayfield and Reif demonstrate how strongly a vortex ring influences the motion of a trapped ion in an electric field, particularly at the lower temperatures 0.3 - 0.6°K where the probability

of capture is high and the probability of escape is low (Donnelly.) At $0.8^{\circ}K$ - $1.1^{\circ}K$ where Gaeta observed the increase in current, an ion will only remain trapped for a short time, nevertheless, the probability that one ion in a column will remain trapped sufficiently long to escape one chance of recombination is quite high. When this occurs the distribution of positive and negative ions along the column is disturbed such that one more ion, not necessarily the one originally trapped, can escape from the column.

Donnelly has shown that the trapping probability decreases exponentially with increasing relative velocity of ion and vortex.

Consequently, when an ion is slowed down by an inelastic collision, its chances of capture by a slow moving vortex ring are considerably enhanced. The higher probability of trapping results in an increase in the number of ions which can escape recombination.

It is not clear what should happen when the applied field strength is increased beyond the critical value. The probability of an exciting collision increases with increasing field, but the ion is not slowed down so much in the process. If one assumes that only the negative ions are trapped, which is approximately true, then at the higher fields the positive ions are removed more quickly from the range of influence of the negative ions.

In summary, the increase in current observed by Gaeta below a certain temperature and correlated with the critical velocity for the ions, is attributed to an enhanced trapping of the negative ions in

particular, such that the columnar recombination coefficient is reduced. It is suggested that the excitation of an ion increases the probability of its capture by a vortex ring.

Next, the author wishes to review briefly a series of papers, experimental and theoretical, connected with the structure of the ions in liquid helium. These papers have significance here since the size and structure of the ions are necessary for calculations of the frequency of vibration.

Atkins [9] (1959) suggested a structure for the ions which accounts for their surprisingly low mobility. One may expect ions to have a similar diffusion coefficient to He^3 atoms in He^4 liquid, but in fact the diffusion coefficient and hence also the mobility of the ions, is much less. Atkins suggested that in the region around the ion, the density of the liquid is increased by the electro-striction effect. This is the electrical polarisation of the surrounding atoms such that an ion drags around with it a large number of He^4 atoms. In this way the mobility and diffusion coefficient are reduced.

Substituting the molar polarisability into the Clausius-Mosotti formula and using thermodynamic arguments, Atkins derives the dependence of density ρ on the distance from the centre of the ion

$$\rho - \rho_o \propto \frac{1}{r^4} \qquad \text{----------} \qquad (41)$$

It is then a simple matter to calculate the extra mass associated with an ion of a given size. Also the extra mass outside a sphere of radius r_c not associated with the core of the ion, is given by

$$M_e = \frac{2\pi\gamma N\alpha_o e^2}{V_o u_1^2 \varepsilon_o r_c^2} \qquad \text{----------} \quad (42)$$

where $N\alpha_o$ = molar polarisability

u_1 = velocity of first sound

ε_o = dielectric constant

γ = ratio of specific heats

He shows that close to the ion the effective pressure is sufficient to solidify the helium. Knowledge of the dependence of pressure on radius enabled the extent of the solid region to be calculated.

The core of the ion is considered further. The effect of the electrostriction depends on whether the zero point motion of the charge in the core is faster than the velocity of sound, or not.

The motion of a positive hole between neighbouring neutral He. atoms, is considered. The average time between jumps from one neutral atom to the next would be given by

$$\bar{t} = \frac{h}{2z\Delta E} \qquad \text{----------} \quad (43)$$

where z = Number of neighbouring atoms

ΔE = energy separation

Putting in reasonable values, Atkins shows that the velocity during a single jump is $\gg u_1$. The effective velocity by random walk is then

$$\bar{v} = \frac{\delta}{n^{\frac{1}{2}} \bar{t}}$$

where δ = average interatomic distance

When $\frac{\delta}{n^{\frac{1}{2}}t} = u_1$, electrostriction can follow the motion. This occurs when $n = 10^5$. This would lead to such a large cloud of charge that electrostriction effects would be obliterated.

Atkins points out, however, that the preceding argument is for a monoatomic positive ion and argues that a polyatomic ion is much more likely. He then shows how electrostriction may give a reasonable approximation for the positive ion in this case.

Atkins suggests that, in the case of the negative ion, the electron may move freely between widely spaced atoms. This is the basis of the 'bubble' model for the negative ion developed later by other authors.

He then suggests three ways in which the effective mass of the ion might be investigated.

1. Careful investigation of field dependence of mobility.
2. Cyclotron resonance.
3. Velocity of second sound at low temperatures where ions are the main contribution to the normal component of of the fluid.

The most important points from this paper are the suggested reason for the large ions and the suggestion of different structures for positive and negative ions, leading to different cross-sections and mobilities.

At about the same time as Atkin's paper, Careri, Fasoli and Gaeta[35] published an experimental paper, also aimed at elucidating the structure of ions in liquid helium.

Reviewing Atkins' original suggestions, Careri et al suggest that

the structure of the positive ion, is still in question and there are, in fact, two possible models:-

I. Solid cluster of He. atoms, polarised round a positive charge, which may move within the cluster.

II Charge distributed in large region with density comparable to liquid. Charge jumping from one atom to another.

Similarly, three models are suggested for the negative ion:-

I. Solid cluster as for I above.

II. Cloud of charge self-trapped by shell of polarised atoms.

III. Free electron moving in large region of the density of the liquid, escaping by tunnelling any trapping which might occur.

IV. Charged impurity.

Their experiment was to measure the field dependence of ion current in a simple diode, completely filled or partly filled, with a classical liquid (CCl_4 and N_2) or liquid helium. When the cell was partly filled, the liquid gas phase boundary was parallel to and between the two electrodes. The classical liquids behaved as expected, giving identical results for positive and negative ions. In liquid helium, however, some important differences are noted:

(a) Above T_λ the current collected at a given field, was the same for filled or partly filled diode.

(b) Just below T_λ the field dependent positive ion current for the partly filled diode is much less than the negative ion current.

(c) At $T < 1^{\circ}K$ in the partly filled diode, the positive and negative ion current measured was negligibly small.

(d) When the helium in the cell was solidified, the current fell practically to zero.

Careri et al point out that the results for the partly filled diode may be readily understood. Ions need to acquire energy from excitations in the liquid in order to 'evaporate' from the surface. As the temperature drops below T_{λ} the number of excitations decreases rapidly and hence the current collected under these conditions falls rapidly. That the positive ion current is less than the negative ion current under these conditions, suggests that the positive ion is a more massive entity requiring a bigger 'push' to free it from the liquid surface. This immediately rules out structure I and IV. Little or no positive or negative ion current was measured at low temperature when a liquid gas interface was present in the cell, suggesting that tunnelling is absent or negligible, ruling out structure III for the negative ion.

The solid helium experiment rules out tunnelling by the positive ion, hence structure II must be discarded.

Careri et al therefore suggest that the positive ion is a cluster and the negative ion an empty bubble.

Later work supports these models and gives the present author a model from which to calculate vibrational energies.

Kuper[11] gives a more advanced theoretical foundation for the structure of the positive and negative ions and also calculates their scattering cross-section. He reperforms Atkins' calculation of the extra

mass associated with an ion subject to electrostriction. Kuper does this starting from the Hamiltonian of N He atoms and one ion, and then considers an ion at the origin of co-ordinates and calculates the volume of elements containing, on average, the same number of atoms as a fraction of their distance from the ion. Pressure increases on approaching the ion and so the volume elements decrease in size. Kuper obtains the same result as Atkins from this calculation

$$\int_{p_o}^{p} V\,dp = \frac{N_o \alpha e^2}{2\varepsilon^2 r^4} \qquad \text{----------} \qquad (44)$$

Integrating and using the equation of state for $^{+}$He gives a positive ion with a central solid sphere of radius $r_+ = 6.3\text{Å}$.

Kuper gives the excess mass for transport properties of the ion to be composed of three parts.

(a) The mass of the solid core as calculated by Atkins.

(b) The displacement mass $\frac{4}{3}\pi\rho_o r_+^3$ since when the solid core moves it must displace this amount of bulk liquid.

(c) 'Hydrodynamic' mass $= \frac{1}{2} \cdot \frac{4}{3}\pi\rho_o r_+^3$

This gives a total effective mass for the positive ion of $\sim 80\ m_{He}$. Kuper gives $100\ m_{He}$.

Kuper argues that the correct model for the negative ion is a single electron bound within a shell of helium atoms in the form of a 'bubble'. To calculate the size of this 'bubble' the radius is adjusted such that the pressure exerted by the electron outwards on the liquid, is equal to the pressure exerted by the liquid on the electron. The

pressure of liquid on the 'bubble' wall has components.

1. Pressure due to zero point motion

$$p_o = 60 \text{ atm.}$$

2. Pressure due to the Van der Waals attraction of He. atoms outside the 'bubble'.

$$p_{v.d.w.} = -38\left(1 - \frac{c^2}{r}\right) \text{ atm.} \quad \text{----------} \quad (45)$$

3. Electrostatic interaction gives a pressure

$$p_{es} = \frac{\rho e^2 \alpha}{2r^4} m_{He} \text{ atm.} \quad \text{----------} \quad (46)$$

4. The outward pressure exerted by the electron is

$$p_{kin.} = \frac{\pi h^2}{4mr^5} \text{ atm.} \quad \text{----------} \quad (47)$$

In equilibrium

$$p_o + p_{es} + p_{v.d.w.} = p_{kin.} \quad \text{----------} \quad (48)$$

Kuper solves this graphically and obtains $r_- = 12.1\text{Å}$.

The effective mass calculated from this radius is $= 100\ m_{He}$.

Kuper then goes on to compare theoretical and experimental ion-roton and ion-He^3 scattering cross-sections. He states that in ion-He^3 collisions, persistence of velocity is significant while in the ion-roton case, there is negligible persistence of velocity. While this is certainly true at low fields, this cannot be said for ion-roton collisions for ions having a velocity $v > v_c$, as shown elsewhere.

The collision cross-sections, experimental and theoretical, are shown to agree fairly well.

Kuper then comments that pressure should affect the positive and negative ions differently. The solid positive ion should grow, while the bubble-like negative ion should shrink under the influence of increasing pressure. He cites the experiments of Meyer[37] and Careri[38] where the mobility of the negative ion increased till at 7 atm. the two ions had identical mobilities. There was no evidence for the growth of the positive ion 'snowball'.

Finally, Kuper postulates that the observed limiting value of velocity $\cong 40$ m/sec. is due to ions creating bound excitations at this velocity.

The effect of pressure on ion mobility, as mentioned above, gives important evidence about the ion structure and size. Experiments have been performed by Careri's group and by Meyer and Reif to determine these effects of pressure on ions.

Cunsolo and Mazzoldi[39] used the 'time of flight' method for determining the mobility of ions at various pressures. They performed their measurements at 1.1 - 1.9°K with pressures up to the melting pressure at the lower temperature and up to the λ point at 1.9°K.

The mobility of the positive ion decreased monotonically with increasing pressure until, at the melting pressure, no current was collected. At the λ-transition, the mobility pressure curve dips rapidly downwards.

For negative ions the mobility pressure curve first rises then falls with increasing pressure. Cunsolo and Mazzoldi suggest that the drop in mobility observed for positive ions, is due to at least two things; (a) the dependence of the scattering cross-section and (b) the number density of rotons on pressure. They suggest also that the results obtained for the negative ion are consistent qualitatively with the 'bubble' model. Initial pressure increases reduced the bubble size so that mobility increases and then further pressure increases cause a decrease in mobility for reasons similar to those for the positive ions.

Meyer and Reif[37] performed similar experiments with their ion velocity spectrometer in which they determined the pressure dependence of mobility down to $\cong 0.5^{\circ}K$. They showed that at constant pressure $\log\mu$ is a linear function of T^{-1} the slope of these lines decreasing with increasing pressure. These results were essentially the same as those of Cunsolo and Mazzoldi except that in addition, they showed that above 7 atm. the mobilities of positive and negative ions were identical. They go on to discuss the scattering cross-section of ions with He^3 atoms and rotons and to show how persistence of velocity increases the effective scattering cross-section. Assuming ion effective mass and ion-roton cross-section are unaffected by density changes in the fluid, Meyer and Reif predict a temperature dependence given by

$$\ln.\,\mu \propto T^{-1} \text{ and pressure dependence by}$$

$$\mu \propto p_o^{-2} \exp.\left(\frac{\Delta}{kT}\right) \qquad \text{----------} \qquad (49)$$

They show that their observed pressure dependence agrees very well

with these formulae and that the decreasing mobility can almost completely be accounted for by the change in the dispersion relations in characterising the elementary excitations of the superfluid. In other words the ion size has little effect on the result. These results then do not support Atkins' suggestions that at high pressure the positive ion 'snowball' should increase in size. The negative ion is still doubtful. The fact that above 7 atm. the mobility of the negative and positive ions becomes equal suggests that the negative ion 'bubble' has 'collapsed' and that the structure is similar to the positive ion.

Careri, Dupre and Modena[40] have measured the mobility of ions at $0.2^{\circ}K$ by means of a magnetic deflection method. The mobilities obtained are low compared with the predicted values obtained from extrapolating measurements of mobility at higher temperature down to $0.2^{\circ}K$. The line drawn through the points on the graph given, seems rather pessimistic, however, and the zero-field mobility should be at least $\geqslant 10^4$ $cm^2/volt.sec.$ It seems likely that even at these low fields the ions create vortex rings and become trapped.

Meyer[41] reports a similar experiment in which he applies a transverse magnetic field to slowly moving ions. The mobilities in this case are consistent with the extrapolated value. In this case, however, the temperature is $0.415^{\circ}K$ while the field remains the same.

The paper most pertinent to the subject of periodic discontinuities in the drift velocity of ions is that recently published by Huang and Olinto[42]. They propose a phenomenological theory, different from that of the present author, to explain the results of Rayfield and Reif[13], and of

Careri, Cunsolo and Mazzoldi[1]. It will be reviewed in detail here.

Huang and Olinto suggest that all of the experiments on ion mobilities can be explained by postulating that ions create vortex rings at the critical velocity v_c and that under certain conditions the ion is trapped in this ring. Under an appropriate field the ions accelerate to v_c where they begin to create turbulence. They continue to travel at v_c while converting electrical energy into turbulent energy until sufficient energy has been transferred for the formation of one vortex ring of unit circulation.

For comparatively low electric fields in the region where Careri et al observed the discontinuities, the ion having created a vortex ring, breaks free and accelerates to its terminal velocity. The extra drag experienced at v_c manifests itself as a drop in apparent mobility. However, for very high electric fields (above the 'giant' discontinuity) or at low temperatures (experiments of Rayfield and Reif) the ion can become permanently trapped by the vortex ring it has just created. In this case the motion of the ion is dominated by the vortex ring; energy is fed from the electric field through the ion to the 'charged vortex ring' system which expands in size and slows down drastically.

Huang and Olinto make the following assumptions in developing this model:-

1. The vortex ring at creation moves with the velocity of the creating ion. A vortex ring of unit circulation, travelling at 5.2 m/sec. has a radius of 98Å and an energy of 0.22 eV.

2. At multiples nv_c of the initial critical velocity v_c, vortex rings

of circulation n are created. In other words a ring of unit circulation cannot be created at $2v_c$. Thus the vortex rings created are all of the same radius, 98Å, and their energy is $0.22n^2$eV.

3. The ion begins to create turbulence when its velocity is such as to satisfy the equation

$$\Theta vR = \frac{nh}{m} \quad (n = 1, 2, 3, \ldots) \qquad (50)$$

where Θ = a dimensionless number

v = velocity of ion

R = radius of ion

substituting

$n = 1$ and $v = 520$ cm/sec.

gives

$\Theta R^+ = 190$Å for positive ions.

Huang and Olinto put $R^+ = 10$Å and find that $\Theta = 6\pi$. However, the bulk of evidence is for a positive ion somewhat smaller than this $6.3 \rightarrow 8$Å; this would yield $\Theta = 30 \rightarrow 24$, or in HO notation $8\pi \rightarrow 10\pi$. So the choice of R = 10Å leading to $\Theta = 6\pi$ has no firm foundation.

4. Charged vortex rings have a life-time long compared to the time required for velocity measurements to be made.

Huang and Olinto consider the application of this model to the results obtained by Rayfield and Reif. These experiments were performed at $0.4 \rightarrow 0.7^\circ$K. At these temperatures the mean-free-path of an ion or a charged vortex ring is much longer than the length of the path across the cell. An ion under the influence of an electric field accelerates and in a negligibly small time, reaches 5.2 m/sec., at which velocity it creates

a vortex ring as described above. Because of the long mean-free-path, there is no mechanism for energy loss, consequently the ion is always captured and remains captured by the first ring it creates. The charged vortex ring then continues to gain energy from the electric field and, in doing so, slows down. The extremely good fit of the experimental points of Rayfield and Reif to a theoretical curve of velocity against energy for a vortex ring, strongly suggests that this is a true picture of the ion's journey across the cell under these circumstances.

The present author's description of these results also suggests that the ion is trapped by a vortex ring but gives a different mechanism for the creation of this vortex ring. Huang and Olinto suggest that the ion cannot accelerate beyond 5.2 m/sec. under these conditons whereas the present author postulates that the ion accelerates to $\sim$40 m/sec. where it has sufficient energy to create one roton. The two situations are indistinguishable in Rayfield and Reif's apparatus since the creation process occurs before the charged vortex ring reaches the measuring space.

Huang and Olinto give an argument for the stability or instability of an ion-vortex ring combination. They suggest that the viscous force on a charged vortex ring has two components, the viscous force on the ring itself and that due to the presence of the ion.

The total drag on the charged vortex ring is

$$F(v_1,T) = F_1(v,T) + \xi F_2(v,T) \qquad (51)$$

where F_1 = viscous drag on a neutral vortex ring

F_2 = viscous drag on an independent ion

ξ = undetermined parameter

Huang and Olinto suggest that $\xi = \frac{1}{3}$ and derive the total viscous force

$$F(v,T) = n\alpha(T)[\beta(v) - \frac{1}{4} - \frac{\ln}{n}\cdot(1 - \frac{v}{v_o})] * \quad (52)$$

(* see footnote.)

where n = number of units of circulation of vortex ring

$\alpha(T)$ = temperature dependent coefficient derived from Rayfield and Reif's results

$\beta(v) = \frac{8R(v)}{a}$ $R(v)$ = radius of vortex ring

a = radius of core of vortex ring

v_o = limit of velocity = 58 m/sec. from roton kinematics.

This viscous drag force has a minimum at a velocity $v_1 = 33$ m/sec.

For steady state motion, the accelerating force due to the field of strength ε must balance the viscous drag force.

$$e\varepsilon = n\alpha(T)[\beta(v) - \frac{1}{4} - \frac{\ln}{n}\cdot(1 - \frac{v}{v_o})] \quad (53)$$

If the applied field is insufficient to balance even the minimum drag force then steady state motion is impossible.

In this case the charged vortex ring breaks up, the ion slowing down

---

* If the value $\xi = 1/3$ is conscientiously substituted into the original formulae, the logarithmic term in equation (52) should be multiplied by 1.54. This does not alter the general shape of the curve but shifts the minimum to $v = 25$ m/sec. However, since the choice of $\xi = 1/3$ was somewhat arbitrary and since the value obtained by Huang and Olinto for $v = 33$ m/sec. ties in well with experiment, it would probably be better to adjust ξ in order to give a minimum at the right value. 1/4.5 would be approximately correct.

due to energy loss and the freed vortex ring accelerating.

If the field applies a force in excess of the minimum drag force, there are by the nature of the function $[\beta - \frac{1}{4} - \frac{\ln}{n}\cdot(1 - \frac{v}{v_o})]$, two possible values of velocity which will satisfy the steady state condition. Huang and Olinto assume that the lower of these two possibilities is the most likely.

In deriving a theoretical curve to agree with the experimental results of Careri, Cunsolo and Mazzoldi, Huang and Olinto first fit an exponential type curve to all the known mobility results in order to find a general form for the relation between terminal velocity v and applied field ε. This curve has to satisfy the two conditions

$$\begin{aligned} v_\infty &\underset{\varepsilon \to \infty}{\longrightarrow} v_o \\ v_\infty &\underset{\varepsilon \to o}{\longrightarrow} \mu_o \varepsilon \end{aligned} \qquad (54)$$

where v_o = velocity limit calculated from roton kinematics = 58 m/sec. and μ_o = zero field mobility.

The suggested dependence is

$$v_\infty(\varepsilon, T) = v_o[1 - \exp.(\frac{-\varepsilon}{\varepsilon_o})] \qquad \text{.....} \qquad (55)$$

where $\varepsilon_o = \frac{v_o}{\mu_o}$

To this curve Huang and Olinto apply regular perturbations at v_c, $2v_c$, etc. where ions create vortex rings. The periodicity of these discontinuities in the exponential curve is purely a result of the original condition for the creation of turbulence by an ion;

namely:

$$\theta v_{ion} R_{ion} = \frac{nh}{m} \qquad (56)$$

The critical velocities for the creation of turbulence are strictly v_c, $2v_c$, $3v_c$, etc. However, the measured critical drift velocities will appear progressively more closely spaced with increasing velocity. At a field giving $v = 3v_c$, for example, the ion will have spent a significant amount of time travelling at v_c and $2v_c$ while creating the first two vortex rings, before finally being accelerated to $3v_c$. Consequently the measured drift velocity will be less than $3v_c$ and the discontinuity associated with the creation of vortex rings of circulation $3\frac{h}{m}$, will appear at this reduced velocity.. Knowing the external field, the energy of the created vortex rings and the viscous forces involved, the time required to create each vortex ring can be calculated. In this way Huang and Olinto calculate the average drift velocity of the ions for increasing fields. This gives the detailed shape of the discontinuity. In a very rough way they compare the shape of the velocity-field curve thus obtained with Careri's results. The critical velocities and fields calculated by this method agree well with the experimentally determined values.

At very high fields, Careri observes a giant discontinuity. Huang and Olinto correlate this phenomenon with the high field trapping of the first vortex ring created by the ion. The ring is created at 5.2 m/sec., traps the ion and then adjusts its velocity to satisfy the lower root of equation (53).

The velocity of the ions falls off rapidly for fields increasing

beyond ε_c in accordance with equation (53) and in agreement with experiment.

The present author wishes to question some of the assumptions made in the Huang and Olinto paper and to compare more carefully the predictions with the experimental results of Careri and himself.

1. Why should the terminal velocity v_∞ of the ion necessarily approach exponentially the roton creation velocity $v_o = 58$ m/sec. as outlined in the condition

$$v_\infty(\varepsilon,T) \underset{\varepsilon \to \infty}{\to} v_o \qquad (57)$$

This is indeed a limit to the velocity of the ions, but one would expect this limit to occur as a discontinuity in the curve of increasing velocity with field. It would seem more consistent with experiment in fact, if the velocity curve was made to approach 50 m/sec. in agreement with Reif's results. This velocity, 50 m/sec. is however, the measured drift velocity and might, on Huang and Olinto's model, be less than the true terminal velocity of the ion v_∞. Therefore experiment rather than theory suggests that the terminal velocity should approach a velocity somewhat in excess of 50 m/sec. exponentially.

2. The final close agreement with experiment, particularly at low fields, is purely a result of the choice in the first place, of a curve which fitted existing experimental results.

3. There seems little doubt that the equation describing the form of the

$\langle v \rangle$ against ε curve beyond the giant discontinuity, is essentially correct and that the motion in this region is that of an ion trapped on a vortex ring of unit circulation. It still requires to be settled how and at what ion velocity the vortex ring is created.

4. Reif and Meyer observed ion velocities in excess of 40 m/sec. This contradicts the basic assertion of Huang and Olinto that the maximum possible drift velocity is $\sim$33 m/sec.

Employing their model, these results could be explained in two ways:

(a) The charged vortex ring chooses to adjust its velocity to the higher root of equation (53).

(b) The field in which the ion moves immediately prior to entering the measuring space, is sufficient to give the ion a velocity $v > nv_c$ ($n = 1, 2, 3, \ldots\ldots$) so that when the ion enters the accelerating field it accelerates to $(n + 1)v_c$ where it creates a vortex ring with circulation $(n + 1)$. The minimum of the function $[\beta - \frac{1}{4} - \frac{\ln}{n}(1 - \frac{v}{v_o})]$ increases with increasing n. For instance the minimum occurs at a velocity of $\sim$42 m/sec. for a charged vortex ring with two units of circulation. Therefore Meyer and Reif's observations of high velocities could be consistent with the ion having entered the measuring space with a velocity already in excess of $2v_c$.

This could readily be verified in Careri's apparatus. Variation of the grid-source field should then alter the position of the giant discontinuity.

5. At $1^{\circ}K$ Donnelly has shown that only the negative ion has a finite capture probability on a vortex. This would affect the model in the region of the giant discontinuity where capture of the ion by the vortex ring is a fundamental requirement. It seems possible that the ion may not be captured in the core of the vortex ring, but that the vortex ring is held in the wake of the ion. At ~ 33 m/sec. the vortex ring is sufficiently small for this to seem reasonable. This would obviate the difficulty.

6. The model of Huang and Olinto seems to be least satisfactory in the low field region where the periodic discontinuities are observed. The idea of a gradually produced vortex ring is not easy to grasp particularly in liquid He II where circulation $< \frac{h}{m}$ cannot exist in a stable state.

7. It is also difficult to visualise how a positive ion of radius $\sim 7\text{Å}$ can create a vortex ring of radius 98Å and a negative ion radius $\sim 12\text{Å}$ create a vortex ring 252Å in radius.

Careri also postulates the creation of a vortex ring of this size justifying this by saying that the effect of the charge on the density of the surrounding liquid extends a long way beyond the solid core of the ion. While agreeing with this last statement, the present author feels that, since the effect of the charge at 100Å is very small, the 'size' of the ion complex cannot have a distinct value of 98Å attributed to it. The velocity of vortex rings of this order of magnitude is also quite sensitive to radius so an ion of rather arbitrary radius would lead to a very ill-

defined critical velocity.

Atkins has suggested that the density excess due to the presence of a charge is $\propto \frac{1}{r^4}$. This would mean that 100Å from the ion the excess density is 15×10^{-8} grm/cm^3. This is negligible in comparison to the bulk liquid density of 14×10^{-2} grm/cm^3. Perhaps a small vortex ring of the dimensions of the ion radius is first produced and is prevented from overtaking the ion, growing in size as it gains energy from the field through the ion until its size is consistent with the velocity of the ion.

8. Huang and Olinto suggest that having created a vortex ring, the ion then accelerates to the terminal velocity appropriate to the applied field. This prompts the question:- Why doesn't the ion, having just created a vortex ring, start immediately to create another? In fact, how can an ion ever accelerate beyond the first critical velocity? May be, after creation, the presence of the vortex ring enables the ion to accelerate, by preventing the immediate production of a second ring. Once clear of the critical velocity, the ion cannot satisfy equation (56) and cannot, therefore, create turbulence.

9. At $v = nv_c$ a ring having n-units of circulation, is created. This results in rings having the same radius independent of n. This condition would have seemed reasonable had the vortex ring and ion been of approximately the same size, but they are not by at least an order of magnitude. One must ask if this limitation is necessary. The model states that an ion travelling at $v = 2v_c$, for

example, creates a vortex ring with two units of circulation, whereas there seems no reason why it should not create the less energetic and small singly quantised rings.

10. The size of the discontinuity in the mobility of positive ions at $v = nv_c$ as calculated from Huang and Olinto's equations, are:

Velocity	% Drop in μ
5.2 m/sec.	1.2
10.3 m/sec.	2.1
15.1 m/sec.	2.7
19.7 m/sec.	3.2

These are considerably smaller discontinuities than those observed by Careri and by the present author. The average discontinuity observed at 52 m/sec. was $\sim 7\%$.

There seems to be no way of correcting their theory to allow for this.

11. As will be seen from the above figures the size of the discontinuity was gradually increasing with increasing velocity. Such an increase has not been observed.

12. On this model, the size of the discontinuity would be strongly dependent on the length of the flight path of the ion. (See Appendix 7) The shorter the path of the ion, the bigger the effect of the creation process on the overall measured drift velocity. Suspecting a process of this kind, the present author varied the grid-collector distance and observed no significant change in the size of the discontinuity. (See Fig.32)

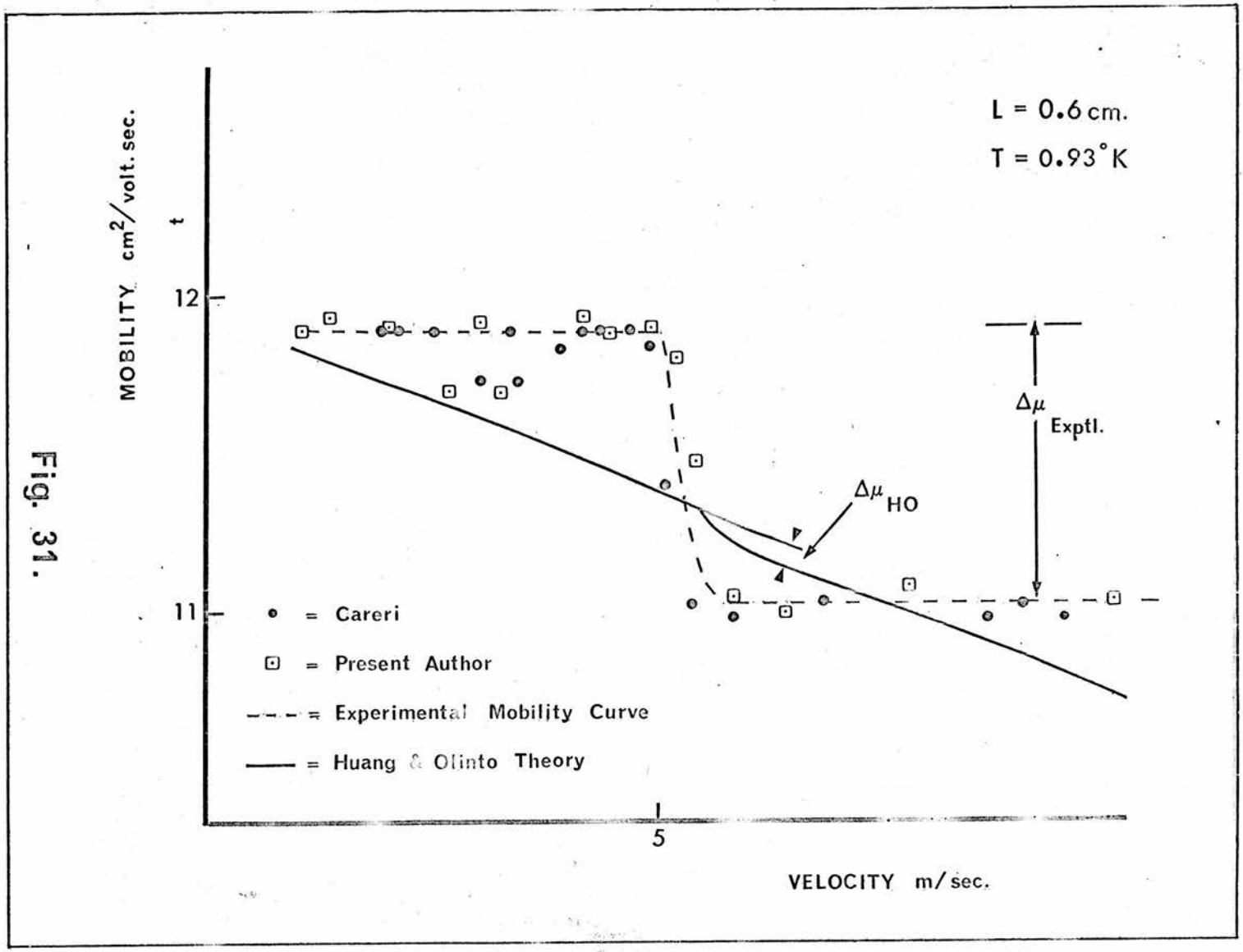
L = 0.6 cm.
T = 0.93°K
MOBILITY cm²/volt.sec.
12
11
Δμ Exptl.
Δμ HO
= Careri
= Present Author
= Experimental Mobility Curve
= Huang & Olinto Theory
5
VELOCITY m/sec.

Fig. 31.

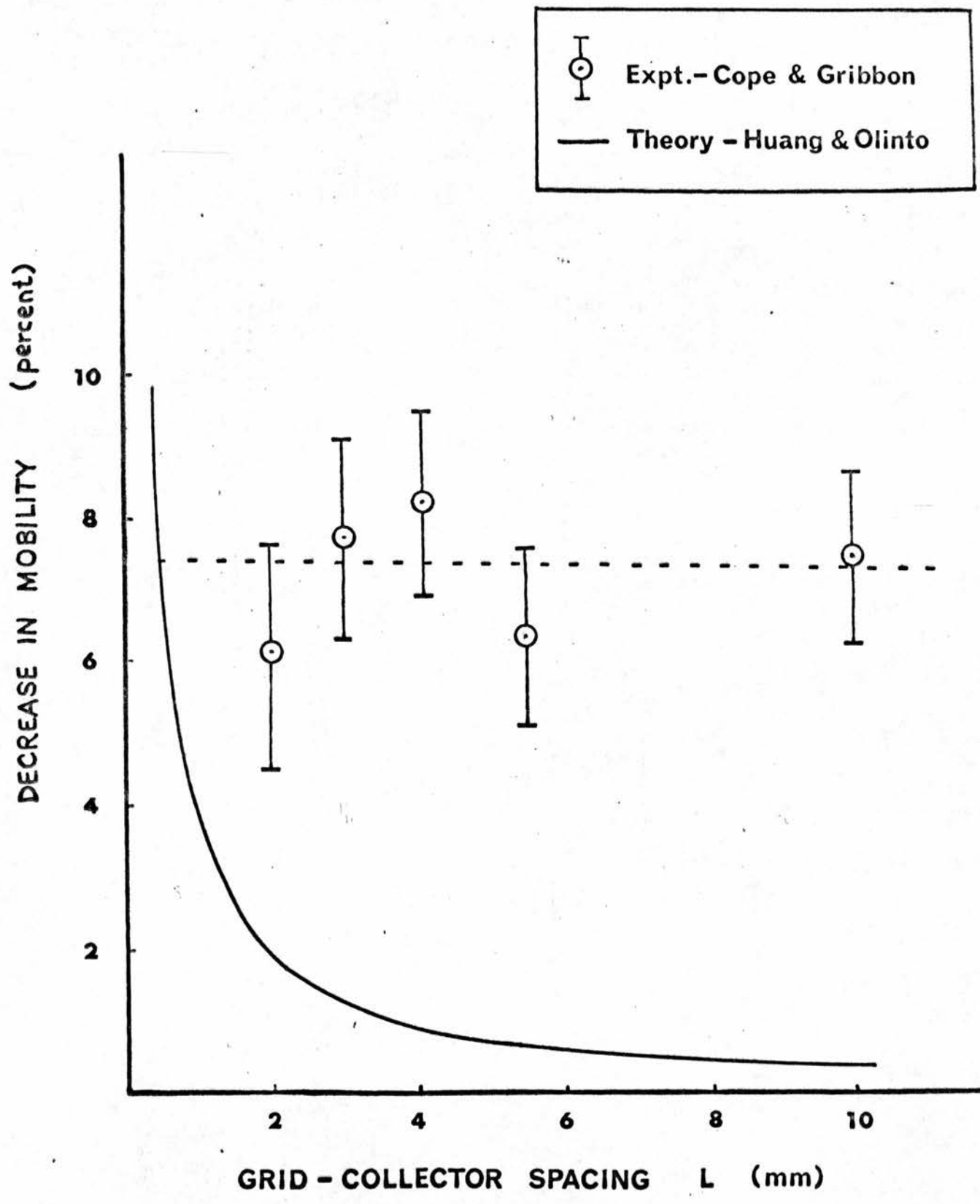
Expt.– Cope & Gribbon
Theory – Huang & Olinto
DECREASE IN MOBILITY (percent)
10
8
6
4
2
2
4
6
8
10
GRID – COLLECTOR SPACING L (mm)

FIG. 32.

13. In favour of Huang and Olinto's model are the author's results on the variation of discontinuity size with grid-source field. Increasing the grid-source field so that ions could have acquired $v = v_c$ before penetrating the grid, drastically reduced the size of the discontinuity. This would be easily explained on the present model by saying that for high grid-source fields the dissipative creation process occurs within the grid-source space and the ion had acquired its terminal velocity before entering the measuring space.

14. The calculated shape of the mobility versus field curves, differs somewhat from experimental observations. Measured mobility has successively smaller but constant values while the theoretical curve shows a continuously decreasing mobility with discontinuities superimposed. This is simply due to the original choice of an exponential curve to fit all the results. A better approximation could be made for low field results which would give the observed discontinuity shape.

Considerable doubt was thrown upon the quantum nature of the periodic discontinuities when Henson[45] published a paper reporting discontinuities in the mobility of ions in liquid Ar. and N.

Henson used a field ionisation ion source of a type described by Muller. He passed the ions through a velocity spectrometer similar in principle to that used in the Reif experiments, but somewhat different in operation.

The mobilities of ions in both Argon and Nitrogen were observed to

be constant over a range values of field changing abruptly in a stepwise fashion, to a new constant level. Zero field mobilities of ions in Argon are 6.0×10^{-4} and in Nitrogen 2.5×10^{-3} $cm^2/volt.sec$. All mobility steps were downwards with increasing field, except the first one in Argon which was upward. The step positions in relation to field, were dependent on the source field and the shutter field. The steps though not strictly periodic, they were approximately evenly spaced in velocity. There is such a strong resemblance to the results in liquid helium that it seems most likely that the phenomena demonstrates the same basic effect. Since in classical liquids there is no restriction on circulation, it seems unlikely that the results can be described by the formation of quantised vortex rings. However, vibrational states of fundamental and harmonic frequencies could be excited. In fact Henson suggests that this might be the solution to his results. The near periodicity in the case of the discontinuities in liquid helium was due to the fact that

$$\frac{2p_o^2}{m} \simeq \frac{1}{2} kT$$

If these two quantities are not equal, as may be the case in Argon and Nitrogen, equally spaced but not periodic discontinuities would be predicted.

CONCLUSION

The aims of the original experiment have been achieved at least in part. The existence of the periodic discontinuities has been confirmed and the effect of varying certain parameters has been investigated.

The author has measured the critical velocity for the first discontinuity for both positive and negative ions, and was in fact, the first to observe the first discontinuity for negative ions.

It has been postulated that the results for ions can be explained in terms of the excitation of vibrational states and the dynamics of ion-roton collisions.

The theory explains:

(i) The value for the first critical velocity more closely than the vortex ring theory

(ii) The difference between the critical velocities for negative and positive ions

(iii) The periodicity

(iv) The giant discontinuity at 28 m/sec.

(v) The variation of discontinuity size with grid-source field

The following experiments are suggested for further study:-

(a) The measurement of ion velocities with greater accuracy, preferably better than 0.1%, would enable the investigation of the ion velocities close to the discontinuity to see whether the average drift velocity v_d is less than v_c at fields just in excess of E_c. Definite evidence on this

point would favour one of the two models proposed for the discontinuity.

(b) The determination of the detailed velocity-field curve for ions using a 'Meyer and Reif' type velocity spectrometer. It would be valuable to have an independent observation of the critical velocities using this different measuring technique.

(c) The measurement of ion velocities in a normal fluid 'wind-tunnel'. More elaborate and meaningful results could be obtained if a uniform normal fluid flow could be superimposed over the whole flight-path of an ion. The 'wind-tunnel' would require careful designing in order to preserve uniform field conditions with uniform normal fluid velocity.

(d) The effect of the grid-source field on the giant discontinuity would be of interest. If the Huang and Olinto model is accepted, the giant discontinuity should be affected by the velocity of the ion prior to its entry into the measuring space. If the ion velocity in the grid-source space is greater than v_{c_1}, the giant discontinuity should not occur until the ion acquires v_i = 42 m/sec. in the measuring space. Higher ion velocities in the grid-source space should retard the appearance of the giant discontinuity even further.

REFERENCES

Part I - Radial Flow of Superfluid Helium Over a Horizontal Plate

1. Jackson, L. C. and Grimes, L. G.
Advanc. Phys., 7, 435, (1958)

2. Allen, J. F.
Proc. Int. School Phys. 'E. Fermi',
Varenna, P. 305, (1961)

3. Atkins, K. R.
'Liquid Helium' (Cambridge University
Press) P. 200, (1959)

4. Robinson, J. E.
Phys. Rev., 82, 440 (1951)

5. Manchester, F. D. and Brown, J. B.
Canad. J. Phys., 35, 483, (1957)

6. Dzyaloshinskii, I. E., Lifshitz, E. N.
and Pitaevskii, L. P.
Sov. Phys., J.E.T.P., 37, 161, (1960);
Advanc. Phys., 10, 165, (1961)

7. Gribbon, P. W. F., and Cope J. A.
Phil. Mag., 8, 2047, (1963)

Part II - Ion Mobility Discontinuities in Liquid Helium

1. Careri, G., Cunsolo, S. and Mazzoldi, P. 'Periodic Discontinuities in the Drift Velocity of Ions in Superfluid Helium', Proc. VIII Conf. Low Temp. Phys., London, P. 90, (1962)

2. Careri, G., Cunsolo, S. and Mazzoldi, P., 'Periodic Discontinuities in the Drift Velocity of Ions in Liquid Helium II', Phys. Rev., 136, A303, (1964)

3. Meyer, L. and Reif, F., 'Mobilities of Helium Ions in Liquid Helium', Phys. Rev., 110, 279, (1958)

4. Careri, G., Cunsolo, S. and Dupre, F., 'Ionic Mobilities in Liquid Helium II', Proc. VII Int. Conf. Low Temp. Phys., Toronto, P. 498, (1960)

5. Careri, G., Cunsolo, S. and Mazzoldi, P., 'Critical Drift Velocity of Ions in Liquid Helium', Phys. Rev. Letters 7, 151, (1961)

6. Feynman , R. P., 'Prog. in Low Temp. Phys.', edited by C. J. Gorter (Interscience Publishers Inc., New York.), 1, 34, (1955)

7. Rayfield, G. W. and Reif, F., 'Evidence for the Creation and Motion of Quantized Vortex Rings in Superfluid Helium', Phys. Rev. Letters, 11, 305, (1963)

8. Edwards, M. H. and Woodbury, W. C., 'Compressibility of Liquid He^4', Can. J. Phys. 39, 1833, (1961)

9. Atkins, K. R., 'Ions in Liquid Helium', Phys. Rev., 116, 1339, (1959)

10. Bohr, N., Nature, 137, 344, (1936)

11. Kuper, C. G., 'The Structure and the Mobility of Ions in Liquid Helium', Proc. Int. Summer School Phys., 'E. Fermi', Varenna, P. 414, (1961)

12. Cope, J. A. and Gribbon, P. W. F., 'Vibrating Ions in Liquid He II', Phys. Letters, 16, 128, (1965)

13. Rayfield, G. W. and Reif, F., 'Quantized Vortex Rings in Superfluid Helium', Phys. Rev., 136, A1194, (1964)

14. Atkins, K. R., 'Liquid Helium', (Cambridge University Press), P. 69, (1959)

15. Loeb, L. B., 'Kinetic Theory of Gases', (McGraw-Hill Book Co.) P. 98, (1934)

16. Loeb, L. B., 'Kinetic Theory of Gases', (McGraw-Hill Book Co.) P. 601, (1934)

17. Cohen, M. and Feynman, R. P., Phys. Rev., 107, 13 (1957)

18. Reif, F. and Meyer, L., 'Study of Superfluidity in Liquid Helium by Ion Motion', Phys. Rev. 119, 1164, (1960)

19. Jeans, J. H., 'Dynamic Theory of Gases', (Cambridge University Press), PP. 260, 275, (1921)

20. Cope, J. A. and Gribbon, P. W. F., Proc. IX Conf. Low Temp. Phys., Columbus, Ohio, P. 353, (1965)

21. Henshaw, D. G. and Woods, A. D. B., Phys. Rev., 121, 1266, (1961)

22. Verster, J. L., 'On the Use of Gauzes in Electron Optics', Philips Research Report, 18, 465, (1963)

23. Williams, R. L., 'Ionic Mobilities in Argon and Helium Liquids', Can. J. Phys., 35, 134, (1957)

24. Careri, G., Cunsolo, S. and Vincentini Missoni, M., 'Discontinuity of the Drift Velocity of Ions in He II Detected by the Heat Flush Effect', Proc. VIII Conf. Low Temp. Phys., London, P. 86, (1962)

25. Careri, G., Scaramuzzi, F. and Thomson, J. O., 'Heat Flush and Mobility of Electric Charges in Liquid Helium:- I. Non-Turbulent Flow', Nuovo Cimento, 13, 186, (1959)

26. Careri, G., Scaramuzzi, F. and Thomson, J. O., 'Heat Flush and Mobility of Electric Charges in Liquid Helium:- II. Turbulent Flow', Nuovo Cimento, 18, 957, (1960)

27. Careri, G. and Gaeta, F. S., 'Ionic Recombination in Liquid Helium', Proc. VII Int. Conf. Low Temp. Phys., Toronto, P. 505, (1960)

28. Careri, G., Cunsolo, S. and Vicentini Missoni, M., 'Critical Velocities of Ions in Liquid He II Detected by Heat Flush', Phys. Rev., 136, A311, (1964)

29. Careri, G. and Gaeta, F. S., 'Ionic Recombination in Liquid Helium', Nuovo Cimento, 20, 152, (1961)

30. Gaeta, F. S., 'Ionic Recombination in Superfluid Helium at Supercritical Velocities', Proc. VIII Conf. Low Temp. Phys., London, P. 92, (1962)

31. Lamb, H., 'Hydrodynamics', (New York, DoverPublications), P. 241, (1932)

32. Douglass, R. L., 'Ion Trapping in Rotating Helium II', Phys. Rev. Letters, 13, 791, (1964)

33. Donnelly, R. J., 'Theory of the Interaction of Ions and Quantized Vortices in Rotating Helium II', Phys. Rev. Letters, 14, 39, (1965)

35. Careri, G., Fasoli, U. and Gaeta, F.S., 'Experimental Behaviour of Ionic Structures in Liquid Helium II', Nuovo Cimento, 15, 774, (1960)

37. Meyer, L., 'Ion Motion in Superfluid Liquid Helium under Pressure', Phys. Rev., 123, 727, (1961)

38. Careri, G., 'Ions in Liquid Helium', Proc. Int. School Phys., 'E. Fermi', Varenna, P. 423, (1961)

39. Cunsolo, S. and Mazzoldi, P., 'The Influence of Pressure on the Mobility of Electric Charges in Liquid Helium II', Nuevo Cimento, 20, 949, (1961)

40. Careri, G., Dupre, F. and Modena, I., 'Magnetic Deflection of Positive Ions in Liquid Helium at 0.2^{o}K', Nuovo Cimento, 22, 318, (1961)

41. Meyer, L., 'Ions in Helium II in a Magnetic Field', Proc. IX Int. Conf. Low Temp. Phys., Columbus, Ohio, P. 338, (1964)

42. Huang, K. and Olinto, A. C., 'Quantized Vortex Rings in Superfluid Helium, A Phenomenological Theory', Phys. Rev., 139, A1441, (1965)

43. Vignos, J. H. and Fairbank, H. A., 'Sound Measurements in Liquid and Solid He^3, He^4, and He^3-He^4 mixtures', Phys. Rev., 147, A185, (1965)

44. Griffiths, D. J., Osborne, D. V. and Allen, J. F., 'Velocity Fields of Helium II Carrying a Heat Current', Proc. Roy. Soc., 287, 328, (1965)

45. Henson, R., 'Mobility of Positive Ions in Liquid Argon and Nitrogen', Phys. Rev., 135, A1002, (1964)

46. Brown, D. R., Nature, 202, 868 (1964)

47. Donnelly, R. J., Phys. Rev. Letters, 14, 39 (1965)

48. Allen, J. F. and Jones, H., Nature, 141, 203 (1938)

49. Bowers, R. and Mendelssohn, K., Proc. Phys. Soc. A. 63, 1318

50. See for example - Atkins, K. R. 'Liquid Helium' P. 99.

51. See for example - Newman, F. H. and Searle, V. H. L., 'The General Properties of Matter' Arnold, P.181, Equation (16-15)

52. Allen, J. F. and Misener, A. D., Proc. Comb. Phil. Soc., 34, 299.

53. van Alphen, W. M., van Haasteren, G. J., de Bruyn Ouboter, R. and Taconis, K. W., Phys. Letters, 20, 474.

54. See for example - Coulson, C. A., 'Waves' Oliver and Boyd, P.60.

55. Brown, D. R., Nature, 202, 868 (1964)

56. Wood, A. D. B. and Hollis Hallett, A. C., Can. J. Phys. 41, 596, (1963)

57. Huang K. from 'Quantum Fluids' edited Brewer, D. F., North Holland (1966) P. 332.

58. See for example - Jeans, J. 'The Kinetic Theory of Gases' C. U. P. P.233.

59. Bruschi, L., Mazzoldi, P. and Santini, M. Phys. Rev. Letters, 17, 292, (1966)

60. Dahm, A.J. and Sanders,T.M.Jr. Phys. Rev. Letters, 17, 126 (1966)

NOTATION

I - RADIAL FLOW

a	- Cross sectional area of observation capillary
A	- Cross sectional area of superleak
d	- Depth of liquid on the plate
d_o	- Depth of liquid at which n-fluid flow becomes negligible
f	- Frequency of waves
h	- Height of sessile drop
h_m	- Maximum height of edge drop
ℓ	- Length of the superleak (Page 21)
ℓ	- Film thickness (Page 24)
Q	- Transfer rate across the plate
r	- Radius of Sessile drop
$r_{1,2,3,}$	- Radii of curvature of drop surface
r_c	- Radius on plate at which flow becomes turbulent
s	- Arc length of drop profile
u	- Velocity of surface waves
v	- Velocity of bulk liquid
y	- Depth of liquid below top of drop
ε	- Dielectric constant
θ	- Predicted angle of contact
μ	- Chemical potential

ρ - Bulk liquid density

σ - Surface tension

Ψ - Angle between tangent to drop profile and the horizontal

$\tilde{\omega}$ - Characteristic frequency related to the surface

ω_a - Frequency of adiabatic oscillations

ω_i - Frequency of isothermal oscillations

II - IONS

a - Vortex ring core radius

A - Area of grid

c - Velocity of sound in the ion

d - Mean interatomic distance

d_o - Grid-collector spacing

e - Electronic charge

E - Applied field

E_c - Field necessary for ion to reach the critical velocity

E_{gc} - Grid-collector field

E_{gs} - Grid-source field

E^+ - Energy of vibrating positive ion

E^- - Energy of vibrating negative ion

$\hbar$ - Planck's constant

i - Ion current

I - Ion current

i_o - Ion current for constant field across the measuring space

L - Distance from grid

m - Total mass of vibrating atoms. (Page 100)

m, m_i - Ion mass

m_{eff} - Effective mass of ion

m_r - Mass of roton

M - Mass of liquid drop

$n(E)$ - Number of rotons with energy E

N_r - Number density of rotons

p - Pressure at the ion

p_o - Intrinsic momentum of roton

p_T - Thermal momentum of roton

$\dot{Q}$ - Heat input

r - Vortex ring radius. (Page 93)

R, r - Ion radius. (Page 100)

S - Entropy

S_c - Distance covered by ion while accelerating from v_o - v_c

S_E - Distance travelled between excitations minus S_c

t_c - Time required for ion to accelerate from v_o - v_c

t_E - Time between inelastic collisions minus t_c

u - Velocity of sound in the bulk liquid

v, v_i - Ion velocity

v_c^+ - Positive ion critical velocity

v_c^- - Negative ion critical velocity

v_d - Terminal drift velocity

v_o - Velocity of ion immediately after an inelastic ion-roton collision

v_r - Roton velocity

v' - Ion velocity after any collision

V_n - Volume flow of n-fluid

x - Amplitude of radially pulsating ion

γ - Applied square wave frequency. (Page 34)

γ_c - Cut-off frequency

γ - Vibrational frequency. (Page 97)

Δ - Intrinsic energy of a roton

η - Viscocity of n-fluid

θ - Ion-roton collision diameter

κ - Circulation

κ - Bulk modulus. (Page 97)

λ - Wavelength of ion vibrations

λ_{ir} - Ion-roton mean-free-path

μ - Ion mobility

ρ - Bulk liquid density

ρ - Ion density. (Page 97)

ρ_n - n-fluid density

ρ_s - s-fluid density

σ - Surface tension

τ - Mean-free-time between collisions

$\bar{\omega}$ - Effective mass of rotons from neutron scattering

Appendix 1 (P. 34)

The Variation of Measured Ion Current with the Frequency of the Applied Square Wave Field

Let L = Grid-collector separation

γ = Applied Square Wave Frequency

μ = Ion Mobility

E = Applied Field

n_o = Density of Ions per cm^3

A = Cross-sectional Area of Ion Beam

Then the length of the forward pulse = $\frac{1}{2\gamma}$ secs.

The distances travelled by the ions during this time

$$s = \text{velocity} \times \text{time} = \frac{\mu E}{2\gamma} \quad \text{---------- (a)}$$

All ions travelling further than the distance L from the grid will be collected and eventually pass through the electrometer, which measures the average current over a time long compared to the period of the applied square wave.

$\therefore$ Number of ions N collected during every forward pulse

$$N = A \left(\frac{\mu E}{2\gamma} - L \right) n_o \quad \text{---------- (b)}$$

$\therefore$ Current recorded 'i' = $\frac{\text{Charge collected}}{\text{Period of Square Wave}}$

$$\therefore i = \frac{Ne\gamma}{} \text{ amps.} \quad \text{---------- (c)}$$

where e = ion charge.

For Direct Current conditions the current i_o collected would be

$$i_o = n_o A. \mu E.e \text{ amps.} \quad \text{---------- (d)}$$

From equations (b), (c) and (d)

$$i = i_o \left(\frac{1}{2} - \frac{\gamma L}{\mu E} \right) \text{ ---------- (e)}$$

This is equation (1) Page 34.

N.B. For very low frequency γ of the applied field, the situation approximates the D.C. situation. Under these circumstances the current collected $i \approx \frac{i_o}{2}$ and not i_o since even at very low frequencies the field is reversed for half of the time.

Appendix 2 (P. 39)

Grid Dimensions

	Grid A	Grid B
Number of Holes	22	21
Shape of Holes	Square	Round
Diameter	0.8 mm.	0.8 mm.
Area	64×10^{-4} cm.^{2}	50×10^{-4} cm.^{2}
Total Open Area	.14 cm.^{2}	.11 cm.^{2}
Percentage Open Area	20 % ?	30 % ?

Appendix 3 (P. 66)

Error in $\Delta\mu$ for Varying Grid-Collector Separation L

Now $\Delta\mu = \mu_L - \mu_H$

where μ_L = Low field mobility

μ_H = High field mobility

and $\mu = \frac{\text{ion velocity}}{\text{applied field}} = \frac{2\gamma L}{E}$

where γ = cut-off frequency

Possible error in $\dot{\gamma} \approx 1\%$ (i.e. 5 c/s in 500 c/s.)

Possible error in L = $\pm$ 0.05 mm.

L	Error
2 mm	2.5 %
3 mm	1.7 %
4 mm	1.25 %
5 mm	1.0 %
10 mm	0.5 %

Possible error in E $\sim$ 0.5 %

$\therefore$ Total possible error in μ

Total possible error in μ	L
4.0 %	2 mm
3.2 %	3 mm
2.75 %	4 mm
2.5 %	5 mm
2.0 %	10 mm

Each mobility value is the average of at least six observations.

$\therefore$ Probable error in $\mu = \frac{\text{Possible Error}}{\sqrt{6}}$

$\therefore$ Probable error in μ	L
1.65 %	2 mm
1.3 %	3 mm
1.15 %	4 mm
1.0 %	5 mm
0.8 %	10 mm

If $\mu_L = 10\ cm^2 volt^{-1} sec.^{-1}$

and $\mu_H = 9\ cm^2 volt^{-1} sec.^{-1}$

Then for L = 2 mm.

$$\Delta\mu = 10 \pm 0.165 - 9 \pm 0.15$$

$$= 1 \pm 0.315$$

then

$$\Delta\mu \approx 10\% \pm 3\%$$

Similarly for L = 3, 4, 5 and 10 mms.

Error in $\Delta\mu$	L
$\pm$ 3.3 %	2 mm
2.6 %	3 mm
2.3 %	4 mm
2.0 %	5 mm
1.6 %	10 mm

Appendix 4 (P. 83g)

Mean-Free-Path of an Ion in a Regular Array of Vortex Lines

Suppose there are n vortex lines passing through unit area, each of 'collision' diameter σ.

An ion starts from some point and travels through this array of lines until it approaches within the distance 'd' of one vortex line. It is then captured by the vortex line.

The Probability P_r that the ion will be captured by a vortex line after having travelled a distance between r and r + δr equals the product of the probability P_{o_r} that the ion will not be captured while travelling the initial distance r and the probability $P_{c_{\delta r}}$ of ion capture within a path length δr.

$$\text{Now } P_{c_{\delta r}} = \frac{\text{The capture area presented to the approaching ion at the given section}}{\text{The total area of the section}}$$

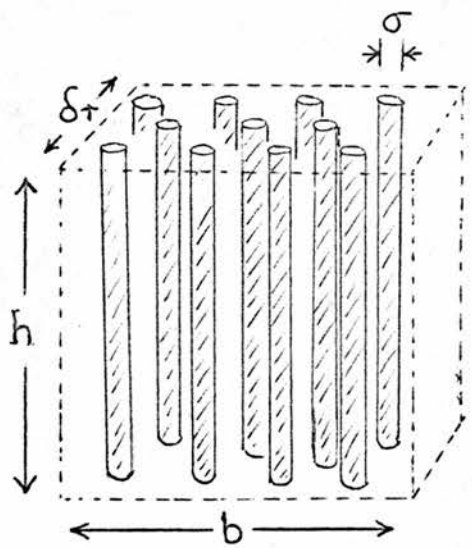

$$= \frac{n.b\ \delta r.\ h.\ \sigma}{b.\ h} = n\ \sigma\ \delta r \quad \text{---------- (f)}$$

$$\therefore \quad P_r = P_{c_{\delta r}} \cdot P_{o_r} = n.\sigma.\delta r \, P_{o_r} \qquad \text{---------- (g)}$$

This gives the probability of an ion free path of exactly 'r'.

The probability P_{c_r} that the ion will have a free path of length 0 - r; or alternatively the probability that the ion will be captured somewhere within the range r, is given by

$$P_{c_r} = \int_o^r P_r \, \delta r = \int_o^r n.\sigma.P_{o_r} \, \delta r \qquad \text{---------- (h)}$$

But P_{o_r} = the probability that the ion will not be captured in the range 0 - r.

$$\therefore \quad P_{o_r} = 1 - P_{c_r} = 1 - \int_o^r n.\,\sigma.\,P_{o_r} \, \delta r \qquad \text{---------- (j)}$$

$$\therefore \quad \frac{dP_{o_r}}{dr} = -n\sigma P_{o_r}$$

$$\therefore \quad P_{o_r} = Ae^{-n\sigma r}$$

Where A = Constant

$$\therefore \quad P_r = Ae^{-n\sigma r} \, n\sigma\delta r \qquad \text{---------- (k)}$$

But the ion is certain to be captured within the range $0 \rightarrow \infty$

$$\therefore \quad \int_0^\infty P_r = 1 = A \int_0^\infty e^{-n\sigma r} \, n\sigma\delta r = A \qquad \text{---------- (m)}$$

$$\therefore \quad A = 1$$

$$\therefore \quad P_r = n\sigma e^{-n\sigma r} \, \delta r$$

The mean free path λ of the ion in this array of vortex lines is then

$$\lambda = \int_0^\infty r P_r \delta r = \int_0^\infty n\sigma r e^{-n\sigma r} \delta r = \frac{1}{n\sigma} \qquad \text{---------- (n)}$$

Appendix 5 (P. 120)

The Sharpness of the Discontinuities

The positive ion critical velocity (5.2 m./sec) at which the first mobility discontinuity occurs, has been determined to within ± 0.1 m/sec. The distinct nature of the discontinuity as shown by this small uncertainty in the critical velocity, is surprising since at 1°K the random thermal velocity of the ions is approximately 8 m/sec. Any model which depends on the instantaneous velocity of the ions would, therefore, predict that the discontinuity would be so 'blurred' that it would not be observed at all.

K. R. Atkins challenged the Huang-Olinto theory on these grounds at the 1965 Sussex Conference.[57] Huang's reply was that "at $\approx$ 1°K the ion mean-free-path is comparable to its radius, so that the ion performs a trembling motion, which can be decomposed roughly into a smooth average motion and a random fluctuation."

In Huang's model the average drift velocity and not the instantaneous thermal velocity operates, since the creation of a vortex ring takes a long time compared to the mean-free-time between ion-roton collisions.

For the 'vibrating ion' model to predict a sharp discontinuity, either

(a) the ions are not 'thermalised' between exciting collisions

or

(b) there must be a long interaction time for the type of inelastic ion-roton collisions which excite vibrations

Suggestion (a) would require a long thermal 'relaxation time'.

Substituting a roton viscosity $\sim 10^{-5}$ poise[56] into Maxwell's expression[58] gives a relaxation time of 5×10^{-9} secs. and therefore the ion can easily acquire thermal velocities between 'exciting' collisions. Therefore suggestion (a) is invalid.

It is necessary to postulate that in the particular inelastic collision which excites ion vibrational states, the interaction time is long compared to the mean-free-time of the ion.

The following sequence of events is suggested:

(i) The ion collides 'head-on' with a roton and interacts with the roton's thermal momentum. (See P. 118). The ion's forward momentum will be very little changed by this.

(ii) The ion-roton pair move under the influence of the applied field, gaining energy from the field.

(iii) The roton is re-emitted in the forward direction of ion motion with intrinsic momentum p_o reversed.

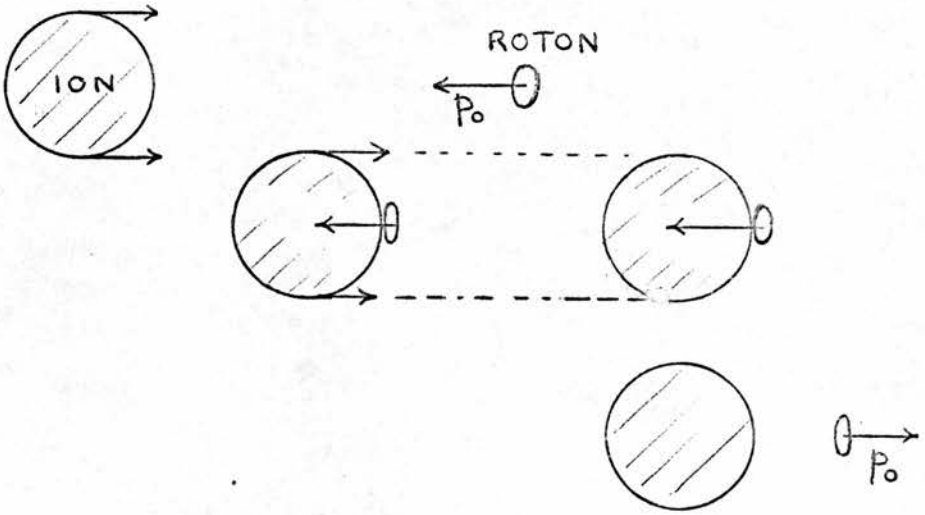

Conservation of momentum gives

$$mv_D - 2p_o = mv_D' \quad \ldots\ldots\ldots\ldots\ldots\ldots\ldots\ldots\ldots\ldots (p)$$

where v_D , v_D' are the ion drift velocity before and after the inelastic collision

m = mass of ion

The energy made available when this type of collision occurs consists of

1. Loss of kinetic energy by ion $\frac{1}{2} m(v_D^2 - v_D'^2)$
2. Energy gained from the applied field during the collision $= e\mathcal{E} v_D t_o$

   where e = electronic charge

   $\mathcal{E}$ = applied field

   t_o = interaction time
3. Possibly the thermal energy of the roton $(\frac{1}{2}kT)$

An inelastic collision will occur when the energy made available in this way equals the lowest energy level for vibration.

$$\therefore \text{ available energy } E = \frac{1}{2} m(v_D^2 - v_D'^2) + e\mathcal{E} v_D t_o + (\tfrac{1}{2}kT) \quad \ldots\ldots (q)$$

From (p) $\qquad v_D' = v_D - \dfrac{2p_o}{m}$

Substituting in (q)

$$E = 2p_o v_D - \frac{2p_o^2}{m} + e\mathcal{E} v_D t_o + (\tfrac{1}{2} kT)$$

The positive root of this equation is

$$\therefore v_D = -c\mu + c\mu \left(1 + \frac{X}{p_o c\mu}\right)^{\frac{1}{2}} \quad \ldots\ldots\ldots\ldots\ldots\ldots\ldots\ldots (r)$$

where $c = \dfrac{p_o}{et_o}$, $\quad X = (\dfrac{2p_o^2}{m} + E_\ell - (\tfrac{1}{2} kT))$ and μ = mobility where $\mu = v/\mathcal{E}$

The values of E_1 and t_o are adjusted to give the best agreement between the experimentally observed v_c and the critical velocities predicted by equation (r).

For positive ions $t_o = 5.6 \times 10^{-10}$ secs.

and $E_1^+ = 2.25 \times 10^{-16}$ ergs.* where E_1 = energy of first excited state

The use of these values in equation (r) together with the measured mobilities μ predict the temperature dependence of v_c. The calculated values are

T °K	v_c (predicted)	(Santini[59]) v_c
0.9	520 cm/sec	520
0.95	505	520
1.0	490	520
1.1	425	520
1.2	367	370
1.3	312	310
1.4	260	520

It can be seen that equation (r) predicts a drop in critical velocity with increasing temperature. The values for v_c agree approximately with the measurements of Santini et al[59] over the range 1.0 → 1.3°K. The theory does not however predict the observed temperature dependence of v_c above 1.3°K.

If the value $t_o = 5.6 \times 10^{-10}$ secs. and $E_1^- = 1.125 \times 10^{-16}$ ergs. $= \frac{E_1^+}{2}$ are substituted into equation (r) the negative ion critical velocities predicted are

---

* This value for E_1 is a factor 2 less than that predicted by the acoustic resonator model [1] (P. 99.)

T °K	v_c (predicted)	v_c (measured)
0.9	266 cm/sec.	
1.0	245	210 cm/sec. *
1.1	221	
1.2	196	
1.3	171	

The agreement is reasonably good.

* Present author.

Appendix 6 (P. 125)

Derivation of Equations (29), (30) and (31)

(29)

In a viscous medium the retarding force on the ion is proportional to its velocity. At the terminal drift velocity v_D

$$\text{Accelerating Force } eE = qv_D \quad \text{---------- (s)}$$

where e = ionic charge

E = field strength

q = constant

At an ion velocity $v < v_D$ the resultant accelerating force = $(eE - qv)$

$$\therefore \text{ Acceleration } \frac{dv}{dt} = \frac{1}{m_i}(eE - qv)$$

Substituting from equation (s)

$$\frac{dv}{dt} = \frac{q}{m_i}(v_D - v) \quad \text{---------- (t)}$$

Integrating

$$\log (v_D - v) = -\frac{q}{m_i} t + \text{Constant} \quad \text{---------- (u)}$$

At time t = 0 the ion velocity $v = v_o$

where v_o = ion velocity immediately after an inelastic collision.

$\therefore$ Constant in equation (u) = $\log (v_D - v_o)$

$$\therefore t = \frac{m}{q} \log \frac{v_D - v_o}{v_D - v} \quad \text{---------- (v)}$$

Therefore the time t_c required for an ion to accelerate from $v_o \rightarrow v_c$

$$t_c = \frac{m}{q} \log \frac{v_D - v_o}{v_D - v_c} \quad \text{---------- (w)}$$

It has been postulated that at an inelastic collision an ion loses a velocity v_c.

$$\therefore \quad v_D - v_o = v_c$$

and from (s)

$$q = \frac{eE}{v_D} = \frac{e}{\mu}$$

where μ = mobility.

$\therefore$ Equation (w) becomes

$$t_c = \frac{m\mu}{e} \log \left(\frac{v_c}{v_D - v_c}\right) \qquad \text{---------- (x)}$$

This is equation (29) in the text.

- - - - - - - - - - - - - -

(30)

The distance S_c travelled by the ion while accelerating from $v_o \rightarrow v_c$ is given by

$$S_c = \int_o^{t_c} v\,dt \qquad \text{---------- (y)}$$

Now from equation (v)

$$v = v_D - v_c e^{-\frac{qt}{m}}$$

$$\therefore \quad S_c = \int_o^{t_c} v_D - v_c e^{-\frac{qt}{m}}\,dt.$$

Integrating

$$S_c = \left(v_D t\right)_o^{t_c} + \left[\frac{mv_c e^{-\frac{qt}{m}}}{q}\right]_o^{t_c}$$

and

$$S_c = v_D t_c + \frac{mv_c}{q}\left(e^{\frac{-qt_c}{m}} - 1\right) \qquad \text{---------- (z)}$$

Substituting for t_c from equation (x)

and rewriting $e^{\frac{-qt_c}{m}}$

$$S_c = \frac{m\mu}{e}\left[v_A \left(1 + \log_e\left(\frac{v_c}{v_A - v_c}\right)\right) - 2v_c \right] \quad \text{--- (aa)}$$

This is equation (30) in the text.

- - - - - - - - - - - - -

(31)

The time t = 0 at which the ion reaches velocity v_c.

The ion travels for a time t_E at a velocity $v > v_c$ before being involved in an inelastic collision.

The distance S_E travelled during this time is given by

$$S_E = \int_0^{t_E} v\,dt.$$

Equation (v) modified gives

$$t = \frac{m}{q} \log \frac{v_A - v_c}{v_A - v} \quad \text{---------- (bb)}$$

$$\therefore \quad e^{\frac{qt}{m}} = \frac{v_A - v_c}{v_A - v}$$

and $$v = v_A + (v_c - v_A)\, e^{-\frac{qt}{m}}$$

$$\therefore \quad S_E = \int_0^{t_E} v_A + (v_c - v_A)\, e^{-\frac{qt}{m}}\, dt. \quad \text{---------- (cc)}$$

Integrating

$$S_E = v_A\, t_E - \frac{m}{q}(v_A - v_c)\left(1 - e^{-\frac{qt_E}{m}}\right) \quad \text{---------- (dd)}$$

This is equation (31) in the text.

Appendix 7 (See P. 179)

The magnitude of the Mobility Discontinuities as predicted by the Huang-Olinto Theory

Equation (35) in the paper by Huang and Olinto gives the ion drift velocity $\langle v \rangle$ as

$$\langle v \rangle = v_\infty \left[1 + \left(\frac{\varepsilon_o}{eEL}\right)\left(\frac{v_\infty}{v_c}\right) g_n\right]^{-1} \quad \text{(Huang-Olinto, 35)}$$

where $\varepsilon_o = 0.22$ eV is the energy of a vortex ring with unit quantised circulation formed by an ion, charge +e, moving at $v_c = 5.2$ m/sec.$^{-1}$; E is the electric field applied over the total flight path L; v_∞ is the drift velocity obtainable in the flight path in the absence of a discontinuity; and g_n is a factor given by

$$g_n = \sum_{\ell=1}^{w} \left[\ell\left(1 - \frac{\ell v_c}{v_\infty}\right) / 1 - \frac{E_\ell}{E}\right] \quad \text{(Huang-Olinto, 36)}$$

where E_ℓ is the critical field at the ℓ^{th} discontinuity.

Writing the Huang-Olinto equation 35 as $\langle v \rangle = v_\infty [1 + A]^{-1}$ for simplicity, the fractional decrease in mobility is given by

$$\frac{\Delta\mu}{\mu} = \frac{v_\infty - \langle v \rangle}{v_\infty} = \frac{A}{1 + A} \qquad \text{(ee)}$$

where $\frac{\Delta\mu}{\mu}$ depends on the grid-collector spacing L through the factor A.

The value of A for a typical experiment can be calculated, e.g. for zero field mobility $\mu_o = 10$ cm^{2}volt^{-1}sec.$^{-1}$, $E_\ell = 54.5$ volt/cm.$^{-1}$ at $\ell = 1$, an applied field E = 80 volt/cm.$^{-1}$ across L = 0.6 cm. gives $v_\infty = 7.47$ m./sec.$^{-1}$ and $g_n = 0.950$, and a value of $A = 6.2 \times 10^{-3}$. Thus in the temperature range 0.85°K to 1.0°K and in the region of the first two discontinuities, $A \ll 1$, and the fractional decrease in mobility is

$$\frac{\Delta\mu}{\mu} \simeq A = \frac{\varepsilon_o}{eEL} \cdot \left(\frac{v_\infty}{v_c}\right) \cdot g_n \qquad \text{(ff)}$$

With equation (ff), the theory and the results, Page 66, can be compared as follows:

(i) A critical test of the Huang-Olinto theory is the variation of the magnitude of the discontinuities with the grid-collector spacing L. Equation (ff) predicts that the discontinuity size $\Delta\mu$ is a function of the ion flight path L. Thus the shorter the ion path, the greater should be the effect of the vortex ring creation process on the measured drift velocity and hence on the size of the discontinuity. However, the results shown in Fig. , indicate that the discontinuity size was independent of the grid-collector spacing. This is in disagreement with the theory.

(ii) The magnitude of a discontinuity from equation (ff) is much less than the measured magnitude. This shows up in Fig. where for example at L = 0.5 cm. the experimental $\Delta\mu = 0.7\mu$ while the theoretical $\Delta\mu = 0.012\mu$.

(iii) The magnitudes of the successive discontinuities should increase with increasing ion velocity. Thus with positive ions equation (ff) predicts $\frac{\Delta\mu}{\mu} = 0.012, 0.021, 0.027, \ldots$ for the first, second, third .... discontinuities. However, the results, (P. 68) show no variation in the magnitudes of the first three discontinuities.

Appendix 8

Recent Measurements of the effective Mass of Ions in Liquid Helium

Dahm and Sanders[60] have measured the effective mass of ions in liquid helium using a microwave technique. They derived the momentum relaxation time from their measurements of the microwave conductivity due to ions injected into a reflection cavity. The ion effective mass is then given by

$$m_{eff} = \frac{et_r}{\mu(0)}$$

where e = electronic charge

t_r = relaxation time

$\mu(0)$ = D.C. mobility

Dahm and Sanders obtained $m_{eff} \approx 40\ m_{He}$ for the positive ion in the temperature range 1.2°K - 1.7°K . The corresponding relaxation time $\approx 1.6 \times 10^{-9}$ secs. is of the same order as the relaxation time calculated from Maxwells' Equation (see Appendix 5 page 202).

The substitution of this new value for the effective mass into the equations (p) and (r) page 203 would affect the predicted critical velocity in two ways.

(a) The factor $\frac{2p_o^2}{m} - \frac{1}{2}kT$ is no longer negligible in comparison to $2p_o v$. The energy available at an inelastic collision is then no longer proportional to v and the predicted critical velocities would not be equally spaced. (see also page 109)

(b) The momentum of the positive ion at 5 m/sec. would be insufficient for it to reflect a roton forwards in an inelastic collision.(i.e. $mv_c < 2p_o$)

It would be necessary to postulate that the first three discontinuities for the positive ions were the result of oblique inelastic ion-roton collisions.

If the positive ion effective mass is correctly $4Om_{He}$ then the vibrating ion model as set out here is unsatisfactory.

However it seems possible that the effective mass obtained by Dahm and Sanders is not necessarily the mass of an ion drifting under the influence of a slowly varying field. They apply a field of frequency 9.3×10^9 c/s and they are measuring relaxation times of the order of the period of the applied field.

If the value of the effective mass ($4Om_{He}$) is substituted into equation (26) page 113 a mobility of 9.9 $cm^2\ volt^{-1}\ sec^{-1}$ is obtained. This is a less satisfactory result than that obtained when an ion mass = 100 m_{He} was substituted (6.1 $cm^2 volt^{-1} sec^{-1}$). The measured mobility at 1°K is 5.9 $cm^2 volt^{-1} sec^{-1}$.

Appendix 9

The Number of Ions in an Excited State

Ions in a field free situation at 1°K have sufficient thermal energy to become vibrationally excited. The number of ions in an excited state at any time depends on

(a) The ease of excitation

(b) The ease of de-excitation.

(a) It has been suggested in Appendix 5 that an ion requires a finite interaction time with rotons in order that it should become vibrationally excited. During the interaction time energy is fed from the field into the ion-roton system. For this reason it is harder for an ion in the field free situation to become excited.

(b) It has been postulated that vibrating ions are easily de-excited.(P.129)

Therefore at any time the excited state is sparsely populated. When the applied field exceeds the critical field for the first discontinuity the population of the first excited state shows a discontinuous increase.